UNIVERSIDADE DO ALGARVE

FACULDADE DE CIÊNCIAS E TECNOLOGIA

LABORATÓRIO DE PROCESSAMENTO DE SINAL

BROADBAND MATCHED-FIELD TOMOGRAPHY

USING

SIMPLIFIED ACOUSTIC SYSTEMS

(Documento provisório)

CRISTIANO SOARES

Tese apresentada à Universidade do Algarve para a obtenção do grau de Doutor no ramo de Engenharia Electrónica e Computação, especialidade Processamento de Sinal.

UNIVERSIDADE DO ALGARVE, FARO

DEZEMBRO 2006

UNIVERSIDADE DO ALGARVE

FACULDADE DE CIÊNCIAS E TECNOLOGIA

Broadband Matched-Field Tomography using simplified Acoustic Systems

(Documento provisório)

Cristiano Soares

LABORATÓRIO DE PROCESSAMENTO DE SINAL (SiPLAB)

Orientador: Doutor Sérgio Manuel Machado Jesus, Professor Associado da Faculdade de Ciências e Tecnologia, Universidade do Algarve

À Telma,
ao pequenino Guilherme,
e aos meus pais.

Acknowledgements

I would like to thank my supervisor Prof. Sérgio M. Jesus for his permanent effort in providing the necessary conditions in the laboratory for accomplishing the objectives of this work, by organizing scientific projects and sea trials for collecting experimental data, his useful advises, and in particular, for his contributions through many suggestions and comments during the writing of this thesis.

I thank also my colleagues in the Signal Processing Laboratory that daily contributed for an enjoyable social environment.

Finally, special thanks to my wife, for her patience and support, specially during the writing of this thesis.

Name: Cristiano José da Palma Soares
College: Faculdade de Ciências e Tecnologia
University: Universidade do Algarve
Supervisor: Doutor Sérgio Manuel Machado Jesus, Professor Associado da Faculdade de Ciências e Tecnologia, Universidade do Algarve
Thesis title: Broadband Matched-Field Tomography using simplified Acoustic Systems

Abstract

Ocean Acoustic Tomography is a remote sensing technique that has been proposed to infer physical properties of the ocean traversed by the sound field. Although its feasibility has been demonstrated, it is still not being used in a systematic way due, in a large extent, to cost and operational difficulties of standard acoustic systems. Current developments of acoustic systems go in the sense of simplifying them, both at the emitting and receiving end. Simplifying an acoustic system may represent a loss or a reduction of the amount of information contained in the observed acoustic field, possibly conducting to degradation in the inversion results. The objective of this thesis is to adapt existing array processing methods to be used in acoustic tomography and geoacoustic inversion taking into account the challenges posed by such simplifications, and to cope with the loss of available information they may represent. Two aspects are exploited with the objective of coping with the reduction of information: one is the development of a broadband data model, and the other is the development of matched-field processors based on that broadband data model, with particular emphasis in high-resolution processors. Matched-field based approaches appear to be suitable to work in conjunction with the simplified acoustic systems used to collect several experimental data sets treated herein. Experimental results using simplified acoustic systems, sparse receiving arrays (active mode) on one hand, or an uncontrolled source (passive mode) on the other hand, show that it is possible to produce environmental estimates of the watercolumn and seafloor in close agreement with ground truth measurements.

Key-words: Acoustic tomography, simplified acoustic systems, broadband, environmental estimation, coherent processing, high-resolution.

Nome: Cristiano José da Palma Soares
Faculdade: Faculdade de Ciências e Tecnologia
Universidade: Universidade do Algarve
Orientador: Doutor Sérgio Manuel Machado Jesus, Professor Associado da Faculdade de Ciências e Tecnologia, Universidade do Algarve
Título da Tese: Tomografia por Ajuste de Campo em Banda-Larga utilizando Sistemas Acústicos simplificados

Resumo

A Tomografia Acústica Oceânica é uma técnica de medida remota que foi proposta para inferir acerca das propriedades físicas do oceano atravessado pelo campo acústico. Embora tenha sido demonstrado que esta técnica é praticável, a mesma não é ainda utilizada de forma sistemática, em larga medida, devido aos custos e dificuldades operacionais dos sistemas acústicos tradicionais. Os desenvolvimentos actuais de sistemas acústicos vão no sentido da sua simplificação, quer do lado da emissão, quer do lado da recepção. A simplificação de um sistema acústico poderá representar uma perda ou uma redução da quantidade de informação contida no campo acústico observado, conduzindo possivelmente a uma degradação nos resultados de inversão. O objectivo desta tese é adaptar métodos de processamento de antenas existentes, de forma a serem utilizados em tomografia acústica e inversões geoacústicas, tomando em consideração os desafios colocados por tais simplificações, e combater a perda de informação disponível que as mesmas representam. Dois aspectos são explorados com o objectivo de combater a redução de informação: um é o desenvolvimento de um modelo de dados de banda larga, e o outro é o desenvolvimento de processadores por ajuste de campo baseados nesse modelo de dados, com particular ênfase nos processadores de alta resolução. Os métodos por ajuste de campo parecem ser apropriados para trabalhar em conjunção com os sistemas acústicos simplificados utilizados para adquirir os vários conjuntos de dados experimentais tratados neste trabalho. Resultados experimentais obtidos com sistemas acústicos simplificados, com antenas de recepção esparsas (modo activo) por um lado, e com uma fonte não-controlada (modo passivo) por outro, mostram que é possível produzir estimativas ambientais da coluna de água e do fundo oceânico de acordo com medidas *in-situ*.

Palavras-chave: Tomografia acústica, sistemas acústicos simplificados, banda-larga, estimação ambiental, processamento coerente, alta resolução.

Contents

List of Figures

List of Tables

Chapter 1

Introduction

Generalities and work motivation

The propagation of sound in the ocean is strongly influenced by the environmental conditions. The sound field is sensitive to the propagation velocity which depends on the geophysical properties of the watercolumn and seafloor. The interaction of the propagating sound with the seafloor is particularly relevant in shallow-water (less than 200 m) as it is reflected at the seafloor and transmitted into the sediments. Being able to predict the acoustic behavior of a given environment is the key to current advances in the usage of acoustics for ocean exploration [1]. This implies that, for example, the sonar detection of a sound source in range and depth depends on the environmental knowledge of a given propagation scenario. Conversely, the interaction between sound waves and the environment allows for retrieving environmental information from the analysis of the emitted and received signals. Acoustic ocean exploration is an appealing complement to classical ocean exploration.

Classical ocean exploration is based on direct measurements of physical quantities of the ocean. Direct *in-situ* measurements of the physical quantities in the watercolumn or in the seafloor are usually time consuming, very expensive and offer poor spatial coverage. In other words, direct methods are generally slow and the regions that can be covered are

small compared to the size of the ocean. Moreover, direct measurements can generally not be made simultaneously at different points of the ocean, nor are they capable to show how slow physical processes vary over time or how these change with seasons or over longer time periods.

The magnitude of the ocean sampling task leads to technologies providing indirect methods for assessing ocean physical quantities. These methods clearly offer the possibility to observe physical quantities in a vast area of the ocean in a systematic way, and at lower cost than direct methods. Indirect methods consist in exploring the interaction of a wave with the media to be characterized, in order to use such interaction and its physical laws to retrieve physical quantities of interest.

An excellent example on the advantages of using indirect methods for ocean observations are satellites such as the TOPEX/Poseidon satellite that has been in service for more than 10 years [2]. This satellite covers 95% of the ice-free oceans every 10 days (!), carrying out a number of tasks such as continuously observing global ocean topography, delivering altimetric data, and observing relevant phenomena such as *el Niño* and *la Niña*.

However, satellites use electromagnetic waves, which are strongly attenuated by sea water and are therefore essentially suitable for observing the ocean surface. Acoustic waves, on the other hand, propagate well in the ocean, providing means to remotely sense the interior of it, using the generic advantages of indirect methods for assessing its physical properties. There are examples of acoustic applications that have been commercially available for several years. The Acoustic Doppler Current Profiler (ADCP), an acoustic device that attempts to produce a record of water current velocities over a range of depths, is now considered an indispensable aid for oceanography, estuary, river and stream flow current measurement.

The side-scan sonar is used for mapping the seabed for a wide variety of purposes such as identification of bathymetric features and understanding material and texture type of the seabed.

One of the most relevant physical properties is the temperature in the watercolumn. Ocean Acoustic Tomography is a remote sensing technique that has originally been proposed to infer this physical property. Although its feasibility has been demonstrated and despite the advantages of this technique, it is still not being used in a systematic way. This concept requires expensive acoustic emitting and receiving equipment to be maintained and operated at several locations in order to obtain sufficient source-receiver propagation paths to cover a given ocean volume. Installing acoustic systems on a long-term or permanent basis may become problematic, since some areas of interest are just not suitable for that. In practice, many acoustic systems operate at low frequencies, implying the use of bulky and expensive sound projectors and large aperture receiving arrays. Operational difficulties arise due to the deployment requirements of those equipments. Most of the acoustic apparatus used today in acoustic tomography are still prototypes and research oriented. From a completely different point of view, biologists and environmentalists have demonstrated concerns on how sound transmissions across the ocean affect marine mammals.

In order to alliviate these problems faced by the sound technology used in ocean acoustic tomography one can operate simplifications either on the emitting end, or on the receiving end of the acoustic system. The simplification of one end of the acoustic system has perhaps to be accompanied by an increase of complexity on the other end in order to prevent a decrease of performance of the whole system. Simplifications on the receiving end can be operated by reducing the number of receivers typically used, and/or by reducing the array

aperture. It is also possible to design a receiving system such that it can be deployed in a free-drifting configuration instead of a moored configuration. Operating these simplifications, one at a time or all together, will essentially reduce the size of those receiving equipments and their deployment requirements. At the emitting end one can reduce the size of the emitting source, which would reduce the deployment requirements, at the cost of an increase of the emitting frequencies. Another possibility is to completely eliminate the source, taking advantage of the fact that the marine environment is naturally noisy, specially due to animal or human activity, and surface hydrodynamic phenomena. Thus, the idea of using sources of opportunity that are naturally present is an appealing alternative to a controlled source in areas where deploying a permanent controlled source is impossible or too costly, in the presence of marine mammals, or for covert military applications.

The characteristics enumerated above, represent a reduction in the complexity of acoustic systems used in acoustic tomography, in comparison to standard acoustic systems. Such reduction in complexity is, in principle, obtained at the cost of a reduction of available information in the observed acoustic field. The objective of the work presented in this thesis is to extend existing or propose new signal processing methods being able to exploit simple and handy acoustic systems for ocean acoustic tomography. The implications and challenges of using such acoustic systems in acoustic tomography have to be identified, in order to understand which observables of the acoustic propagation can be used, together with the field inversion algorithm to be applied.

Ocean acoustic tomography: background

In 1979 Munk and Wunsch [3, 4] proposed Ocean Acoustic Tomography (OAT) as a concept for global ocean monitoring. OAT can be defined as the cross-sectional imaging of a region

from either transmitted or reflected pressure fields collected when insonifying the region from different directions. The problem of Ocean Acoustic Tomography is to infer from precise measurements of travel time, or other properties of acoustic propagation, the state of the ocean traversed by the sound field. The rationale behind that concept is that the ocean is largely transparent to sound, and that sound travel time depends on the temperature (and to a much lesser extent, on salinity). Conversely, measurements of the time that acoustic energy takes to travel from emitter to receiver can provide information about the intervening ocean using inverse methods.

At the same time Matched-Field Processing (MFP) was being proposed for source localization problems [5, 6]. MFP is a full-field signal processing method that takes advantage of the spatial properties of the acoustic field and the knowledge of the ocean properties between source and receiver to retrieve source location (see [7] and references herein). A measured field is compared to model replicas calculated for hypothetical source positions within a specific range and depth search region to form an ambiguity surface whose maximum will indicate the location of the acoustic source provided that the underlying physical model is sufficiently accurate. The comparison between the field and the replicas is done by means of a processor which usually is a correlation function based on statistical assumptions made on signal and noise. Since the acoustic signal is used as an intermediate observable to estimate source location, MFP can be considered to be an inverse problem. However, the calculation of the replica signal is more difficult than in conventional array processing since it involves solving the wave equation on the actual physical scenario. The knowledge on the parameters of the actual physical scenario is of paramount importance in MFP based processing approaches, since the ability to predict the acoustic behavior of this scenario,

and consequently the source location estimation performance will depend on those physical parameters. Hinich [5] was the first to examine source localization with a vertical array, but Bucker [6] is credited to be the first to formulate MFP, as he used realistic environmental models, introduced the concept of ambiguity surface and demonstrated that there was enough complexity of the wave field to allow inversion - localization.

From the algorithmic point of view, there are essentially two types of algorithms for performing ocean acoustic tomography. One is the original concept, by Munk and Wunsch, and is based on the travel times of the sound through multiple paths, and has been termed Travel-Time Tomography (TTT) [3]. The other is Matched-Field Tomography (MFT), which is similar to the Matched-Field Processing (MFP) technique, except that the source location is known, and parameters of the intervening ocean are to be estimated [8, 9, 10, 11]. TTT makes direct use of the multipath nature of the sound propagation in the ocean. One looks for the perturbations of the sound-speed around a background value instead of the sound-speed profile itself. The modeled travel times are calculated taking advantage of linearizable equations making direct inversion possible. This approach was initially proposed for deep water regions where the ray approximation was valid and sound speed could be analytically linked to acoustic ray travel-time [4]. Since it uses absolute travel-times, travel-time based tomography turned out to be highly dependent on the ability to separate closely spaced arrivals and the precise knowledge on the source-receiver relative position at all times. Moreover, it appears to be limited to tomographic problems where the linearization approach is applicable. In shallow-water, TTT suffers degradation due to arrivals that can not be identified or separated. On the other hand, in shallow-water, there is the need to infer seafloor properties, about which little or no information is contained in the travel times.

Instead, MFT is applicable to problems where one looks for the actual value of the parameters rather than their perturbations around a background value. In that case the problem is highly non-linear and a linearization approach is no longer a realistic option. As direct inversion is not possible, the inversion is posed as an optimization problem in an attempt to maximize the match between the measured acoustic field and the replica field calculated for candidate parameter values. Several authors have used this technique for performing geoacoustic inversions of field data [12, 13, 14, 15, 16].

MFT is often applied in shallow water scenarios where the seafloor parameters have an important influence on the field propagation. The seafloor parameters are often unknown, and have therefore to be estimated together with the parameters of the watercolumn. This arises one of the hardest problems to deal with, in MFT, which is the high number of unknowns that may enter the inverse problem. The inverse problem is in general ill-conditioned and the parameter space is usually very large. Thus, there is the inherent risk that the final model estimate may represent an acoustically equivalent but environmentally different model from the true model, leading to erroneous environmental parameter estimates. This problem leads to another important discussion in MF approaches, which is on the ability of the processor to reject sidelobes. In the past much effort has gone into developing processor techniques to suppress sidelobes as much as possible. This issue is particularly important in inverse problems where many parameters are left as unknowns. Depending on the parameters in play, the specific physics of the scenario at hand, and the geometric setup of the experiment, complicated ambiguity patterns might be generated. The ability of discriminating closely spaced acoustic fields depends on the degree of uniqueness of the acoustic pressure field. This can be achieved by using a high number of receivers or eventually by employing

high-resolution methods as discussed by Collins *et al.* [17]. Examples of high-resolution methods are matched-field processors derived from the concepts of minimum-variance [18] or subspaces [19]. These methods offer significantly higher sidelobe attenuation in comparison to Bartlett-like methods and usually involve comparisons beyond simple correlations. However, there have been a reduced number of papers applying either the minimum-variance processor [20, 21], or subspace based methods [22] to real acoustic data with some degree of success.

Ocean acoustic tomography using simplified acoustic systems

Ocean acoustic tomography experiments in deep water regions for large-scale ocean monitoring have used multiple sources and multiple arrays in order to determine the variability of the three-dimensional water temperature field [23, 24, 25]. In shallow-water tomography experiments the simple configuration of a single source and a single vertical array of receivers has been used in several occasions. The acoustic source is usually towed by a research vessel, in order to cover a certain area of interest, and the receiving array traditionally employed has a high number of hydrophones (see e.g. [13, 14, 16]) in order to sufficiently sample higher order normal modes and assure as much as possible uniqueness in the problem solution.

Current developments of receiver systems go in the sense of reducing their overall size along with the length of the array itself and the number of receivers with the objective of reducing the cost and deployment requirements of these systems. This means that the acoustic field will be heavily undersampled representing therefore an additional challenge in terms of conditioning of the inverse problem. The other simplification already mentioned, the free-drifting deployment of the receiver array, poses a challenge in terms of knowledge of the position of the receiving array. A number of papers using sparse vertical arrays exist.

Siderius *et al.* [15] used 4-hydrophone arrays distributed over a range of 40 km to invert range-dependent bottom properties from broadband transmission loss in the frequency band 200-800 Hz. Felisberto *et al.* [26] demonstrated with experimental data that successful inversions for the watercolumn in shallow water can be obtained with a 4-hydrophone vertical array using a known broadband source with a bandwidth of 700 Hz about 10 km away from the vertical array. Here an arrival matching processor was used. Le Gac *et al.* [27] developed a geoacoustic inversion process based on the use of a model-based matched-impulse response using broadband acoustical signals on a single hydrophone. The methods used in all these studies involve the correlation of the received signals with the emitted signal to estimate the channel impulse response, and therefore require broadband signals. More recently Soares *et al.* have obtained tomography inversion results using sparse vertical line arrays with 4 elements [28, 29] and with 3 elements [30, 31]. All results were obtained with cross-frequency MF processors without using knowledge of the emitted waveform. In Refs. [30, 31] high-resolution processors were used.

From the emitter point of view it can be said that the majority of acoustic tomography studies used controlled acoustic sources and therefore fall in the case of active tomography. In opposition, Passive Acoustic Tomography (PAT), a variant of acoustic tomography where the usual controlled source is replaced by a source of opportunity, represents a significant increase of the complexity of the inverse problem in comparison to active tomography. Using a source of opportunity will in principle lead to a loss of signal-to-noise ratio of the received signals. As the emitted waveform is unknown, the extraction of observables as for example travel-times or ray amplitudes of acoustic rays is strongly degradated in terms of accuracy. In that way, travel-times and ray amplitudes in PAT are relative to those of the first arrival,

and no longer absolute quantities as in active tomography. Further attributes of the emitted signal are that it may contain stochastic components, and the signal may suffer fluctuations during the observation time both in strength and bandwidth. Also the position of the source may be unknown and changing over time, and may therefore constitute a nuisance parameter to be added to the parameters of interest to be estimated from received acoustic fields. Furthermore, not knowing the source position implies that other propagation channel characteristics such as waterdepth or seafloor properties are also unknown and must be estimated. There is a generic approach in signal processing called blind system identification for estimating the input signal or system parameters when only the output data are known. A passive acoustic tomography problem with unknown emitted signal and unknown channel properties can be termed blind ocean acoustic tomography (BOAT). The distinction between PAT and BOAT is that the former aims at estimating ocean temperature with alternative passive sources, while the latter produces a full environmental estimate, including water column, bottom properties, and source-receiver geometry as well as a source-emitted power spectrum, without any knowledge or control on the acoustic illuminating source. The tomographic problem suffers significant increase both in complexity and uncertainty when one passes from active mode to passive mode.

A number of papers reporting the idea of using alternative illuminating sources for OAT and geoacoustic inversion exist. Two groups of applications for inferring ocean properties have been proposed in the literature. One uses ship radiated noise and vocalizations of marine mammals for watercolumn or geoacoustic inversion. The other uses surface generated noise for geoacoustic inversion. Chapman [32] describes an approach for geoacoustic inversion using ship noise data collected with a 16-hydrophone vertical line array. Ship noise data

were recorded as a ship followed an arc segment at a range of 3.3 km from the array. Jesus *et al.* [33, 34] applied MFT on ship noise data of a research vessel describing arcs of 1.2, 2.2, and 3.2 km recorded on a 16-hydrophone vertical line array. Thode *et al.* [35] performed global inversions using blue whale vocalizations from 8 elements of a vertical line array to extract information on bottom composition, array shape, and the animal's position. Other authors used ship-towed horizontal arrays recording the noise emitted by the towing-ship itself or by a cooperative ship to estimate ocean parameters [36, 37, 38]. All these studies except [38] used MFP based inversion methods.

Concerning the applications using surface generated noise Buckingham first proposed to use acoustic daylight to form images of silent objects in the ocean [39, 40] and then using ambient noise for geoacoustic inversion [41]. More recently Harrison [42, 43, 44] used sea surface wind induced noise and then Buckingham *et al.* [45] used light aircraft air induced noise, both with the purpose of shallow water geoacoustic inversion.

The simplifications that can be operated in an acoustic system, at the emitting end or at the receiving end, discussed in this chapter basically imply that the amount of information available in the received acoustic field is reduced in comparison to that when a traditional acoustic system is used to emit and receive signals. At the emitting end, using a source of opportunity, such as for example ships or marine mammals, corresponds to a loss of control on one hand, and to a lack of knowledge on emitted waveform on the other hand. On the receiving end, the reduction of available information is essentially a consequence of the sparsity of the receiver elements.

This thesis deals with this important implication by proposing MFP based array processing methods that attempt to cope with the increased ill-conditioning of the underlying

inverse problem by extracting more information from the acoustic signals than conventional processing. The algorithms developed in this thesis can be applied for estimating watercolumn, bottom properties, and source position.

Organization of this thesis

This thesis is organized as follows: chapter 2 briefly reviews some fundamental topics such as the dependence of sound-speed, sound-propagation, and inverse problems in MFP. Chapter 3 develops a broadband data model and discusses some related aspects. Chapter 4 develops three matched-field processors based on the broadband data model: the Bartlett processor, the minimum-variance processor, and the MUSIC processor. Chapter 5 reports a series of computer simulations performed for numerically characterizing and comparing the three processors. Chapter 6 reports experimental results on MFT applied to the MREA'03 data set comparing the three processors developed. Chapter 7 reports experimental results on MFT applied to the MREA'04 data set testing the performance of a high-resolution processor with a varying number of frequencies and a scheme for validating environmental inversions. Chapter 8 reports experimental results on passive acoustic tomography applied to the IN-TIFANTE'00 data set. Finally, chapter 9 draws conclusions on the achievements of this thesis and gives suggestions for future work.

Chapter 2

Theoretical background

The present chapter reviews several concepts used in the remaining text of this thesis. This chapter is broadly divided into two groups of subjects. One is on the underlying physics of the problem by treating concepts such as the sound-speed in the ocean, the modeling of sound propagation in the ocean, and modeling of sound propagation in range-dependent environments (sections 2.1, 2.2, 2.3). The other deals with the inverse problem, by reviewing environmental focalization, an inversion technique based on Matched-Field Processing (section 2.4); and genetic algorithms which is a global search method used in focalization problems (section 2.5).

2.1 The sound-speed

The sound speed in the ocean plays a fundamental role in sound propagation. Through the times the sound speed has been related to physical and chemical parameters, but it can simply be seen as an increasing function of temperature, salinity, and pressure. A simplified expression for this dependence is the Mackenzie formula [46, 47], given as

$$c(\mathsf{T}, z, \mathsf{S}) = 1449.2 + 4.6\mathsf{T} - 0.055\mathsf{T}^2 + 0.00029\mathsf{T}^3 + (1.34 - 0.01\mathsf{T})(\mathsf{S} - 35) + 0.016z, \quad (2.1)$$

where c is the sound speed in m/s, T is the temperature in °C, z is depth in m, and S is salinity in ppt. It can be seen that in shallow water the temperature has the most important contribution for the sound speed. In deep water, and for large depths, the last term containing depth z dominates the sound speed. The speed of sound in the ocean shows only small departures from 1500 m/s, usually less than 1%. Nevertheless the effect of small variations of the sound speed on sound propagation in the ocean is profound.

For estimating the ocean sound speed profile via acoustic tomography, the direct estimation of the sound speed profile is the simplest approach as it directly reflects the parameters required. However, in general a sound speed profile contains a large number of data points - thus, direct estimation of those data points could be cumbersome. The ocean sound speed can be efficiently represented via shape functions. Empirical orthogonal functions (EOF) have extensively been used for ocean sound speed estimation. EOFs are orthogonal shape function [48] that can be obtained from a database and are very efficient to reduce the number of data points. If historical data is available, an efficient parameterization in terms of EOFs leads to faster convergence and higher uniqueness in the optimal solution since a great deal of information is included and the search is therefore started close to the solution, besides representing a way of strongly constraining the solutions that can be obtained [8]. For this purpose, for example, EOFs are constructed from representative data by sampling the depth dependence of the ocean temperature. The EOFs are obtained by computing the singular value decomposition (SVD) of a matrix $\mathbf{C_{TT}}$ with columns

$$[\mathbf{C_{TT}}]_i = \underline{\mathsf{T}}_i - \bar{\underline{\mathsf{T}}}, \tag{2.2}$$

where $\underline{\mathsf{T}}_i$ are the measured profiles available, and $\bar{\underline{\mathsf{T}}}$ is the average profile. The SVD is known

to be

$$\mathbf{C_{TT}} = \mathbf{UDV}, \tag{2.3}$$

where $\mathbf{D}$ is a diagonal matrix with the singular values, and $\mathbf{U}$ is a matrix with orthogonal columns, which are used as the EOFs. The temperature profile is obtained by

$$\underline{\hat{\mathsf{T}}}_{\mathrm{EOF}} = \underline{\bar{\mathsf{T}}} + \sum_{n=1}^{\mathcal{N}} \alpha_n \underline{\mathsf{U}}_n, \tag{2.4}$$

where α_n is a coefficient associated to the EOF $\underline{\mathsf{U}}_n$, and $\mathcal{N}$ is the number of EOFs to be combined, which is selected by observation of the singular values by using some empirical criterion. The criterion used in this study to select the number of relevant EOFs for the available data is

$$\hat{\mathcal{N}} = \min_{\mathcal{N}} \frac{\sum_{n=1}^{\mathcal{N}} \lambda_n^2}{\sum_{m=1}^{\mathcal{M}} \lambda_m^2} > 0.8, \tag{2.5}$$

where the λ_n are the singular values obtained by the SVD, and $\lambda_1 \geq \lambda_2 \geq \ldots \geq \lambda_{\mathcal{M}}$. $\mathcal{M}$ is the total number of singular values. Experimental results have shown that usually the first 1, 2 or 3 EOFs are enough to achieve a high degree of accuracy. The use of EOFs involves historical data that in the case of the water column temperature profile can be acquired over time and space. Thus, one can expect to have sufficient information to enable the model to obtain the profile that best represents the watercolumn over range, depth and time. Figure 2.1 shows temperature profiles measured during several sea trials with the respective EOFs obtained via SVD. They were obtained during different seasons of the year at different places, which can clearly be seen to have a strong influence on their shapes. The temperature and depth scale is the same on all plots for the sake of easy comparison. Figure 2.1(a) shows the profiles measured with XBTs during the INTIFANTE'00 sea trial, which took place off the Portuguese West coast near Setúbal in October 2000 [49]. The mean profile varies 3.6°C between the top and the bottom. Table 2.1 shows the minimum and
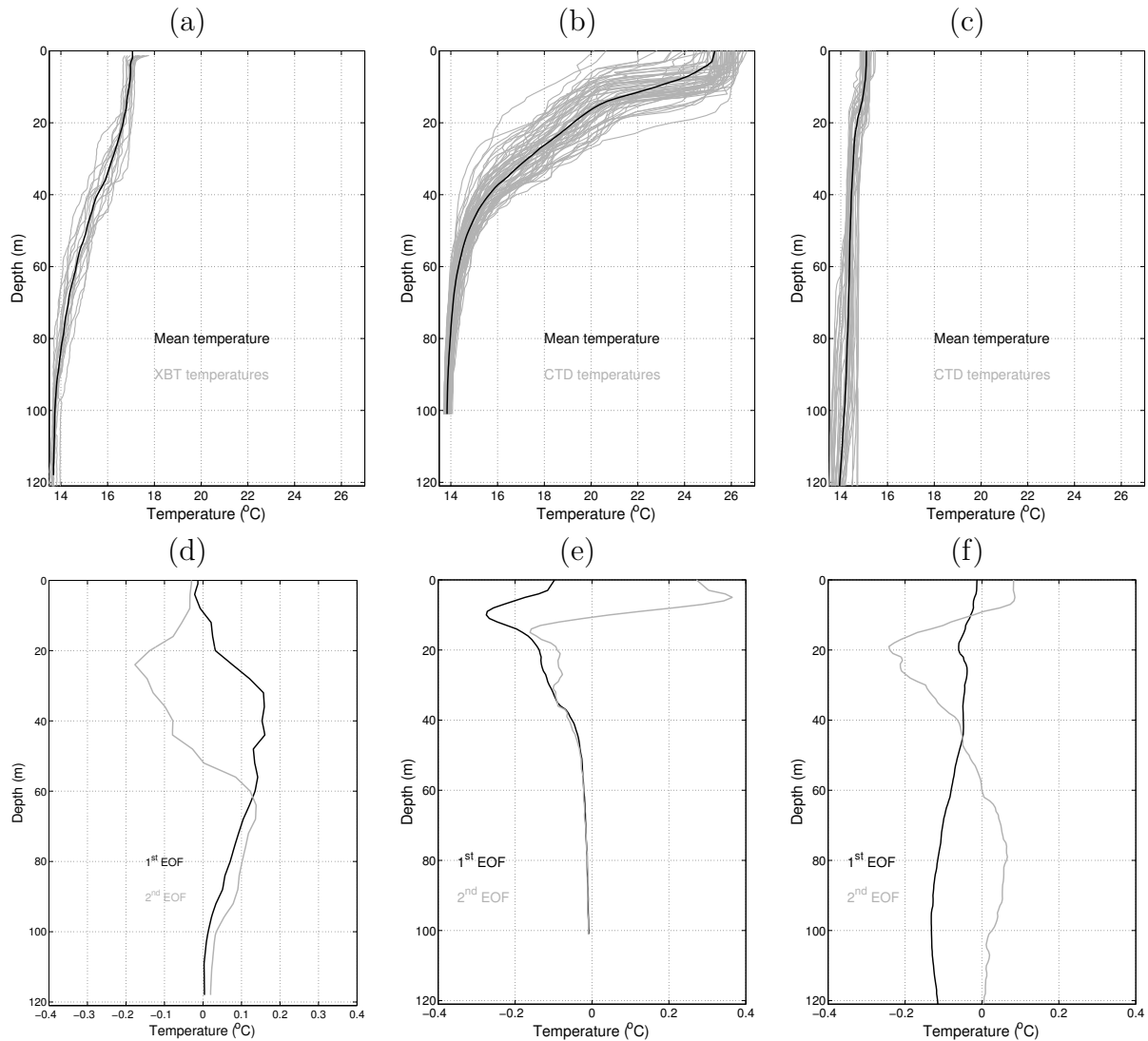
Figure 2.1: Temperature profiles and respective EOFs measured at several places: Portuguese West coast near Setúbal in October 2000 ((a) and (d)); North Elba Island area in June 2003 ((b) and (e)); Portuguese West coast near Setúbal in April 2004 ((c) and (f)).

maximum temperatures of the average profiles considered. Figure 2.1(b) shows the profiles

measured during the MREA'03 sea trial [50] which took place in the North Elba Island area

in June 2003. These are typical Mediterranean Summer profiles with a strong thermocline.

The variation with depth (11.5 °C) is clearly stronger then for those in the Atlantic Ocean.

The MREA'04 took place off the Portuguese West coast near Setúbal in April 2004 and the

mean profile has a variation of 1.1°C between the top and the bottom (figure 2.1(c)) [51].

This is a nearly isovelocity case. Winter propagation conditions are better than those in the

	INTIFANTE'00	MREA'03	MREA'04
min.	13.7	13.8	14.0
max.	17.1	25.3	15.1

Table 2.1: Minimum and maximum values of the mean profile considered at each sea trial.

Summer, since typically during summertime the temperature profile is downward refracting preventing long range propagation.

In the second row are plotted the respective EOFs obtained with the collections of measured temperature profiles. Those profiles will be used for the inversion of the acoustic field in the experimental part of this study. The INTIFANTE'00 and the MREA'03 data satisfied the criterion in equation (2.5) with the first 2 EOFs, while the MREA'04 data satisfied the criterion with just the first EOF. The EOFs have interesting features that are clearly related to the variability of the measured temperatures profiles. The first EOF for the IN-TIFANTE'00 sea trial is close to zero at the top and increases with depth until a depth of 40 m, and then reduced back to zero at the bottom. The first EOF of the MREA'03 sea trial shows high variability in the first layers and then approaches to zero. Finally, the first EOF of the MREA'04 sea trial is close to zero at the top, and increases steadily with depth, indicating that some variability at deeper layers found place during the temperature measurements.

2.2 Acoustic propagation in shallow water

The wave equation in an ideal fluid can be derived from hydrodynamics and the adiabatic relation between pressure and density. Considering that the time scale of oceanographic changes is much longer than the time scale of acoustic propagation, it is assumed that the material properties density ρ and sound speed c are independent of time. The linear approx-

imation of the wave equation involve retaining of only first order terms in the hydrodynamic equations:

$$\rho \nabla (\frac{1}{\rho} \nabla p) - \frac{1}{c^2} \frac{\partial^2 p}{\partial t^2} = 0, \tag{2.6}$$

where p is the acoustic pressure [1]. Note that this is a homogeneous equation, and that ρ and c^2 are space dependent. Several numerical methods exist to solve this equation. The major difference between the various techniques is the mathematical manipulation of the wave equation applied before implementation of the solution. In general the task of implementing the solution of the wave equation is very difficult due to the complexity of the ocean-acoustic environment: the sound speed profile is usually non-uniform in depth and range; the sea surface is rough and time dependent; the ocean floor is typically a very complex and rough boundary which may be inclined, and its properties are usually varying over range.

Shallow water is defined as that part of the ocean lying over the Continental Shelf where the water depth is less than 200 m. At frequencies of a few hundred Hz, the shallow water column is of several wavelengths and act as a waveguide whose boundaries are the surface and the bottom. In this type of environment the acoustic field is usually represented by normal modes. The *Helmholtz equation* is the wave equation in the frequency domain, and can be written in cylindrical coordinates under the assumption of cylindrical symmetry as:

$$\frac{1}{r} \frac{\partial}{\partial r} (r \frac{\partial p}{\partial r}) + \rho(z) \frac{\partial}{\partial z} (\frac{1}{\rho(z)} \frac{\partial p}{\partial z}) + \frac{\omega^2}{c^2(z)} p = -\frac{\delta(r)\delta(z - z_s)}{2\pi r}. \tag{2.7}$$

Using the technique of *separation of variables* the solution being searched has the form $p(r, z) = \Phi(r)\Psi(z)$. Replacing this in (2.7) and after some manipulations,

$$\rho(z) \frac{d}{dz} [\frac{1}{\rho(z)} \frac{d\Psi_m(z)}{dz}] + [\frac{\omega^2}{c^2(z)} - k_{rm}^2]\Psi_m(z) = 0, \tag{2.8}$$

with k_{rm}^2 denoting the separation constant

$$k_{rm}^2 = \frac{1}{\Phi_m(r)}[\frac{1}{r}\frac{d}{dr}(r\frac{d\Psi_m}{dr})], \tag{2.9}$$

and Ψ_m denotes a particular function Ψ obtained with k_{rm}, and denote the modes which build a complete set. The modal equation (2.8) is to be solved with the appropriate boundary conditions, and since the Ψ_m form a complete set of functions, the acoustic pressure can be represented as

$$p(r, z) = \sum_{m=1}^{\infty} \Phi_m(r)\Psi_m(z). \tag{2.10}$$

Thus the solution yields

$$p(r, z; z_s) \approx \frac{i}{4\rho(z_s)\sqrt{8\pi r}}e^{-i\pi/4}\sum_{m=1}^{\infty}\Psi_m(z_s)\Psi_m(z)\frac{e^{ik_{rm}r}}{\sqrt{k_{rm}}}, \tag{2.11}$$

where z_s is the source depth. In reality the wavenumber spectrum is composed by a continuous and a discrete part, corresponding to *evanescent* and *radiating* spectrum respectively. The solution in (2.11) is obtained under the assumption that the spectrum is composed only by the discrete part. Hence the solution is valid only at ranges greater or equal than several water depths away from the source.

An alternative approximation to the wave equation is the so called "high frequency approximation" that consists in representing the acoustic field by the ray solution. The ray solution of the wave equation is a high frequency approximation, that is useful particularly for deep water problems, where generally only a few rays are significant. Ray tracing is satisfactory if the wave length is much less than the length scales in the problem. For ray tracing Snell's law provides a simple formula for calculating the ray declination angle when the channel is modeled as a stratified medium based on the knowledge of the soundspeed at the interface between two layers. A ray connecting the emitter to the receiver is called an

eigenray. Each eigenray represents an arrival at the receiver characterized by a propagation time called arrival time given as

$$\tau = \int_\Gamma \frac{ds}{c},$$

(2.12)

where Γ is the ray trajectory according to the Snell's law. In reality there are multiple eigenrays connecting the source to a receiver each with a different trajectory which means that the propagation media between the emitter and the receiver is multipath, with the impulse response

$$h(t) = \sum_{r=1}^{\mathcal{T}} a_r \delta(t - \tau_r)$$

(2.13)

where $\mathcal{T}$ is the number of arrivals hitting the receiver, τ_r is the arrival time, and a_r is the amplitude associated to the rth arrival.

Ray solutions can be rapidly computed, are highly intuitive and easily visualized. However, diffraction effects and other low frequency behavior are not included, leading to a somewhat coarse accuracy. On the other hand, the main advantage of the normal mode method is the capability to provide highly accurate fields at reasonable computation times and at low frequencies. Since MFP is mostly applied at low frequencies in shallow water, the ray solution is rarely used. In shallow water many significant rays arrive to the receiver, whereas the modes are only a few, which further implies that mode models are preferable to ray tracing models.

2.3   Range dependent environments

In real ocean acoustic applications it is often a good approximation to consider that environmental parameters such as sound-speed profile, water depth and bottom properties are invariant with range. *Range-independence* can only be a simplification of the physical model

for the problem at hand since there will always be some degree of *range-dependence*. Common examples of range-dependence are variations in the bathymetry between emitter and receiver, or variations in the water-column soundspeed caused by e.g. ocean fronts or internal tides. Oceanographic features are also variable in time and require *in situ* measurements to be characterized. This can be done, for example, using satellite images. Range-dependence linked to the bathymetry is easier to handle since it does not evolve with time and accurate description on the bathymetry can be obtained *a priori*. Figure 2.2 shows two bathymetry maps: one corresponds to the area where the INTIFANTE'00 and the MREA'04 sea trials took place which is off the Portuguese West coast near Setúbal (Figure 2.2(a))[49, 51]; and the other corresponds to the area where the MREA'03 sea trial took place, which is the North Elba Island area (Figure 2.2(b))[50]. All these experiments provided field data propagated along tracks with range-dependent bathymetry, which throughout the present work will allow for demonstrating that dealing with range-dependent environments is now a reality in MFP based applications. One decade ago it was not possible to perform acoustic inversions in reasonable computation times for mild range-dependence, although acoustic propagation models able to solve the forward problem for such scenarios were already available. Nowadays this is routine. The ever decreasing price of CPU power enables a small laboratory or a small department to construct its own computer cluster, such that it is possible to process a complete data set within a day, even if range-dependent features are present.

The propagation model used in this thesis is the C-SNAP range-dependent normal modes propagation model with mode coupling [52]. If the environment is range-independent then C-SNAP implements an approximation of equation (2.11) using the M largest-order discrete modes of the problem. The numerical method employed to find the mode amplitudes is
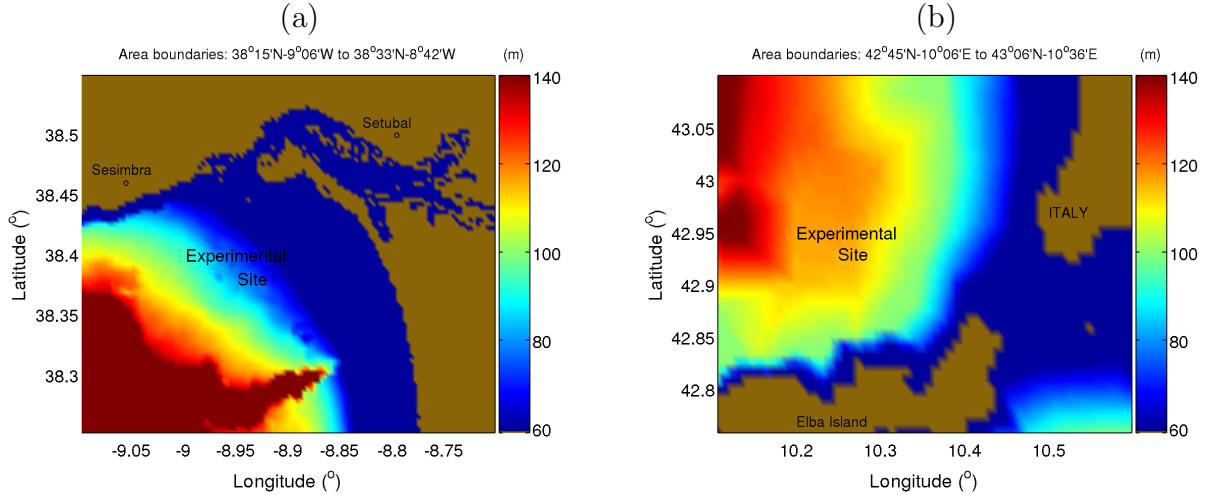
Figure 2.2: Bathymetry maps corresponding to the experimental sites of the: INTIFANTE'00 and MREA'04 sea trials (a); MREA'03 (b).

based on a widely used finite difference algorithm in combination with an inverse iteration technique. If the environment is range-dependent then C-SNAP computes the pressure field as follows: first, it divides the environment into a sequence of range-independent segments, with sloping bottoms treated by the staircase approximation. Environmental properties for the various range subdivisions are obtained through a linear interpolation in range between adjacent profile inputs. Then, the normal modes, the eigenvalues and the pressure field are computed as in the range-independent case until the interface to the next segment is reached. Third, the mode set pertaining to the next segment is computed and the pressure field to the left of the interface is projected onto the new mode set (mode coupling). The resulting mode coefficients are used to carry on the computation of the pressure field in the new segment. This procedure is repeated for each new segment.

Note that eq. (2.11) is the pressure field in the frequency domain. In the case of broadband signals the Helmholtz equation is solved for each frequency. Note also that the mode-functions $\Psi_m(z)$ and the wavenumbers k_{rm} are independent of geometric parameters such as source range and depth, and depend only on the environmental parameters. In

range-independent environments, this allows for the implementation of computationally efficient range-depth source localization algorithms, by pre-calculating the mode-functions and wavenumbers, and then calculating the field replicas for each hypothetical source position in the search region. In inverse problems where environmental parameters are to be estimated, a new set of mode-functions and wavenumbers has to be calculated for each hypothetical parameter set.

2.4   On environmental focalization

The estimation of the position in range and depth of a sound source by matched-field processing of a vertical array involves the generation of a replica field by an acoustic propagation model with specified environmental conditions. Such replica field is then used in the processing of the field received by the array. In this way environmental information is included in the processing scheme. The amount and the accuracy of the information available on the environment is a serious problem to deal with in MFP [53, 54, 55, 56, 57]. The propagation model that solves the Helmholtz equation is fed with given environmental parameters. If the replica is correctly constructed, i.e., if the environmental information is correct, then the maximum of the ambiguity surface will, in principle, appear at the correct source location. Otherwise the quality of the ambiguity function will degrade and its maximum will eventually be at a wrong position. Collecting accurate environmental knowledge is not always possible: for example, seafloor properties in shallow water are often characterized by strong variability, and the employment of seismic surveying and coring for exploring extensive areas is, in general, a very expensive and time consuming task, besides offering poor spatial coverage. Another issue is time coherence of the environment. For example, if a source is to be

located along time, or a moving source is to be tracked, important changes in the hydrology
may occur over time and space. This kind of error have been referred as *model mismatch*
[58]. Model mismatch also occurs when there is uncertainty in the measurement geometry
such as array receiver position [59, 53, 60].

To mitigate model mismatch, the focalization processor [17] and the uncertain OFUP
processors [61] emerged in the last 15 years - the latter with lower degree of success. Collins
et al. have demonstrated that it is possible to overcome mismatch and accurately estimate
source location with limited *a priori* environmental information by expanding the parameter
search space of MFP to include environmental parameters. Focalization has the primary
goal of determining source location and perhaps the secondary goal of determining effective
ocean acoustic parameters. The implementation of this technique was possible thanks to
the simultaneous emergence of efficient computational algorithms such as genetic algorithms
(GA) and simulated annealing (SA). The reason is that a linear growth of the number of
parameters implies an exponential growth of the size of the search space.

Environmental focalization provides a powerful solution for the lack of accurate mea-
sures of the environmental parameters, and to overcome mismatch to allow proper source
localization. This technique clearly allowed enhancing source localization since little success
on source localization with real data was achieved before it was employed [62, 63, 55, 64].
The only successful shallow water continuous source localization results with real data were
reported by Jesus [65]. Since then, there has been a number of papers reporting on successful
source localization results [13, 66, 67, 68, 69, 70]. Soares *et al.* [68, 71, 72] have shown with
experimental data collected in well controlled experimental conditions that the impact of
environmental mismatch can vary with range and frequency. It was also demonstrated how

effective focalization for source localization can be at frequencies up to 1500 Hz and source ranges up to 10 km.

The equivalent model concept

A physical model is generally a simplified representation of the reality, while focalization is employed to determine the most suitable model for the real environmental conditions. For example, in the past very few studies have made assumptions of range-dependence. In fact, a range-independent environment does not exist in practice, but in most cases it is not viable modeling existing range-dependent features. The concept of *equivalent model* allows for simplification of the modeling process by the use of an environmental model that has an alternative set of parameters while giving a similar acoustic response. In practice, errors made in one or more parameters will be compensated by errors made in the other parameters. The existence of an equivalent model is intimately linked to field ambiguity, which in turn strongly relates to field complexity. There are at least two issues arising the ambiguity problem: one is intrinsic to the physical conditions and can be seen in terms of the number of modes effectively comprising the acoustic field, which rules the complexity of the acoustic field and its uniqueness. The other issue is related to the degree of spatial sampling employed. An insufficient sampling of higher-order modes will result in a drawback in the degree of uniqueness of the acoustic field.

The *equivalent model* concept is useful specially when the parameter hierarchy is fortunate [17]. Parameter hierarchy is the relative sensitivity of the acoustic field to the variation of a given parameter. The source location parameters tend to be on the top of the hierarchy. When the main goal of the focalization process is source localization then this hierarchy is fortunate, since it is possible to accurately determine source location even if the model used

is a simplified representation of the reality, provided that a valid equivalent model exists. However, focalization can be employed with the goal of estimating environmental parameters, with known source location or not. In that case the parameter hierarchy can possibly come out of favor, i.e., the parameters of interest are not at the top of the parameter hierarchy, and the concept of equivalent model becomes uninteresting, meaning that high-ranking parameters must be accurately known or must be estimated together with the parameters of interest. Moreover, the the likelihood of ambiguous solutions increase with the dimension of the parameter space. It might be essential to employ high-resolution methods to perform focalization, since these methods have increased capability of suppressing ambiguous solutions. High-resolution methods have been credited as being extremely sensitive to environmental mismatch, and in fact very few studies with experimental data have employed high-resolution methods such as minimum-variance or subspace methods.

2.5   Inverse Problems and Global Optimization using Genetic Algorithms

Determining the range and depth location of an acoustic source in a waveguide from the acoustic field measured on a vertical array of sensors can be seen as an inverse problem. The same applies when estimating the environmental parameters of a waveguide from the receiver acoustic field. Inverse problems are common to many areas of physics and functional analysis.

In general, the solution can not be obtained directly. The inverse problem is usually posed as a nonlinear optimization problem. The formulation of the problem follows by assuming a discrete forward model parameter vector of unknown parameters with a bounded range of possible values for each parameter. The candidate parameter vectors are used to generate

field replicas, which are then compared to the acoustic field by means of an objective function. As a generic concept, inverse problems can be classified as well behaved or ill-conditioned. In the present case the derivation of the acoustic field in given environmental and generic conditions is non-linear and non-analytical, moreover, since the received field is contaminated with noise there is no guaranty of uniqueness.

For such an ill-conditioned inverse problem, the corresponding multi-dimensional objective function may exhibit several maxima where the highest may not correspond to the true solution due to several reasons such as model mismatch and noise. In the last two decades a number of techniques have been proposed in the literature to cope with such optimization problems [48]. Among these techniques, Genetic Algorithm (GA) is a class of stochastic methods that have the following characteristics:

- allow for global optimization;

- asymptotically converge to the true solution.

The GA is an optimization method based on principles of biological evolution of individuals [73]. An individual is a collection of bit chains that represents one of the possible parameter vectors, and a population is a set of individuals that evolves through time as generations. A generation is an iteration in which the fitness of each individual is computed by the so-called objective function. The fitness represents the "quality" of an individual. The probability of an individual to be included into the next generation depends on its fitness, i.e. individuals with higher fitness are more likely to survive. Two probabilistic operators are applied to the individuals: the crossover operator and the mutation operator. The crossover operator joins individuals into pairs without considering their fitness, and a given number of bits is exchanged with a given probability. The mutation operator inverts every bit with

a given probability. This operator is important to avoid the loss of individuals' diversity. The loss of diversity in a population can lead to convergence to local extrema. Therefore the mutation probability should be set high enough to keep the search algorithm being able to escape from local maxima but low enough to not slowdown convergence to the global extremum - basically it is a compromise between speed and accuracy. At the beginning a random population of all possible vectors is selected. The fitness of each individual is computed. The operators crossover and mutation are applied to get a new population - the children. The fitness is improved from generation to generation through evolutionary mechanisms. An evolutionary step consists of selection of individuals based on individuals' fitness.

The GA should in principle be able to reach the maximum by sampling a very small number of points of the objective function. However, there are at least two characteristics that cause major difficulties to global search methods. One, intimately related to the ambiguity when a high number of unknowns enter the search space, is the *multi-modality*. Most optimization problems in the real world are multi-modal, which means that they have many local sub-optima. Such sub-optima might be close to the same level. In that case the search is difficult due to the presence of false attractors. When the number of local sub-optima is high, then it is said that the so-called *fitness landscape* is massively multi-modal. This characteristic causes difficulties to any search algorithm. The opposite problem is *isolation*. A problem with such characteristic is the "needle in the haystack" problem, where a global optima (needle) exists somewhere in the search space (haystack), which consists of solutions all with similar fitness and much less than that of the solution. There is no information available such that the search could proceed in some direction. In that way any meta-heuristic

(a)   (b)
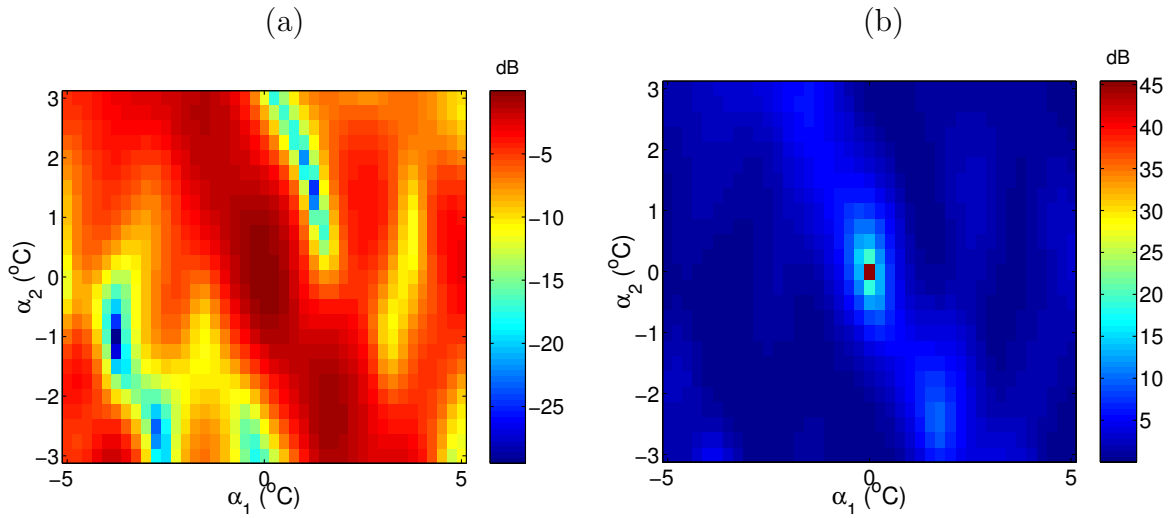
Figure 2.3: Factors of difficulty for a global search algorithm: Multi-modality (a); isolation (b).

has the same performance as a simple random search, where solutions are randomly taken from the search space without following any heuristic rule. In figure 2.3 are shown two plots representing cost-functions with the goal of estimating the EOF coefficients α_1 and α_2 of the expansion in eq. (2.4). The parameter vector $[\alpha_1 \alpha_2]^T$ was $[0\ 0]^T$, and the data was generated with a SNR of 39 dB using three receivers and three frequencies. The cost-function in figure 2.3(a) is the broadband coherent Bartlett processor (developed in chapter 4). It is an extremely multi-modal function where the sidelobes are at a level close to that of the maximum. Many sidelobes are only 1 or 2 dB below the maximum. The colorbar scalar is about 30 dB wide. Figure 2.3(b) is the opposite case represented by an example of the application of the coherent broadband MUSIC processor (developed in chapter 4) where the maximum is clearly isolated. Note that the colorbar scale is 45 dB wide.

2.6   Summary

This chapter reviewed several basic concepts that will be used throughout the following chapters. The topics treated herein were:

- The relation of the sound-speed with temperature, salinity, and depth.

- Empirical Orthogonal Functions (EOF) as an efficient mean to represent temperature or sound-speed profiles.

- Normal modes and ray models; discussion of their applicability in real world problems.

- Range-dependent propagation media, and discussion on the applicability of range-dependent assumptions; normal modes propagation model in range-dependent propagation media.

- Introduction to common concepts and difficulties encountered in focalization; discussion of its applicability for the estimation of environmental parameters.

- The inverse problem as an optimization problem; global optimization by means of genetic algorithms; common difficulties found.

Chapter 3

The Data Model

The Green's function in (2.11), the solution of the Helmholtz equation, forms the basis for representing the signals used in MFP based processing techniques. The derivation of a processor relies on a data model that incorporates the Green's function representing the media response and statistical assumptions made on signal and noise components. In other words, the received signals are characterized as time, space, and frequency processes with certain statistical assumptions.

MFP techniques were initially applied in a narrowband fashion to deep water problems [54]. However, as the interest of the underwater acoustic community shifted towards shallow-water scenarios, it was soon recognized that the complex interaction of the sound with the sea bottom boundary, which frequently is inaccurately known, presented an additional challenge to the estimation problem (source localization). In an effort to increase the robustness of MFP techniques to bottom modeling inaccuracy, broadband MFP has been employed by using multiple frequency information. Using multiple frequencies can be regarded as a mean for obtaining increased amount of information from the acoustic field.

The simplifications in the acoustic system being considered in the present thesis represent the loss of capability in earning information in the form of acoustic data, either by using

receiving systems with a reduced number of receiver elements, or by using an uncontrolled source possibly emitting a reduced number of spectral components with sufficient SNR.

As an effort to compensate that loss of information, the present chapter proposes a broadband data model formally contemplating a source radiating multiple frequencies, i.e., a broadband source, with the objective of making an efficient use of the spectral components considered. This allows for explicitly incorporating the relationships of the acoustic signal and noise across frequency in the form of second order statistics. The exploitation of spatial coherence of the acoustic field, a key factor in MFP techniques, can eventually be extended to the exploitation of the spectral coherence of the acoustic field.

The development of the broadband data model includes a discussion on the parameterization of the propagation channel in the context of acoustic tomography, on signal models and how this model handles time variability of the acoustic channel parameters, and on noise models. The model is then expressed in terms of second-order statistics. Another issue on the data model is the subspace view, where possible solutions of the eigen-problem for different assumptions on the signal component are hypothesized. Finally, Cramer-Rao Lower Bounds on the proposed broadband data model are calculated.

3.1   The convolution equation

Throughout this study, only the case of a single source and a single vertical line array (VLA) will be considered. Thus, one can define the horizontal range of the emitting source to the VLA as R_s, and the source depth as Z_s, with the subscript s standing for *source*. The VLA consists of L receivers, positioned at depths Z_l, with $l = 1, 2, \ldots, L$, denoting receiver index. Source range and source depth can be included into vector $\underline{\theta}_s$ denoting the source location

in the 2-dimensional plane.

A waveform $s(t)$ emitted by a single source, exciting a horizontally stratified waveguide, is received by a VLA of hydrophones and observed during time T. The propagation channel connecting the source at depth Z_s to a receiver at depth Z_l and range R_s is represented by its impulse response $h(t, \underline{\theta}_s, Z_l, \underline{\Theta})$, where $\underline{\Theta}$ is a generic parameter vector characterizing the propagation channel. The array impulse response can be represented by a vector

$$\underline{h}(t, \underline{Z}, \underline{\theta}_s, \underline{\Theta}) = [h(t, Z_1, \underline{\theta}_s, \underline{\Theta}) \cdots h(t, Z_l, \underline{\theta}_s, \underline{\Theta}) \cdots h(t, Z_L, \underline{\theta}_s, \underline{\Theta})]^T. \tag{3.1}$$

The channel is assumed linear, causal, and time invariant. Thus, the signals received at the VLA are given by the convolution equation

$$\underline{y}(t) = \int_0^\infty \underline{h}(t - \tau)s(\tau)d\tau + \underline{n}(t), \tag{3.2}$$

where $\underline{h}(t) = \underline{h}(t, \underline{Z}, \underline{\theta}_s, \underline{\Theta})$, and $\underline{n}(t)$ is additive zero-mean Gaussian noise. This is the theoretical view of the system representation of the waveguide.

3.2 Frequency-domain snapshot model

In several applications, parameter estimation techniques are implemented in the frequency domain. The snapshot model aims at dividing the total observation time T into N disjoint intervals of length ΔT. These intervals are n-indexed:

$$n = 1 \quad 0 \leq t < \Delta T$$

$$n = 2 \quad \Delta T \leq t < 2\Delta T$$

$$\vdots$$

$$n = n \quad (n-1)\Delta T \leq t < n\Delta T$$

$$\vdots$$

$$n \;\; = \;\; N \quad (N-1)\Delta T \leq t < N\Delta T, \tag{3.3}$$

and serve to generate a set of space-frequency complex vectors by Fourier transforming the data corresponding to the time intervals above. Such complex vectors are usually referred as *frequency-domain snapshots* [74].

As part of the development it is necessary to establish the criteria for choosing ΔT which is directly related to the impulse responses across the array. The impulse response connecting the acoustic source to the lth receiver, can be represented as a sum of Dirac functions with delays τ_r and amplitudes a_r:

$$h(t, Z_l, \underline{\theta}_s, \underline{\Theta}) = \sum_{r=1}^{\mathcal{T}} a_r \delta(t - \tau_r) \tag{3.4}$$

where $\mathcal{T}$ is the number of arrivals or so-called eigenrays hitting the lth receiver, and $\tau_1 \leq \ldots \leq \tau_r \leq \ldots \leq \tau_{\mathcal{T}}$. This representation of the impulse response is often seen as a transient response since for the emission of an impulse $s(t) = \delta(t)$, the lth receiver will sense energy only during the time interval between τ_1 and $\tau_{\mathcal{T}}$. In general the signal component received at the lth receiver will be given as

$$x(t, Z_l) \;\; = \;\; h(t, Z_l, \underline{\theta}_s, \underline{\Theta}) * s(t) = \sum_{r=1}^{\mathcal{T}} a_r s(t - \tau_r).$$

The Fourier transform of $x(t, Z_l)$ is

$$X(\omega, Z_l) \;\; = \;\; S(\omega) \sum_{r=1}^{\mathcal{T}} a_r \exp(-j\omega\tau_r) \tag{3.5}$$

$$= \;\; S(\omega) A(\omega, \underline{a}, \underline{\tau}) \exp[j\Phi((\omega, \underline{a}, \underline{\tau})], \tag{3.6}$$

where A and Φ are the polar coordinates of the sum in eq.(3.5). This equation points out the dependence of the frequency response on the a_r and the τ_r, and therefore the representation above will be obtained only if ΔT is long enough to include all delayed versions of the emitted

signal $s(t)$, i.e., all $s(t - \tau_r)$ for $r = 1, \ldots, \mathcal{T}$. Note that the frequency response in eq. (3.6) is a function of the complete set of a_r and τ_r. Thus, if a waveform of length T_s is considered, then

$$\Delta T > \mathsf{T}_s + \tau_\mathcal{T} - \tau_1 \tag{3.7}$$

is the theoretical condition to be accomplished upon the length of the interval to generate a snapshot.

3.3 The narrowband snapshot model

The data model in equation (3.2) assumes a band limitation $\mid \omega \mid < \Omega$. The output of the receivers is sampled at a rate $\omega_s > 2\Omega$, i.e. a sampling period $\Delta_s < \pi/\Omega$. The frequency-domain snapshot model is obtained through the discrete Fourier transform of $\underline{y}(t)$ which is given by

$$\underline{Y}(\omega) = \Delta_s \sum_{i=1}^{I} w_{\Delta_s T}(\Delta_s i) \underline{y}(\Delta i) e^{-j\omega\Delta_s i}, \tag{3.8}$$

where I is the number of samples in the interval ΔT. The window $w_{\Delta T}(t)$ is zero outside the interval $[0, \Delta T]$, and normalized, such that $\int_{-\infty}^{\infty} w_{\Delta T}(t)^2 dt = \Delta T$. Thus, the vector with the received signals can be written in the frequency domain as

$$\underline{Y}(\omega) = \underline{H}(\omega, \underline{Z}, \underline{\theta}_s, \underline{\Theta})S(\omega) + \underline{N}(\omega), \tag{3.9}$$

where the elements in vector $\underline{H}$ are solutions of the Helmholtz equation considering the depths of the L receivers. $S(\omega)$ represents the scalar source waveform, whose assumptions will be made later on. The noise vector $\underline{N}(\omega)$ is Gaussian zero mean.

With the development of methods for acoustic inversion using deterministic signals, it has been observed that repeated emissions at very high SNR resulted in successive receptions suffering rapid changes in short time intervals possibly caused by small scale environmental

perturbations, source and/or receiver motion, and sea surface and bottom roughness, which, partially or all together, contribute to unmodeled fluctuations in the signal part of (3.9). Since such changes cannot be attributed to the noise due to the high SNR, a complex random factor $\alpha(\omega) = a \exp(j\phi)$ can be included such that the data model is written as

$$\underline{Y}(\omega) = \underline{H}(\omega, \underline{Z}, \underline{\theta}_s, \underline{\Theta})S(\omega)\alpha(\omega) + \underline{N}(\omega). \tag{3.10}$$

The noise $\underline{N}(\omega)$ is assumed to be uncorrelated with random factor $\alpha(\omega)$. Note that random factor $\alpha(\omega)$ is space invariant but is assumed to be frequency dependent. For the design of optimal estimators it is useful to assume that it is zero-mean and Gaussian distributed. The distribution of the random factor is discussed in Ref. [75] where estimation of the random factor with real data suggested that the distribution of its amplitude A was approximately Rayleigh but its phase was not uniformly distributed as usually assumed.

In this study, concerning the frequency-domain snapshot model, the chief interest is in the development of the broadband snapshot model, which will represent the signals as an aggregate of frequency components, accounting for their cross-frequency correlations.

3.4   The broadband snapshot model

A broadband data model for the acoustic data received at an L-receiver array can be written as a concatenation of K narrow-band signals

$$
\begin{aligned}
\underline{Y} &= [\underline{Y}^T(\omega_1), \cdots, \underline{Y}^T(\omega_k), \cdots, \underline{Y}^T(\omega_K)]^T \\
&= \mathbf{H}(\underline{Z}, \underline{\theta}_s, \underline{\Theta})\tilde{\underline{S}} + \underline{N}
\end{aligned}
\tag{3.11}
$$

in order to introduce, as much as possible, a common frame for the narrowband and broadband cases [75]. The main objectives are to proceed into a generalization in terms of

frequency band, and to account for the signals' cross-frequency correlations. The matrix $\mathbf{H}(\underline{Z}, \underline{\theta}_s, \underline{\Theta})$ is the channel response matrix given as

$$\mathbf{H}(\underline{Z}, \underline{\theta}_s, \underline{\Theta}) = \begin{bmatrix} \underline{H}(\omega_1, \underline{Z}, \underline{\theta}_s, \underline{\Theta}) & \cdots & \underline{0}_{k-1} & \cdots & \underline{0}_{K-2} \\ \underline{0}_1 & \cdots & \underline{H}(\omega_k, \underline{Z}, \underline{\theta}_s, \underline{\Theta}) & \cdots & \underline{0}_1 \\ \underline{0}_{K-2} & \cdots & \underline{0}_{K-k} & \cdots & \underline{H}(\omega_K, \underline{Z}, \underline{\theta}_s, \underline{\Theta}) \end{bmatrix}, \quad (3.12)$$

where the $\omega_k, k = 1, \ldots, K$ represent the discrete frequencies of interest, and K is the number of frequencies considered. $\underline{0}_k$ is a vector with kL zeros. Note the construction of the channel matrix: it reminds the channel matrix typically used for modeling in classical array processing for multiple emitters. In the present case, each column is relative to a frequency ω_k, however, the channel vectors do not overlap across the columns - they are indeed orthogonal. This construction of the channel matrix accounts for the uncorrelatedness of the Fourier coefficients when the emitted signal is stochastic. The channel matrix has KL rows, and K columns. The vector $\underline{\tilde{S}}$ has entries $S(\omega_k)\alpha(\omega_k)$ i.e., the source spectrum multiplied by the random perturbation factor at each frequency $\omega_k \in [\omega_1, \omega_K]$. The vector $\underline{N}$ represents the noise and has obviously the same notation as $\underline{Y}$ in eq. (3.11).

In the following subsections assumptions on the signal model will be discussed. Assumptions on the degree of knowledge and statistical properties of the propagation channel, emitted waveform, and noise will be worked out with the application scenario in mind.

3.4.1 The propagation channel and its parameterization

The propagation channel is represented by matrix $\mathbf{H}(\underline{Z}, \underline{\theta}_s, \underline{\Theta})$, formed by its frequency components $\underline{H}(\omega_k, \underline{Z}, \underline{\theta}_s, \underline{\Theta})$. The first aspect to be referred is the choice of the parameterization. The receivers' depths vector $\underline{Z}$ and signal emitter's location $\underline{\theta}_s$, that from now on will be called geometric parameters, have been made explicit since these parameters are usually under the experimenter's control in acoustic tomography. Further, this emphasizes that the

experimental setup consists of a vertical receiver array with nominal depths $Z_l, l = 1 \ldots, L$, and a single emitter described by $\underline{\theta}_s$ denoting its position on a range-depth plane. In general, the geometric parameters will be accurately known, and will eventually be taken as unknowns only in the spirit of environmental focalization to allow for the improvement of model fit.

In blind ocean acoustic tomography, the source will be known with reduced accuracy, and will be treated as an unknown. Geometric parameters will be regarded as nuisance parameters, whether they are controlled by the experimenter or not. Finally, the channel is also parameterized by $\underline{\Theta}$ which is a generic vector of parameters that holds virtually any parameter characterizing the propagation channel, independently of the degree of *a priori* knowledge.

Concerning their statistical properties, all parameters described above will be assumed deterministic. This working hypothesis might certainly be unrealistic since the ocean - the propagation channel - is subject to many randomly fluctuating inhomogeneities. However, statistical information on the parameters is usually not available, and the mathematical problem is difficult to address. In the next subsection it will be shown how parameter randomness or variability can be treated in the context of this data model.

3.4.2   Signal component models

The assumptions on the waveform vector of equation (3.11) will be discussed assuming that the channel matrix $\mathbf{H}$ is deterministic although this is not necessarily true in reality. This choice was made in order to allow easier tractability from the mathematical point of view, as it will be seen in the subsequent development.

Each entry in the signal vector $\underline{\tilde{S}}$ has two contributions, which are the emitted waveform $S(\omega_k)$ and the random perturbation $\alpha(\omega_k)$. The signal vector $\underline{\tilde{S}}$ is to be modeled either as a deterministic vector, or as a random vector. In the case of a deterministic signal component the emitted waveform $s(t)$ is deterministic and $\alpha(\omega_k) = 1$. In this case $\underline{\tilde{S}} = \underline{S}$, where the entries of $\underline{S}$ are $S(\omega_k)$. In the case of a random signal component, i.e. when $\underline{\tilde{S}}$ is assumed to be a random vector, two situations should be considered. One is when the emitted waveform $s(t)$ is random: in this case the spectral components $S(\omega_k)$ are random and asymptotically uncorrelated for increasing observation windows. The other situation is when $\alpha(\omega_k)$ is assumed random due to ocean inhomogeneities, in which case $\alpha(\omega_k)$ can be assumed to be zero mean. In matched-field processing it is fundamental to make assumptions on the second-order statistics, which, in the present case, is to make assumptions on $\mathrm{E}[\alpha(\omega_i)\alpha(\omega_j)]$. This rules the degree of spectral coherence of the received signals. The assumption of incoherent spectral components corresponds to $|\mathrm{E}[\alpha(\omega_i)\alpha(\omega_j)]| = 0, i \neq j$, and the assumption of fully coherent spectral components corresponds to $|\mathrm{E}[\alpha(\omega_i)\alpha(\omega_j)]| = 1$. It is interesting to note that in this particular case, if a deterministic waveform s(t) is emitted then the signal matrix

$$\mathbf{C}_{SS} = \mathrm{E}[\underline{\tilde{S}}\,\underline{\tilde{S}}^H] \tag{3.13}$$

$$= \underline{S}\,\underline{S}^H, \tag{3.14}$$

which means that the elements $[\mathbf{C}_{SS}]_{ij}$ are just $S(\omega_i)S(\omega_j)$ and therefore no contributions of the random perturbation factor appear on the final expression of the signal matrix.

This situation may be too optimistic in some cases. Besides the ocean inhomogeneities that may introduce random amplitude and phase perturbations into the acoustic field, the experimental scenarios of the application considered in this thesis consist of a free drifting receiver array and/or towed acoustic source, which means that emitter and receiver positions

may be changing while the acoustic field is being collected. The point is that if the observation time is too long or if the channel parameters are quickly changing, then the assumption of time invariance will eventually be violated. Considering a deterministic waveform, an appropriate data model assuming parameter variations would be

$$\underline{Y}_n = \mathbf{H}(\underline{Z}, \underline{\theta}_s^n, \underline{\Theta}_n)\underline{S} + \underline{N}_n, \tag{3.15}$$

where $\underline{\theta}_s^n$ and $\underline{\Theta}_n$ denote respectively the source location and the environmental parameters for snapshot index n. Depending on the degree of parameter variation, the snapshot dependence will in fact cause the channel to decorrelate during the total observation time, inducing loss of spectral and eventually spatial coherence. This is a relatively complex modeling, since now the data will be a function of an ensemble of $\underline{\theta}_s^n$ and/or $\underline{\Theta}_n$. It is in general impossible to observe all the $\underline{\theta}_s^n$ and $\underline{\Theta}_n$ from the data, neither it would have a practical interest. A reasonable modeling choice to deal with the parameters' variation along time, is to keep the assumption that the channel matrix $\mathbf{H}$ is deterministic while considering an alternative parameter set, and assume a certain degree of spectral incoherence, which is equivalent to assume that $|\mathrm{E}[\alpha(\omega_i)\alpha(\omega_j)]|$ assumes values in the interval $[0; 1]$, whose value depends on ω_i and ω_j. This is equivalent to assuming that small changes in $\underline{\theta}_s$ and $\underline{\Theta}$ can be represented by phase perturbations in the acoustic field that are dependent on frequency but independent on space. The parameter variations will ultimately rule the structure of the signal matrix $\mathbf{C}_{SS}$.

3.4.3 Noise models

The noise component has received considerable attention in the underwater acoustic literature [76, 7] and will be briefly discussed in the context of the broadband data model. Noise

has roughly been classified in three main categories: (1) White noise, also known as sensor noise, is uncorrelated, and has covariance matrix $\sigma_N^2 \mathbf{I}$; (2) Distributed noise, generated for example at the ocean surface, is structured according to the same ocean environment that determines the signal propagation. Since distributed noise is of stochastic nature it is, in principle, realistic to assume that it is uncorrelated across frequency. (3) Discrete noise sources due to human activity or marine animals are structured across space and stochastic components may be assumed uncorrelated across frequencies.

The noise structure is usually not known *a priori* and is typically considered as uncorrelated for that reason. It can eventually be estimated if silence periods exist, and if it is statistically stationary. For the sake of generality, throughout the theoretical development, the noise vector $\underline{N}$ will be assumed $\mathsf{N}(\underline{0}, \sigma_N^2 \mathbf{C}_{NN})$ distributed, whenever appropriate.

3.4.4 The spectral density matrix

Now that different assumptions on signal and noise components have been made one can express the respective spectral density matrix (SDM) models. One of the conclusions of section 3.4.2 is that the choice of the data model relies largely on the choice of a model for the signal matrix $\mathbf{C}_{SS}$. This section will express models for the SDM following strictly the cases hypothesized in section 3.4.2. First, let

$$
\begin{aligned}
\mathbf{C}_{YY} &= \mathrm{E}[\underline{Y}\,\underline{Y}^H] \\
&= \mathbf{H}\mathrm{E}[\underline{\tilde{S}}\,\underline{\tilde{S}}^H]\mathbf{H}^H + \mathrm{E}[\underline{N}\,\underline{N}^H] \\
&= \mathbf{H}\mathbf{C}_{SS}\mathbf{H}^H + \sigma_N^2 \mathbf{C}_{NN} \\
&= \mathbf{C}_{XX} + \sigma_N^2 \mathbf{C}_{NN}
\end{aligned}
\tag{3.16}
$$

be a generic definition of the SDM for $\underline{Y}$ defined in (3.11). The dimensions of the SDM $\mathbf{C}_{YY}$

are $KL \times KL$ consisting of $L \times L$ cross-frequency SDMs

$$\mathbf{C}_{YY}(\omega_{k_1}, \omega_{k_2}) = \mathrm{E}[\underline{Y}(\omega_{k_1})\, \underline{Y}^H(\omega_{k_2})], \quad k_1, k_2 = 1, \ldots, K. \tag{3.17}$$

The signal-to-noise ratio of each $\mathbf{C}_{YY}(\omega_{k_1}, \omega_{k_2})$ matrix block will obviously depend on the

element $[C_{SS}]_{k_1 k_2}$ and on $\mathbf{C}_{NN}(\omega_{k_1}, \omega_{k_2})$. The deterministic signal assumption discussed in

section 3.4.2 represents fully coherent signal receptions and its correlation matrix is given

as $\mathbf{C}_{SS} = \underline{S}\,\underline{S}^H$, which is of rank equal 1. On the other hand, if the emitted waveform is a

random signal, then

$$\mathbf{C}_{SS} = \mathrm{diag}[\sigma_S^2(\omega_1), \cdots, \sigma_S^2(\omega_k), \cdots, \sigma_S^2(\omega_K)], \tag{3.18}$$

where $\sigma_S^2(\omega_k) = \mathrm{E}[\alpha^*(\omega_k)\alpha(\omega_k)S^*(\omega_k)S(\omega_k)]$. In that case the rank of the signal matrix

is equal K. Note that for this case the SDM $\mathbf{C}_{YY}$ consists only of block matrices in the

diagonal. The intermediate case is represented by the last case discussed in section 3.4.2,

where the rank of the signal matrix can vary between 1 and K, representing partial frequency

cross-correlation. This model is the most generic in the framework of a full broadband data

model.

At this point, the sample SDM used for experimental data can be written as

$$\hat{\mathbf{C}}_{YY} = \frac{1}{N} \sum_{n=1}^{N} \underline{Y}_n \underline{Y}_n^H, \tag{3.19}$$

where $\underline{Y}_n$ is the nth realization of $\underline{Y}$.

Finally, note that for $k_1 \neq k_2$ the cross-frequency noise SDMs are assumed to be $\mathbf{0}$ if the

noise is random at the source, which can be applied to any of the noise categories mentioned

in section 3.4.3, or if it is spectrally incoherent, which is more applicable to discrete noise

sources.

3.4.5 The subspace approach

The broadband data model has been discussed in subsection 3.4.2 in the context of system variability and ocean inhomogeneities. This subject rises the question of the dimensionality of the signal subspace. Historically the subspace approach has been reported in the framework of classical beamforming and detection of emitters. The present case consists of a single emitter radiating at several frequencies. In general the SDM defined in 3.16 can be expressed in terms of the eigendecomposition

$$\mathbf{C}_{YY} = \mathbf{U}_S \mathbf{\Lambda}_S \mathbf{U}_S^H + \sigma_N^2 \mathbf{U}_N \mathbf{U}_N^H \tag{3.20}$$

where the data space is separated into signal and noise eigenspaces. This is an ordinary eigen-factorization with the fact that the eigenvalues and eigenvectors appear separated, with the subscripts $_S$ and $_N$ respectively denoting signal subspace and noise subspace.

In the current section, the idea is to characterize the signal subspace for the different assumptions on the data model, i.e., explicit solutions for $\mathbf{U}_S$ and $\mathbf{\Lambda}_S$. In other words, the goal is to hypothesize the solution of the eigen-problem of the SDM $\mathbf{C}_{YY}$, in particular, for the eigenvalues greater than σ_N^2 - those spanning the signal subspace.

For the deterministic signal model it can be noted that

$$\mathbf{C}_{YY} \frac{\mathbf{H}(\underline{\theta}_0)\underline{S}}{||\mathbf{H}\underline{\theta}_0)\underline{S}||} = [\underline{S}^H \mathbf{H}^H(\underline{\theta}_0)\mathbf{H}(\underline{\theta}_0)\underline{S} + \sigma_N^2] \frac{\mathbf{H}(\underline{\theta}_0)\underline{S}}{||\mathbf{H}\underline{\theta}_0)\underline{S}||} \tag{3.21}$$

which is to say that $\frac{\mathbf{H}(\underline{\theta}_0)\underline{S}}{||\mathbf{H}\underline{\theta}_0)\underline{S}||}$ is an eigenvector (the first eigenvector) of $\mathbf{C}_{YY}$, associated with eigenvalue $\underline{S}^H \mathbf{H}^H(\underline{\theta}_0)\mathbf{H}(\underline{\theta}_0)\underline{S} + \sigma_N^2$. This is in fact the only eigenvalue greater than σ_N^2 which means that the signal subspace has dimension equal 1.

Conversely, for the model of uncorrelated frequencies, where the SDM has K $L \times L$ blocks in the diagonal, and therefore $\mathbf{C}_{SS}$ is diagonal (see equation (3.18)), the signal subspace will

be spanned by vectors

$$[\underline{0}^T \cdots \underline{0}^T \; \frac{\underline{H}^T(\underline{\theta}_0, \omega_k)}{||\underline{H}(\underline{\theta}_0, \omega_k)||} \; \underline{0}^T \cdots \underline{0}^T]^T, \tag{3.22}$$

respectively associated with eigenvalues $\sigma_S^2(\omega_k)||\underline{H}(\underline{\theta}_0, \omega_k)||^2 + \sigma_N^2$. Unlike classical array processing for direction-of-arrival estimation, in the case of uncorrelated emitters, the eigenvectors can be explicited using the columns of the channel matrix. This is due to the separation of the spectral components when the Fourier transform is performed, leading to the orthogonality of the columns of the channel matrix. In this case the signal subspace dimension is equal to the number of frequencies K, which is the maximum dimension that this data model can handle.

The case for a generic signal matrix is more difficult to handle mathematically since, in that case, $\mathbf{C}_{SS}$ has a rank varying between 1 and K. Anyway, one can say that the generic span of the signal subspace is given by the columns of

$$\frac{\mathbf{H}(\underline{\theta}_0)\mathbf{C}_{SS}^{\frac{1}{2}}}{\sqrt{\text{tr}[\mathbf{H}(\underline{\theta}_0)\mathbf{C}_{SS}\mathbf{H}^H(\underline{\theta}_0)]}}. \tag{3.23}$$

Here it should be noted that the dimension of the signal subspace is equal the rank of $\mathbf{C}_{SS}$.

The solutions of the eigenproblem of the SDM obtained in this section will be used later on for formulating subspace based methods.

3.5   The Cramer-Rao Lower Bound

Understanding the potential performance of parameter estimation techniques is very useful in practice [74, 77]. Commonly the accuracy is posed in terms of local errors, which, in general, makes sense when the signal-to-noise ratio is sufficiently high in order to identify the global maximum. The estimation accuracy would be best expressed in terms of mean-square errors (MSE), but this is often difficult or impossible to workout analytically.

In such cases, it is possible at least to place lower bounds on the performance of an estimator, provided that certain regularity conditions are satisfied. There are a few such bounds in the literature, where the most extensively employed is the Cramer-Rao Lower Bound (CRLB). This bound provides the lower bound on the variance of any unbiased estimator by exploring the underlying probability density function (PDF) for that data, which is indeed very intuitive: the CRLB is, in fact, a measure of the PDF's *sharpness*, which, in turn reflects the degree of dependence of the data on a given parameter, and determines how accurately the parameter can be estimated. Besides providing a lower bound on the variance of any unbiased estimator, it allows, at best, to assert that an estimator is the minimum-variance unbiased estimator, which will be the case if the estimator attains the bound for all values of the unknown parameter.

In the following the CRLB for estimators of $\underline{S}$ and $\underline{\theta}_0$ under the proposed broadband data model will be derived. The subsequent development will explore the Cramer-Rao Lower Bound theorem (see Appendix A), which states the possibility of finding an estimator for the given unknown, and places a lower bound on any unbiased estimator, both for signal estimation or for parameter estimation.

3.5.1 The CRLB of a deterministic signal estimator

The likelihood function for the deterministic signal component and uncorrelated noise with variance σ_N^2 is given as

$$p(\underline{Y};\underline{S}) = \frac{1}{\sqrt{2\pi}(\sigma_N^2)^{KL}} \exp\left\{-\frac{1}{2\sigma_N^2}[\underline{Y} - \mathbf{H}(\underline{\theta}_0)\underline{S}]^H[\underline{Y} - \mathbf{H}(\underline{\theta}_0)\underline{S}]\right\}, \qquad (3.24)$$

which considers a single snapshot. The first step will always be to check the regularity condition stated in the CRLB theorem. The first derivative of the log-likelihood function is

computed with respect to the signal vector $\underline{S}$:

$$\frac{\partial \ln p(\underline{Y}; \underline{S})}{\partial \underline{S}} = \frac{1}{2\sigma_N^2} \frac{\partial}{\partial \underline{S}} \{ [\underline{Y} - \mathbf{H}(\underline{\theta}_0)\underline{S}]^H [\underline{Y} - \mathbf{H}(\underline{\theta}_0)\underline{S}] \} \tag{3.25}$$

$$= \frac{1}{\sigma_N^2} \mathbf{H}^H(\underline{\theta}_0)[\underline{Y} - \mathbf{H}(\underline{\theta}_0)\underline{S}]. \tag{3.26}$$

It can be easily seen that the mathematical expectancy of (3.26) equals zero for any value of $\underline{S}$. Thus, regularity condition of the CRLB theorem is verified. The second derivative of the log-likelihood function with respect to the signal vector is given as

$$\frac{\partial^2 \ln p(\underline{Y}; \underline{S})}{\partial \underline{S} \partial \underline{S}^H} = \frac{\mathbf{H}^H(\underline{\theta}_0))\mathbf{H}(\underline{\theta}_0))}{\sigma_N^2}, \tag{3.27}$$

which is the so-called Fisher matrix. Since the regularity condition has been satisfied, then any unbiased estimator $\hat{\underline{S}}$ will satisfy the condition

$$\mathbf{K}_{\hat{S}\hat{S}} \geq \sigma_N^2 [\mathbf{H}^H(\underline{\theta}_0))\mathbf{H}(\underline{\theta}_0))]^{-1}, \tag{3.28}$$

which places a lower bound on the covariance matrix $\mathbf{K}_{\hat{S}\hat{S}}$. This condition is indeed very intuitive since it clearly means that the CRLB reflects the actual SNR imposed by the channel gain and the noise power.

As referred above the CRLB theorem also serves the purpose of finding an unbiased estimator. If the first derivative with respect to the signal vector can be written in the form

$$\frac{\partial \ln p(\underline{Y}; \underline{S})}{\partial \underline{S}} = \mathbf{J}(\underline{S})[\underline{g}(\underline{Y}) - \underline{S}] \tag{3.29}$$

for some function $\mathbf{J}$ and $\underline{g}$, then $\hat{\underline{S}} = g(\underline{Y})$ is the minimum-variance unbiased estimator. In fact,

$$\frac{\partial \ln p(\underline{Y}; \underline{S})}{\partial \underline{S}} = \frac{1}{\sigma_N^2} [\mathbf{H}^H(\underline{\theta}_0)\mathbf{H}(\underline{\theta}_0)][\mathbf{H}^+(\underline{\theta}_0)\underline{Y} - \underline{S}], \tag{3.30}$$

which allows to assign $\mathbf{J}(\underline{S}) = \frac{1}{\sigma_N^2}[\mathbf{H}^H(\underline{\theta}_0)\mathbf{H}(\underline{\theta}_0)]$ and $\underline{g}(\underline{Y}) = \mathbf{H}^+(\underline{\theta}_0)\underline{Y}$, with $\mathbf{H}^+$ denoting the pseudo-inverse of matrix $\mathbf{H}$. Note that matrix $\mathbf{J}$ is coincident with the second derivative

in (3.28). Furthermore, a minimum-variance unbiased (MVU) estimator of $\underline{S}$ has been found, $\hat{\underline{S}} = g(\underline{Y})$, which is the best scenario stated by the CRLB theorem.

3.5.2 The CRLB for an estimate of a deterministic parameter

This subsection aims at placing a lower bound on the variance of an estimate $\hat{\theta}_0$ using the generic data model in (3.16). Note that for this data model the rank of the K-frequencies signal matrix $\mathbf{C}_{SS}$ can vary between 1 and K. This rises the question on how does the randomness of signals and propagation channel impact the performance of an estimator of a parameter $\hat{\underline{\theta}}_0$. Thus, a random zero mean signal vector is assumed, and the likelihood function is

$$p(\underline{Y}; \underline{\theta}_0) = \frac{1}{\sqrt{2\pi} \det \mathbf{C}_{YY}} \exp\{-\underline{Y}^H \mathbf{C}_{YY}^{-1} \underline{Y}\}. \tag{3.31}$$

For the sake of simplicity and with no loss of generality the development will be carried out for the ith element of $\underline{\theta}_0$, θ_i. The partial derivative with respect to θ_i is

$$\frac{\partial \ln p(\underline{Y}, \underline{\theta})}{\partial \theta_i} = -\text{tr}[\mathbf{C}_{YY}^{-1} \frac{\partial \mathbf{C}_{YY}}{\partial \theta_i}] + \text{tr}[\underline{Y}^H \mathbf{C}_{YY}^{-1} \frac{\partial \mathbf{C}_{YY}}{\partial \theta_i} \mathbf{C}_{YY}^{-1} \underline{Y}]. \tag{3.32}$$

The regularity condition is verified, but for the current case it is straightforward that the MVU estimator for θ_i cannot be found using the CRLB theorem. Thus, it remains to find the CRLB for any MVU estimator of θ_i. The second derivative with respect to θ_j is given as

$$\frac{\partial^2 \ln p(\underline{Y}, \underline{\theta})}{\partial \theta_i \partial \theta_j} = -\text{tr}[\mathbf{C}_{YY}^{-1} \frac{\partial \mathbf{C}_{YY}}{\partial \theta_i} \mathbf{C}_{YY}^{-1} \frac{\partial \mathbf{C}_{YY}}{\partial \theta_j} + \mathbf{C}_{YY}^{-1} \frac{\partial^2 \mathbf{C}_{YY}}{\partial \theta_i \partial \theta_j}] - \text{tr}[\underline{Y}^H \mathbf{C}_{YY}^{-1} \frac{\partial^2 \mathbf{C}_{YY}}{\partial \theta_i \partial \theta_j} \mathbf{C}_{YY}^{-1} \underline{Y}],$$
$$\tag{3.33}$$

whose mathematical expectancy results in the Fisher information matrix with elements

$$[\mathbf{J}(\theta_0)]_{ij} = \text{tr}[\mathbf{C}_{YY}^{-1} \frac{\partial \mathbf{C}_{YY}}{\partial \theta_i} \mathbf{C}_{YY}^{-1} \frac{\partial \mathbf{C}_{YY}}{\partial \theta_j}]. \tag{3.34}$$

Any estimator of the parameter vector $\underline{\theta}_0$ will satisfy the condition

$$\mathbf{K}_{\hat{\theta}_0 \hat{\theta}_0} \geq \mathbf{J}^{-1}(\underline{\theta}_0), \tag{3.35}$$

where $\mathbf{K}_{\hat{\theta}_0\hat{\theta}_0}$ is the covariance matrix on the parameter vector estimates. This bound states that the accuracy to which $\underline{\theta}_0$ can be estimated depends on the sensitivity of the correlation matrix $\mathbf{C}_{YY}$ on the parameter vector. This is certainly a feature that is intrinsic to the propagation channel and is closely related to the concept of parameter observability. The observability of each parameter varies with several factors such as the environment itself, frequency and experimental setup.

It would be interesting to theoretically compare the CRLB for the incoherent and coherent cases. This is, however, a cumbersome task and will, therefore be carried out with numerical computer simulations. Nevertheless, it can be anticipated, that the CRLB relative to the coherent cases will evolve much faster towards zero with the increase of the number of frequency bins than in the incoherent case. This is due to the much higher number of cross-terms involved in the estimation problem.

3.6   Summary

In this chapter a broadband data model was proposed (section 3.4). This model is based on a matrix consisting of orthogonal columns each one containing the vectors with the acoustic response of the channel at the different frequencies considered, which has been denoted as channel matrix. This model allows for making assumptions on the cross-frequency relations of both received signals and noise in a systematic way. More precisely, the spatial coherence of the acoustic field, a key factor in MFP, can be extended to the frequency domain.

This is based on an important feature of this model, which is the introduction of a random factor in the signal component, called perturbation factor. This perturbation factor is a function only of frequency and independent of space, whose objective is to take into

account unmodeled ocean inhomogeneities and possibly time-variance of the channel acoustic response.

After stating the broadband data model, several aspects are discussed:

- the parameterization of the channel matrix, in the context of ocean tomography, using a source-receiver array pair, which is made dependent on three parameter vectors containing: the receiver depths; the range-depth source location; the parameters of the intervening ocean;

- section 3.4.2 discusses models for the signal component. The signal model depends on assumptions made for the emitted waveform and the random perturbation vector. One interesting aspect discussed is parameter variability. It is suggested that the random perturbation factor can be used also for modeling time-variance since in practice this can be seen as adding phase contributions over the observation time, which can merely be seen as a loss of spectral coherence;

- noise models are suggested in the context of the broadband data model (section 3.4.3). It can be remarked that it is realistic to assume that noise is uncorrelated across frequency for the three noise categories mentioned (electronic noise, surface distributed noise sources, discrete noise sources). i.e., it is realistic to assume noise free cross-frequency blocks in the SDMs. This feature is advantageous in terms of signal-to-noise ratio;

- the SDM on the broadband model is calculated suggesting that the SNR is increased when the signal is coherent across frequencies;

In section 3.4.5 the geometric solutions for the eigen-problem of the spectral density

matrix are hypothesized according to the different statistical assumptions that can be made on the signal component.

Finally, the CRLBs for the estimators of deterministic signals and deterministic channel parameters are obtained. In the case of estimators of deterministic signals the estimation performance directly depends on the channel gain and on the noise power. In this case the CRLB theorem allows for finding a minimum-variance estimator for the emitted signal. In the case of estimators of deterministic channel parameters the estimation performance depends on the sensitivity of the SDM on the parameter.

Chapter 4

Broadband MFP for parameter estimation

The previous chapter has proposed the broadband data model with the main objective of compensating the loss of information resulting from the simplifications in the acoustic system considered in this thesis. This model allows for extending signal coherence to the frequency domain (spectral coherence). In the context of environmental parameter estimation via MF techniques, the exploitation of spectral coherence has been seen as a mean of using extra information contained in the received field.

This chapter makes the state-of-the-art of the *coherent/incoherent processing debate*, and will be dedicated to the derivation of various coherent broadband (BB) processors, based on well known array processing techniques, to be used in matched-field tomography with simplified acoustic systems:

- the BB Bartlett processor;

- the BB minimum-variance processor;

- and the BB MUSIC processor.

Processors of the Bartlett family have been widely used in a variety of problems typically

applying MF based techniques such as source localization, matched-field tomography (MFT), and geoacoustic inversion. The other two processors are considered high-resolution methods and have not been used in MFT and geoacoustic inversion so far. The idea is to adapt these methods to ocean acoustic tomography and geoacoustic inversion in order to take advantage of the increased capability of high-resolution methods in the attenuation of sidelobes, rather than to obtain high-resolution ocean parameter estimates. The main motivation of the application of high-resolution methods is the simplification of acoustic systems used in the collection of field data considered in this thesis, that may contribute for the loss of uniqueness in the problem's solution. High-resolution methods appear to be suitable to cope with this difficulty.

An additional characteristic required is that the proposed coherent BB processors should be able to work under the assumption of unknown emitted waveforms. This is achieved by representing the emitted signal in terms of second order statistics by the signal matrix, which also allows to account for ocean inhomogeneities or parameter variability possibly inducing loss of spectral coherence seen as random features introduced by the channel. Then a subspace based method is used to estimate the signal matrix in order to account for the emitted signal and the random features in the processing.

Finally, useful pre-processing algorithms for enhancing the spectral coherence and possibly the SNR are given.

4.1   Coherent and incoherent matched-field processors: state-of-the-art

One discussion that became almost classical throughout the past decade in the MFP related literature was on how to process the acoustic field in the frequency domain. The question is

whether to process the acoustic field incoherently or coherently. Historically, the processors using only auto-frequencies were called incoherent processors, and those using also cross-frequencies were called coherent processors. In this context, these terms were adopted in order to reflect the need to adjust the replica fields to the emitted signal or not (coherent and incoherent respectively), mainly in order to account for the signal relative phases.

Incoherent processing was first proposed by Baggerorer *et al.* [76], where geometric averaging was found to be effective to reduce sidelobes in a range-depth ambiguity surface. Later Tolstoy[78] suggested the use of a coherent frequency approach under the hypothesis that the signals across frequencies are correlated. The main problem with this class of approaches was the lack of knowledge of the emitted signal spectrum in order to account for the phase relationship across frequency. Michalopoulou *et al.* [20, 79] and Orris [80] suggested algorithms to overcome the lack of knowledge of the emitted signal spectrum. In Ref. [20] it is proposed to scale the data and replica vectors such that they have zero phase on the phone with best signal-to-noise ratio (SNR). A potential problem with this algorithm is that this scaling is dependent on the SNR of a single phone. Later, Orris *et al.* proposed the matched-phase coherent processor that copes with the lack of knowledge of the emitted source spectrum by including the unknown relative phases in the cost function and searching for them as free parameters using an SA search algorithm [80]. However, Soares *et al.* [75] proposed an alternative to overcome the burden of estimating the relative phases included in the matched-phase processor. It was recognized that if the unknown relative phases are set appropriately then a sum of real numbers is carried out and that this is equivalent to summing the absolute values of the complex cross-correlation terms. The alternative processor proposed was named cross-frequency incoherent processor and the maximum of the

ambiguity surface obtained is exactly the same as that obtained with the matched-phase processor with no phase parameters search.

All implementations suggested in the references mentioned above are said to be broadband or multi-frequency, but none of them were formally based on a broadband statistical data model. A significant part of the discussion came from the fact that the emitted source spectrum is unknown in most of the applications, and that the relative phases are therefore unknown, which causes the coherent processors to suffer degradation. The lack of a true broadband data model has perhaps conducted to a poor understanding of the acoustic behavior in terms of cross-frequency correlation, and why and when a coherent method provides a better detection or better localization performance than an incoherent method.

Application of deconvolution techniques should therefore be a natural step to cope with the lack of knowledge on the emitted waveform. Multichannel deconvolution has received some attention in the underwater acoustic literature. Mignerey *et al.* [81] proposed a Bayesian based multichannel deconvolution algorithm for extracting source signature spectra which is a *maximum a posteriori* (MAP) estimator. In this case a vertical array was used, and a narrowband linear data model was assumed. Knowledge on environmental conditions and previously estimated source location enter as *a priori* information. Transient source signatures were successfully extracted using real data collected in a scenario with 5.2 km nominal depth when the source location was correctly estimated. This study was then continued by Finette *et al.* [82] using a statistical approach to extend the deconvolution processor to spatially correlated noise-fields in order to discuss the degradation of the deconvolution processor in the presence of noise mismatch. To evaluate the fidelity of the reconstructed source waveform the transmitted signature was cross-correlated with estimates obtained from the

MAP estimator described in Ref. [81] and a Gauss-Markov estimator. This correlation was seen as a coherent matched-field beamformer incorporating *a priori* knowledge of the source signature to locate the known source while rejecting other sources that may be present.

4.2 Conventional matched-field processing

Conventional or Bartlett matched-field processors are most popular in underwater acoustic estimation problems, since they have been used in virtually every study on MFP. Beside the conventional processor other well known processors belonging to that class are the minimum variance, the multiple constraint, and the matched mode processor [6, 83].

The frequency domain Bartlett processor, also called linear processor, performs matched-field beamforming by weighting the output of the array elements at different frequencies and summing over all elements:

$$P(\underline{\theta}) = \mathrm{E}\,\mathrm{tr}[\mathbf{W}^H(\underline{\theta})\underline{Y}(\underline{\theta_0})\underline{Y}^H(\underline{\theta_0})\mathbf{W}(\underline{\theta})] \tag{4.1}$$

where $\mathbf{W}$ is a weighting matrix with K columns. Note that it is assumed that the acoustic field is zero mean without loss of generality. This criteria is to be maximized with respect to $\mathbf{W}(\underline{\theta})$:

$$\hat{\mathbf{W}}(\underline{\theta}) = \arg\max_{\mathbf{W}} \mathrm{E}\,\mathrm{tr}[\mathbf{W}^H(\underline{\theta})\underline{Y}(\underline{\theta_0})\underline{Y}^H(\underline{\theta_0})\mathbf{W}(\underline{\theta})]. \tag{4.2}$$

The trace and the expectation operators are interchangeable, so

$$\begin{aligned}
\hat{\mathbf{W}}(\underline{\theta}) &= \arg\max_{\mathbf{W}} \mathrm{tr}[\mathbf{W}^H(\underline{\theta})\mathrm{E}[\underline{Y}(\underline{\theta_0})\underline{Y}^H(\underline{\theta_0})]\mathbf{W}(\underline{\theta})] \\
&= \arg\max_{\mathbf{W}} \mathrm{tr}[\mathbf{W}^H(\underline{\theta})\mathbf{C}_{YY}(\underline{\theta_0})\mathbf{W}(\underline{\theta})],
\end{aligned} \tag{4.3}$$

which allows the SDM to be calculated. This can be replaced by the generic structure given

in eq. (3.16):

$$\hat{\mathbf{W}}(\underline{\theta}) = \arg\max_{\mathbf{W}} \text{tr}[\mathbf{W}^H(\underline{\theta})[\mathbf{H}(\underline{\theta_0})\mathbf{C}_{SS}\mathbf{H}^H(\theta_0) + \sigma_N^2\mathbf{C}_{NN}]\mathbf{W}(\underline{\theta})]$$

$$= \arg\max_{\mathbf{W}} \text{tr}[\mathbf{W}^H(\underline{\theta})\mathbf{H}(\underline{\theta_0})\mathbf{C}_{SS}\mathbf{H}^H(\theta_0)\mathbf{W}(\underline{\theta}) + \sigma_N^2\mathbf{W}^H(\underline{\theta})\mathbf{C}_{NN}\mathbf{W}(\underline{\theta})] \quad (4.4)$$

The tr operator can be split, and the constraint

$$\text{tr}[\mathbf{W}^H(\underline{\theta})\mathbf{C}_{NN}\mathbf{W}(\underline{\theta})] = 1 \tag{4.5}$$

is applied in order to obtain an ambiguity function whose structure is independent of the

noise structure $\mathbf{C}_{NN}$, and of the signal amplitude associated to each test solution. The

functional is maximum when

$$\hat{\mathbf{W}}(\underline{\theta}) = \frac{\mathbf{H}(\theta)\mathbf{C}_{SS}^{\frac{1}{2}}}{\sqrt{\text{tr}[\mathbf{H}^H(\theta_0)\mathbf{C}_{NN}\mathbf{H}(\theta_0)\mathbf{C}_{SS}]}}. \tag{4.6}$$

Replacing back into (4.1) the following function is obtained:

$$P(\underline{\theta}) = \frac{\text{tr}[\mathbf{H}^H(\underline{\theta})\mathbf{C}_{YY}\mathbf{H}(\underline{\theta})\mathbf{C}_{SS}]}{\text{tr}[\mathbf{H}^H(\underline{\theta})\mathbf{C}_{NN}\mathbf{H}(\underline{\theta})\mathbf{C}_{SS}]}. \tag{4.7}$$

This is the broadband Bartlett processor for generic assumptions on the emitted signal

component. According to the discussion of section 3.4.2 other particular cases can be written.

One is the Bartlett processor assuming a deterministic waveform, meaning that $\mathbf{C}_{SS} = \underline{S}\,\underline{S}^H$,

and thus,

$$P(\underline{\theta}) = \frac{\underline{S}^H\mathbf{H}^H(\underline{\theta})\mathbf{C}_{YY}\mathbf{H}(\underline{\theta})\underline{S}}{\underline{S}^H\mathbf{H}^H(\underline{\theta})\mathbf{C}_{NN}\mathbf{H}(\underline{\theta})\underline{S}}, \tag{4.8}$$

which is coherent across space and frequency. The other is when the emitted waveform is

random, then (3.18) applies and the cross-frequency terms completely vanish, resulting in

an incoherent Bartlett processor:

$$P(\underline{\theta}) = \frac{\sum_{k=1}^{K}\sigma_S^2(\omega_k)\underline{H}^H(\underline{\theta},\omega_k)\mathbf{C}_{YY}(\omega_k)\underline{H}(\underline{\theta},\omega_k)}{\sum_{k=1}^{K}\sigma_S^2(\omega_k)\underline{H}^H(\underline{\theta},\omega_k)\mathbf{C}_{NN}(\omega_k)\underline{H}(\underline{\theta},\omega_k)}. \tag{4.9}$$

Note that the normalization of the cost-function is done over the whole set of frequencies considered.

4.3 The minimum-variance processor

The above matched-field processor has important limitations in terms of sidelobe attenuation. This might become a major difficulty in multi-parameter estimation problems, when several unknown parameters are considered. As an attempt to alleviate such limitation Capon [18] proposed a processor commonly known as Minimum Variance Distortionless Response (MVDR) processor. For the broadband data model the optimization problem is to find $\mathbf{W}_{MV}$ such that

$$\hat{\mathbf{W}}_{MV} = \arg \min_{\mathbf{W}_{MV}} \text{tr}[\mathbf{W}_{MV}^H(\underline{\theta})\mathbf{C}_{YY}(\underline{\theta_0})\mathbf{W}_{MV}(\underline{\theta})], \qquad (4.10)$$

under the constraint of no distortion

$$\text{tr}[\mathbf{W}_{MV}^H(\underline{\theta})\mathbf{W}(\underline{\theta})] = 1 \qquad (4.11)$$

where $\mathbf{W}$ is the signal component in a noiseless situation. The statement made by this constraint is that no distortion is introduced by the filter $\mathbf{W}_{MV}$. The minimization is carried out using Lagrange multipliers. The functional

$$\mathcal{L} = \text{tr}[\mathbf{W}_{MV}^H\mathbf{C}_{YY}\mathbf{W}_{MV}] + \mu\{\text{tr}[\mathbf{W}_{MV}^H(\underline{\theta})\mathbf{W}(\underline{\theta})] - 1\} \qquad (4.12)$$

is to be minimized by applying the derivative with respect to $\mathbf{W}_{MV}^H$ [84]:

$$\begin{aligned} \nabla_{\mathbf{W}_{MV}^H}\mathcal{L} &= \mathbf{C}_{YY}\mathbf{W}_{MV} + \mu\mathbf{W} \\ &= \mathbf{0}, \end{aligned} \qquad (4.13)$$

which yields $\hat{\mathbf{W}}_{MV} = -\mu\mathbf{C}_{YY}^{-1}\mathbf{W}$. This allows for solving the constraint in eq. (4.11)

$$\text{tr}[-\mu\mathbf{W}^H\mathbf{C}_{YY}^{-1}\mathbf{W}] = 1 \qquad (4.14)$$

with respect to μ

$$\mu = -\frac{1}{\text{tr}[\mathbf{W}^H \mathbf{C}_{YY}^{-1} \mathbf{W}]}. \tag{4.15}$$

Substituting back into eq. (4.13) the MV filter is obtained

$$\hat{\mathbf{W}}_{MV}^H = \frac{\mathbf{C}_{YY}^{-1} \mathbf{W}}{\text{tr}[\mathbf{W}^H \mathbf{C}_{YY}^{-1} \mathbf{W}]}. \tag{4.16}$$

This can be replaced in equation (4.1), resulting in the sought processor

$$P(\underline{\theta}) = \frac{1}{\text{tr}[\mathbf{W}^H \mathbf{C}_{YY}^{-1} \mathbf{W}]}. \tag{4.17}$$

Inserting the weight obtained in equation (4.6) the broadband minimum-variance processor is obtained

$$P(\underline{\theta}) = \frac{\text{tr}[\mathbf{H}^H(\underline{\theta}) \mathbf{C}_{NN} \mathbf{H}(\underline{\theta}) \mathbf{C}_{SS}]}{\text{tr}[\mathbf{H}^H(\underline{\theta}) \mathbf{C}_{YY}^{-1} \mathbf{H}(\underline{\theta}) \mathbf{C}_{SS}]}. \tag{4.18}$$

Note that the constraint in equation (4.5) is reflected in the numerator of the minimum-variance processor. With regard to calculations, the MV processor presents the need to invert the SDM $\mathbf{C}_{YY}$, which can be done in a straightforward fashion provided that the SDM is of rank KL. In practice, this requires $N \geq KL$. Otherwise, it may be necessary to add a small quantity to the diagonal, as suggested in [85].

The particular cases of deterministic and uncorrelated frequencies are respectively obtained by assuming $\mathbf{C}_{SS} = \underline{S}\,\underline{S}^H$ on one hand,

$$P(\underline{\theta}) = \frac{\underline{S}^H \mathbf{H}^H(\underline{\theta}) \mathbf{C}_{NN} \mathbf{H}(\underline{\theta}) \underline{S}}{\underline{S}^H \mathbf{H}^H(\underline{\theta}) \mathbf{C}_{YY}^{-1} \mathbf{H}(\underline{\theta}) \underline{S}}, \tag{4.19}$$

and by assuming eq. (3.18) for the signal matrix on the other hand,

$$P(\underline{\theta}) \frac{\sum_{k=1}^{K} \sigma_S^2(\omega_k) \underline{H}^H(\underline{\theta}, \omega_k) \mathbf{C}_{NN}(\omega_k) \underline{H}(\underline{\theta}, \omega_k)}{\sum_{k=1}^{K} \sigma_S^2(\omega_k) \underline{H}^H(\underline{\theta}, \omega_k) \mathbf{C}_{YY}^{-1}(\omega_k) \underline{H}(\underline{\theta}, \omega_k)}. \tag{4.20}$$

The latter expression can be expressed by explicit summations because the SDM $\mathbf{C}_{YY}$ becomes a block matrix which allows to individually compute the inverse of the auto-frequency SDMs $\mathbf{C}_{YY}(\omega_k)$, for each frequency ω_k.

4.4 The MUSIC processor

Section 3.4.5 provided geometric solutions of the eigen-problem of the SDM $\mathbf{C}_{YY}$, in particular, those solutions spanning the signal subspace. According to Schmidt [19] the signal subspace can also be defined by its orthogonal complement - the noise subspace. This is acceptable due to the orthogonality between the columns of $\mathbf{U}_S$ and $\mathbf{U}_N$ in eq. (3.20). Due to equation (3.23) condition

$$\mathbf{U}_N^H \{ \frac{\mathbf{H}(\underline{\theta}_0)\mathbf{C}_{SS}^{\frac{1}{2}}}{\sqrt{\text{tr}[\mathbf{H}(\underline{\theta}_0)\mathbf{C}_{SS}\mathbf{H}^H(\underline{\theta}_0)]}} \} = \mathbf{0} \tag{4.21}$$

is verified. In practice, an estimate $\hat{\mathbf{C}}_{YY}$ of the SDM is obtained, and its eigenvectors are separated into signal and noise eigenvectors as in equation (3.20). Then the so-called orthogonal projector onto the noise subspace is estimated as

$$\hat{\mathbf{\Pi}}^\perp = \hat{\mathbf{U}}_N \hat{\mathbf{U}}_N^H. \tag{4.22}$$

The MUSIC processor or *parameter spectrum* is defined as

$$P_{\text{MUSIC}}(\underline{\theta}) = \frac{\text{tr}[\mathbf{H}^H(\underline{\theta})\mathbf{H}(\underline{\theta})\mathbf{C}_{SS}]}{\text{tr}[\mathbf{H}^H(\underline{\theta})\hat{\mathbf{\Pi}}^\perp\mathbf{H}(\underline{\theta})\mathbf{C}_{SS}]} \tag{4.23}$$

so that the solution parameter occurs at the maximum of $P_{\text{MUSIC}}(\underline{\theta})$. The degree of the solution uniqueness will certainly depend on the dimension of the signal subspace. The orthogonality in eq. (4.21) works as a constraint of the solutions satisfying the condition. The smaller the signal subspace dimension the larger the dimensionality of that constrain, thus, reinforcing the solution uniqueness. The dimensionality of the noise subspace will in general be high. In theory, estimates of an arbitrary accuracy can be obtained if the observation time is sufficiently long, if the SNR is adequate, and if the signal model is sufficiently accurate. The important limitations of this method are the failure to correctly

estimate the parameter with a low number of observations and a poor SNR. This method has been credited as being highly sensitive to model mismatch.

One fundamental issue is on how the signal and noise subspaces are separated, which is equivalent to estimating the dimension of the signal subspace. For this purpose the so-called information criteria [86, 87, 88] are often used. Later on, it will be shown that in practice this is not a straightforward task, even thinking of the non-subjective nature of the information criteria, and that the success of this processor in estimating the parameter vector is extremely dependent on that step.

Finally, as in previous sections, particular cases are given. The MUSIC processor for deterministic or coherent signals is portrayed as

$$P_{\text{MUSIC}}(\underline{\theta}) = \frac{\underline{S}\mathbf{H}^H(\underline{\theta})\mathbf{H}(\underline{\theta})\underline{S}}{\underline{S}^H\mathbf{H}^H(\underline{\theta})\hat{\mathbf{\Pi}}^\perp\mathbf{H}(\underline{\theta})\underline{S}}, \tag{4.24}$$

where it should be noted that here it is assumed that the signal subspace has dimension 1, and therefore the rank of the orthogonal projector is $KL - 1$. The case concerning uncorrelated signals is given as

$$P_{\text{MUSIC}}(\underline{\theta}) = \frac{\sum_{k=1}^{K}\underline{H}^H(\underline{\theta}, \omega_k)\underline{H}(\underline{\theta}, \omega_k)\sigma_S^2(\omega_k)}{\sum_{k=1}^{K}\underline{\tilde{H}}^H(\underline{\theta}, \omega_k)\hat{\mathbf{\Pi}}^\perp\underline{\tilde{H}}(\underline{\theta}, \omega_k)\sigma_S^2(\omega_k)}, \tag{4.25}$$

where $\underline{\tilde{H}}(\underline{\theta}, \omega_k)$ is a column of matrix $\mathbf{H}(\underline{\theta})$. For completeness, it remains to say that the rank of the orthogonal projector is $KL - K$.

This method can be summarized as follows:

1. Collect data and estimate the sample SDM.

2. Estimate the dimension of the signal subspace. This can be done using an information criterion.

3. Estimate the signal subspace or its complement.

4. Estimate intersections of the signal subspace with the set of acoustic replicas.

4.5 Estimating the emitted signals

In the previous sections three methods based on the broadband data model were developed. It can be remarked that the development was carried out assuming knowledge on the emitted waveform - either such as it was emitted, when representing it by $\underline{S}$, either using its second order statistic, when using $\mathbf{C}_{SS}$. The fact behind the latter case is the eventual existence of unmodeled propagation channel inhomogeneities or channel variability, even when the signal is deterministic.

The main problem now is that in practice the knowledge of the emitted signal is often not available, or even if it is, its knowledge can not be used due to unmodeled ocean inhomogeneities that introduce random features in the channel response. The lack of knowledge of the emitted signal leads to the requirement of estimating $\underline{S}$ or $\mathbf{C}_{SS}$ depending on the statistical assumptions made. Such estimation problem is analog to deconvolution. Deconvolution has received extensive attention in the literature [81, 82, 89, 90]. Classical deconvolution assumes full knowledge of the source location and of the environmental parameters, which is not the case in parameter estimation problems.

Concerning the signal estimation problem two cases are to be treated:

- Case 1: the deterministic case, where it suffices to account for first order statistics;

- Case 2: the random case, allowing assumptions on spectral coherence from fully coherent signals to incoherent signals.

Concerning Case 1, in section 3.5.1 it was possible to write the first derivative of the likelihood function of the received signal in such a form that effectively an MVU estimator for the emitted signal $\underline{S}$ could be found. However, that case was treated assuming that just a single snapshot interval was available. If N snapshots are available then an estimator for $\underline{S}$ can be written as

$$\hat{\underline{S}} = \frac{1}{N} \sum_{n=1}^{N} \mathbf{H}^+(\underline{\theta}_0) \underline{Y}_n \qquad (4.26)$$

$$= \mathbf{H}^+(\underline{\theta}_0) \frac{1}{N} \sum_{n=1}^{N} \underline{Y}_n, \qquad (4.27)$$

which is based on the mean over N realizations of the received signal. Case 2 is much more complex and could not be solved using the CRLB theorem.

One classical way for estimating $\mathbf{C}_{SS}$ is obtained using the likelihood function of the received signal. It is a maximum likelihood estimate given as

$$\hat{\mathbf{C}}_{SS,\mathrm{ml}} = \hat{\mathbf{H}}^+(\hat{\theta}_0)[\hat{\mathbf{C}}_{YY}(\theta_0) - \hat{\sigma}_N^2 \hat{\mathbf{C}}_{NN}][\hat{\mathbf{H}}^+(\hat{\theta}_0)]^H, \qquad (4.28)$$

where it is assumed that all estimates involved are consistent under the typical regularity conditions assumed [74]. However, in the literature it is often referred that in general $\hat{\mathbf{C}}_{SS,\mathrm{ml}}$ is indefinite since the columns of $\mathbf{H}(\underline{\theta}_0)$ must be estimated and do not need to exactly span the same subspace the signal eigenvectors $\hat{\underline{u}}_1, \ldots, \hat{\underline{u}}_M$ do.

An alternative is to use signal subspace methods. The matrix $\mathbf{C}_{XX}$ (eq. (3.16)) can be estimated together with σ_N^2. Using the eigenvalue representation $\lambda_1 \geq \ldots \geq \lambda_M$ and the orthonormal eigenvectors $\underline{u}_i, (i = 1, \ldots, M)$ of $\mathbf{C}_{YY}(\underline{\theta}_0)$ spanning the signal subspace, and assuming that $\lambda_M \geq \lambda_{M+1} = \ldots = \lambda_{KL} = \sigma_N^2$, one can write

$$\mathbf{C}_{XX} = \sum_{i=1}^{M} (\lambda_i - \sigma_N^2) \underline{u}_i \underline{u}_i^H. \qquad (4.29)$$

The eigenvalues λ_i and the eigenvectors $\underline{u}_i$ can be estimated from the sample SDM $\hat{\mathbf{C}}_{YY}(\underline{\theta_0})$).

For estimating σ_N^2 the following criterion may be used [91]:

$$\ln[L(\underline{\theta_0}; \sigma_N^2)] = -\ln|\mathbf{C}_{XX} + \sigma_N^2\mathbf{I}| - \text{tr}[\hat{\mathbf{C}}_{YY}(\mathbf{C}_{XX} + \sigma_N^2\mathbf{I})^{-1}], \tag{4.30}$$

which is written in terms of eigenvectors and eigenvalues as

$$\ln[L(\underline{\theta_0}; \sigma_N^2)] = -\sum_{i=1}^{M} \ln\lambda_i - (KL - M)\ln\sigma_N^2 - \sum_{i=1}^{M}\lambda_i^{-1}\underline{u}_i^H\hat{\mathbf{C}}_{YY}\underline{u}_i - \frac{1}{\sigma^2}(\text{tr}\hat{\mathbf{C}}_{YY} - \sum_{i=1}^{M}\underline{u}_i^H\hat{\mathbf{C}}_{YY}\underline{u}_i). \tag{4.31}$$

The optimum estimates for λ_i and $\underline{u}_i$ are determined from $\hat{\mathbf{C}}_{YY}$, and the estimate of σ_N^2 is given as

$$\hat{\sigma}_N^2 = \frac{\text{tr}\hat{\mathbf{C}}_{YY} - \sum_{i=1}^{M}\hat{\lambda}_i}{KL - M}, \tag{4.32}$$

which is equivalent to the arithmetic mean of the $KL - M$ smallest eigenvalues of $\hat{\mathbf{C}}_{YY}$:

$$\hat{\sigma}_N^2 = \frac{1}{KL - M}\sum_{i=M+1}^{KL}\hat{\lambda}_i. \tag{4.33}$$

Now the estimate $\hat{\sigma}_N^2$ can be used in equation (4.29) to estimate $\mathbf{C}_{XX}$. Finally, the estimate of $\mathbf{C}_{SS}$ proceeds by filtering out the channel response:

$$\hat{\mathbf{C}}_{SS} = \mathbf{H}^+(\underline{\hat{\theta}_0})\hat{\mathbf{C}}_{XX}[\mathbf{H}^+(\underline{\hat{\theta}_0})]^H. \tag{4.34}$$

The estimation of the $\mathbf{C}_{SS}$ signal matrix can be summarized as follows:

1. Use an information criterion to estimate the dimension of the signal subspace, i.e., estimate M.

2. Estimate σ_N^2 using equation (4.33).

3. Estimate $\mathbf{C}_{XX}$ using equation (4.29).

4. Filter the channel response $\mathbf{H}(\underline{\theta_0})$ using equation (4.34).

In step 4) one problem persists: generally $\underline{\theta}_0$ is unknown, and the deconvolution algorithm cannot be completed. In the framework of parameter estimation one can replace $\underline{\theta}_0$ with $\underline{\theta}$, making $\hat{\mathbf{C}}_{SS}$ dependent on $\underline{\theta}$, and then replacing it in the processor expressions obtained in the above sections. It is possible to demonstrate that the lack of knowledge on the emitted waveform will lead to a drawback in the parameter estimation performance. The amount of knowledge on the structure of the emitted waveform can be seen as the amount of *a priori* information entering the parameter estimation algorithm.

4.6   Coherence and coherence restoration

Let $\phi_l(t) = \phi_l(t, \omega_k), l = 1, \ldots, L$ be the phase at receiver l and frequency ω_k along time t. The problem at hand is to find a function $x(t)$, which will be called *coherence restoration function*, such that the variability of

$$
\begin{aligned}
\Phi_1(t) &= \phi_1(t) + x(t) \\
&\vdots \\
\Phi_l(t) &= \phi_l(t) + x(t) \\
&\vdots \\
\Phi_L(t) &= \phi_L(t) + x(t)
\end{aligned}
\tag{4.35}
$$

is minimum. This can be achieved via a least-squares problem during the observation time:

$$
\begin{aligned}
\mathcal{J}(x) &= \frac{1}{T} \int_0^T [\Phi_l(t) - \phi_l(0)]^2 dt \\
&= \frac{1}{T} \int_0^T [\Phi_l(t) - 2\Phi_l(t)\phi_l^2(0)] + \phi_l^2(0)]dt.
\end{aligned}
\tag{4.36}
$$

If $\Phi_l(t)$ is explicited then

$$
\mathcal{J}(x) = \frac{1}{T} \int_0^T [\phi_l^2(t) + 2\phi_l(t)x(t) + x^2(t) + 2\phi_l(t)\phi_l(0) + 2\phi_l(0)x(t) + \phi_l(0)]dt.
\tag{4.37}
$$

Now the derivative with respect to $x(t)$ is applied to the functional and equated to zero

$$\frac{d\mathcal{J}(x)}{dx(t)} = \frac{1}{T}\int_0^T [0 + 2\phi_l(t) + 2x(t) + 0 + 2\phi_l(0) + 0]dt \qquad (4.38)$$

$$= 0. \qquad (4.39)$$

The equation above is to be solved with respect to $x(t)$, yielding as a trivial solution

$$x(t) = -[\phi_l(0) + \phi_l(t)]. \qquad (4.40)$$

The actual development has been carried out only for receiver l, but the objective is to suit $x(t)$ to the L receivers. Thus, the next problem is to solve an equation system with L equations and only one unknown:

$$\begin{cases} x(t) = -[\phi_1(0) + \phi_1(t)] \\ \vdots \\ x(t) = -[\phi_l(0) + \phi_l(t)] \\ \vdots \\ x(t) = -[\phi_L(0) + \phi_L(t)] \end{cases} \qquad (4.41)$$

It can be shown that in the sense of the least-squares the optimal solution for this overdetermined problem is

$$x(t) = -\frac{\sum_{l=1}^L \phi_l(0) + \sum_{l=1}^L \phi_l(t)}{L}. \qquad (4.42)$$

It is interesting to verify that the initial phases and the phases along all receivers are equally taken into account for obtaining the coherence restoration function. If at a given frequency ω_k the signal components across the receiver array are fully coherent, and assuming that the noise power is σ_N^2 at all receivers, then the mean variance of $x(t)$ during the observation time due to noise will be $\frac{\sigma_N^2}{L}$.

An alternative method, deducted from a proposal of Michalopoulou [79] using a reference receiver, is going to be developed. A reference receiver is chosen for compensating both the lack of knowledge on the emitted waveform and the spectral incoherence. The reference

receiver would ideally be that with highest SNR, but in Ref. [79] always the top receiver was taken.

Assuming that the noise component consists only of uncorrelated noise one can perform a test based on correlations to find out what receiver has the highest SNR at a given frequency. Let

$$\underline{\phi}_n(\omega_k) = [e^{j\angle \underline{Y}_n(Z_1)} \cdots e^{j\angle \underline{Y}_n(Z_l)} \cdots e^{j\angle \underline{Y}_n(Z_L)}]^T \tag{4.43}$$

be the vector with the complex phases in the observed acoustic field at snapshot n. Taking only the phases will avoid taking a decision strongly dependent on the channel gain or the noise power at a given receiver since all elements in vector $\underline{\phi}_n(\omega_k)$ will have an amplitude equal to 1. The next step is the computation of a sample correlation matrix

$$\mathbf{C}_{\phi\phi}(\omega_k) = \frac{1}{N} \sum_{n=1}^{N} \underline{\phi}_n(\omega_k) \underline{\phi}_n^H(\omega_k) \tag{4.44}$$

and then take the receiver respective to the column with highest absolute mean value. The rationale behind this algorithm is to assume that the noise component is uncorrelated or at least nearly uncorrelated across space, and therefore the signal with best SNR will in average have highest correlation with all the other signals in the remaining receivers. This second alternative relies only on a single receiver, which might be advantageous in comparison to the former when the noise power is strongly dependent on space or when the number of receivers is reduced.

The phase normalization proposed above is specially suitable and effective when the experimenter is certain that the SNR at the reference receiver is very high. An alternative scheme can be applied when a large number of frequencies is available. One can proceed by optimizing the frequencies to be used for parameter estimation. The cost-function can be based on the eigenvalues of the spectral density matrix. Assuming that the λ_i are sorted one

can simply take

$$\Lambda(\lambda_1, \lambda_2) = \frac{\lambda_1}{\lambda_2} \tag{4.45}$$

as the cost-function to be optimized over the available frequency search space. The idea is to choose combinations of frequencies such that partitioning of energy into different eigenvectors is reduced, and most energy is concentrated on the first eigenvector. This cost-function can be seen as an abbreviation of the well known Information Theoretic Criteria. Such criteria are based on the eigenvalues of the SDM and perform a minimization that serves the purpose of separating the signal subspace from the noise subspace. One is the Akaike Information Criterion (AIC) [86, 92] given for the broadband data model as

$$\text{AIC}(k) = -2\ln\left(\frac{\prod_{i=k+1}^{KL} \lambda_i^{KL-k}}{\frac{1}{KL-k}\sum_{i=k+1}^{KL} \lambda_i}\right)^{(KL-k)N} + 2k(2KL - k), \tag{4.46}$$

where $k = 0, \ldots, KL$. The Minimum Description Length (MDL) [87, 88, 92] criterion is given by

$$\text{MDL}(k) = \ln\left(\frac{\prod_{i=k+1}^{KL} \lambda_i^{KL-k}}{\frac{1}{KL-k}\sum_{i=k+1}^{KL} \lambda_i}\right)^{(KL-k)N} + \frac{1}{2}k(2KL - k)\ln N, \tag{4.47}$$

where $k = 0, \ldots, KL - 1$. It can be shown that the MDL yields consistent estimates on the dimension of the signal subspace, and that the AIC is inconsistent since it tends, asymptotically, to overestimate the dimension of the signal subspace.

The choice between the eigenvalues ratio $\Lambda(\lambda_1, \lambda_2)$ or the information criteria can be based on the number N of snapshots available. For a low number of snapshots, say $N \approx KL$ (provided that $N \geq KL$), the estimates of the λ_i are in principle poor, in particular those for $i \approx KL$, causing the information criterion to completely fail to correctly separate the signal and noise subspaces. In other words, the optimization can implicitly be made in the sense of minimizing the signal subspace dimension, by maximizing the eigenvalues ratio. If N is large compared with KL then the eigenvalue estimates tend to have a lower variance

and the optimization can explicitly be made for minimizing the signal subspace dimension, using the information criteria.

The computational effort for computing the eigenvalues depends on the number of frequencies and receivers. If KL is small it is reasonable to perform an exhaustive search over the whole frequency search space by testing all possible frequency combinations. Otherwise, if KL is large then the computational burden for computing the eigenvalues is high, and a global search algorithm such as a GA can be employed in order to optimize the frequencies.

4.7   Summary

Three coherent broadband MF processors were derived using the broadband data model proposed in chapter 3:

- the Bartlett processor (section 4.2);

- the minimum-variance processor (section 4.3);

- and the MUSIC processor (section 4.4).

The derivation of these BB processors could be carried out as traditionally found in the literature for the narrowband case, with some adaptation to the fact that the channel vector turned into a channel matrix, and the scalar representing the emitted waveform turned into a vector, according to the broadband data model. Most BB processors found in the literature are in fact a superposition of the single-frequency processor computed at several frequencies and are usually the result of an algorithmic rationale. The BB processors herein are formally obtained from the BB data model.

These processors were derived by representing the emitted waveform as a second order matrix, the signal matrix $\mathbf{C}_{SS}$, which remained with unspecified assumptions. The advantage of proceeding this way is that the final processor expression obtained is generic and valid for any degree of cross-frequency correlation. This also introduces flexibility, since the signal assumptions are ruled by assumptions made on the signal matrix. The signal matrix appears always as a weighting factor in the processor expression and can be suitably replaced in agreement to the assumptions made. This was done herein by particularizing for fully coherent and fully incoherent signals.

Another possibility is to keep unspecified assumptions on the signal component (on the signal matrix), and include the estimation of the signal matrix in the processing. The estimator of the signal matrix proposed here is based on the signal subspace. The estimate of the signal matrix is then replaced in the processor expression. Note, however, that due to back-dependence on the unknown parameter, the estimation of the signal matrix is coupled with the parameter search, i.e., since the parameter of interest is unknown, an estimate of the signal matrix is calculated for each hypothetical value of the search parameter.

Coherent matched-field processing without knowledge of the emitted signal is very appealing, since coherent processing usually requires full knowledge of the emitted signal, which has been seen as a major problem in the MFP literature. The scheme proposed here constitutes a significant relaxation of this constraint. Moreover, by splitting the data into signal and noise subspaces, it is possible to work under partial spectral coherence, which constitutes a generalization in terms of the statistical assumptions on the signal component.

Finally, several pre-processing schemes to ameliorate the data quality in terms of spectral coherence are proposed. Two of these schemes seek for enhancing field coherence by normal-

izing the phases at the receivers using a reference phase. The other performs a selection of

frequencies using criteria based on the eigenvalues of the cross-frequency SDM.

Chapter 5

Matched-Field Processors: a synthetic study

Three methods have been applied to the proposed broadband data model. These processors can be characterized as follows:

1. the Bartlett processor directly correlates the measured data with the replica data, and the output power is the squared magnitude of that correlation;

2. the minimum-variance processor is classified in the category of the adaptive beamformers, and also considered a high-resolution estimation method;

3. finally, the MUSIC method was introduced in the framework of signal and noise subspaces separation. The subspace based approaches rely on certain geometrical properties of the assumed data model, resulting in an extremely high-resolution capability, which (in theory) is not limited by the array aperture, provided the data observation time and/or SNR are sufficiently large.

The Bartlett processor is simply based on correlations. Due to its wide use, it is well known in the underwater acoustic signal processing literature, where it has been credited to be robust against physical and statistical mismatch, and its implementation is straightfor-

ward.

The MV and MUSIC high-resolution processors go beyond simple correlations and their computation requires additional steps. The computation of the MV processor involves the inversion of the SDM matrix, which has been remarked as a difficulty in the MFP literature. The MUSIC processor involves splitting the data into signal and noise subspaces, whose correct estimation is fundamental for its success. High-resolution methods are credited to be highly sensitive to physical and statistical mismatch, which are possible impairments to their successful application to the problem at hand.

In the context of the proposed processors several issues are of concern at this point:

- each processor can be implemented combining the assumptions of coherent or incoherent spectral components, with known or unknown signal structure. In the case of unknown signal structure, its estimation is coupled with the estimation of the parameter of interest. It is unknown how these processors behave under different working conditions, neither how they will compare in terms of sidelobe structure;

- another aspect of concern is related with statistical mismatch. The main question is under which conditions a given processor produces parameter estimates with the expected performance. Here, it is interesting to measure the performance as a function of signal-to-noise ratio and number of data observations;

- another important issue is the coupling of a processor with the search method employed to maximize the cost-function. In this thesis a genetic algorithm will be used in the MFT inversion procedure. Sidelobes in the cost function represent a difficulty to a meta-heuristic search method such as a genetic algorithm. The application of high-

resolution processors in MFT is motivated too a large extent by the possibility of significantly improving the performance of the search method due to their increased ability in the attenuation of sidelobes (less false attractors, see section 2.5).

- other issues treated in this chapter are the application of coherence restoration when parameters vary during the observation time, and cost-function sensitivity to parameter variation.

As it can be seen there are several issues to be investigated in order to understand the potential of these methods in MFT. So far, high-resolution methods have not been used in MFT or geoacoustic inversion. The objective of this chapter is to perform a simulation study in order to compare the three proposed processors covering the issues presented above. Although all three processors will be analyzed with the same depth, the Bartlett processor will be seen as the reference in terms of performance and some more focus will be on the high-resolution methods, since these somewhat constitute a novelty for this application.

The synthetic data is obtained using the baseline model for the North Elba site in order to use the same model used with experimental data (see section 6.2). The forward problem is solved using the normal modes propagation model C-SNAP.

5.1 Portraying estimators as cost functions

A Matched-Field processor can be seen as a function of the hypothetical parameter vector $\underline{\theta}$, and is often called cost-function in the context of inverse problems. Concerning the behavior of a processor, assuming absence of noise and model mismatch of any type, the important characteristics are the ratio between the maximum value of the processor and the so-called sidelobes, on one hand, and on the other hand the resolution. These capabilities

are generally an implication of underlying constraints applied during the construction of an estimator. The behavior of a processor is also highly dependent on the unknown parameter or, when it comes to multi-parameter estimation, it depends on the sensitivity of the field to variations of the individual parameters, and also on the ambiguity patterns in play when several unknowns are searched.

The main interest is to illustrate how the matched-field processors obtained in chapter 4 compare in terms of sidelobe attenuation and resolution, and how the assumptions of known or unknown waveform, or the assumption of coherent or incoherent signals impact on these characteristics. This can be carried out numerically by calculating each cost-function as a function of physical parameters of interest. Computer simulations were performed using the baseline model of the MREA'03 experiment. The source was supposed to be at a 6 km range and at a 60 m depth, and receivers were at depths 15, 60, and 75 m ($L = 3$). The acoustic field was considered for frequencies 400, 450, and 500 Hz ($K = 3$). The spectral density matrix was computed using (3.16). The noise power σ_N^2 was set as the mean of the first K eigenvalues of the $\mathbf{C}_{XX}$ matrix (the SDM of the signal component):

$$\sigma_N^2 = \frac{1}{K} \sum_{k=1}^{K} \lambda_k, \tag{5.1}$$

in order to obtain auto-frequency SDMs with the same SNR, in both coherent and incoherent cases. The noise matrix is the identity matrix. At this point it can be noted that under the assumption of coherent signals $\lambda_1 > 0$ and $\lambda_2 = \cdots = \lambda_K = 0$, and for the incoherent case, in general, $\lambda_k^2 > 0, k = 1, \ldots, K$. Note also that for computing the SDM, $\mathbf{C}_{SS} = \mathbf{1}$ for the coherent case, and $\mathbf{C}_{SS} = \mathbf{I}$ for the incoherent case. Some more remarks are necessary before proceeding: (a) along this remaining chapter, the emitted waveform will always be represented by second order statistics, i.e., by matrix $\mathbf{C}_{SS}$; (b) in this section, for computing
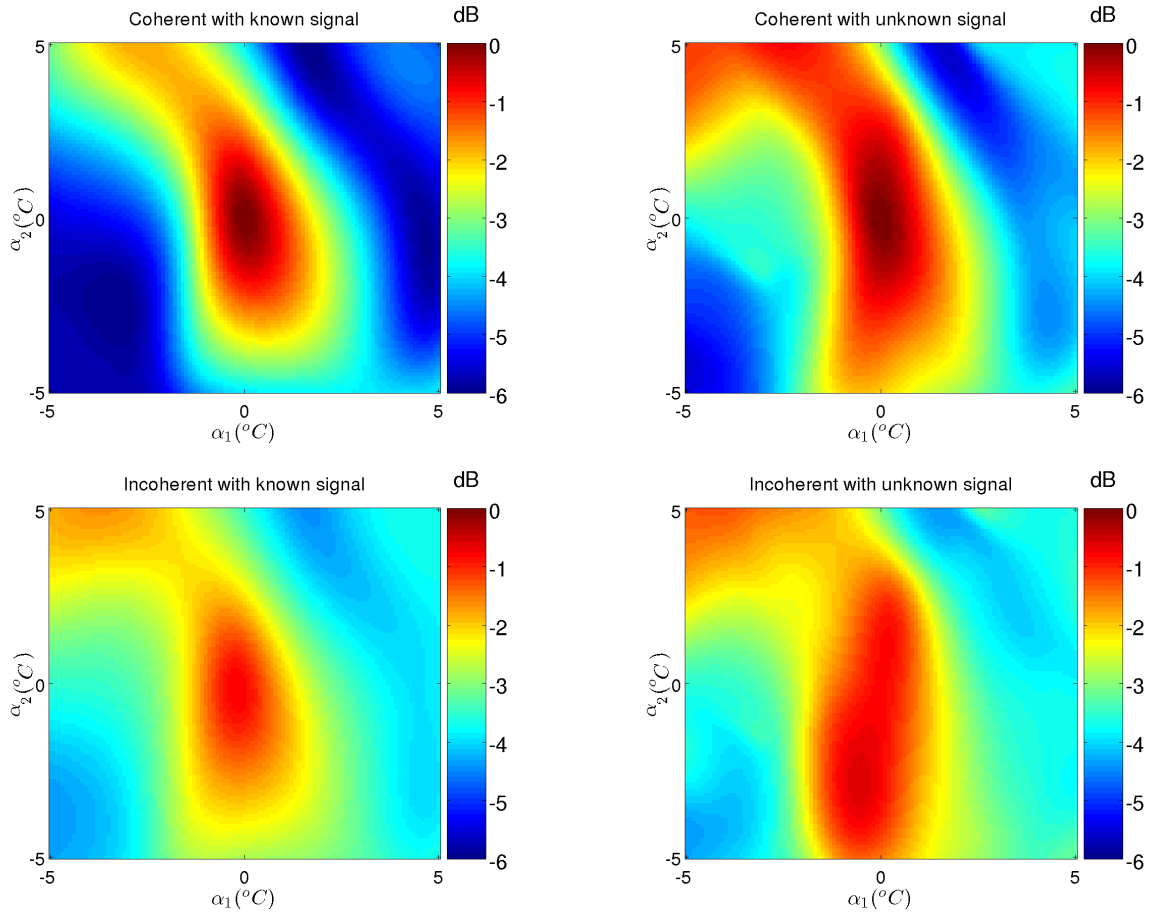
Figure 5.1: The behavior of the broadband Bartlett processor for the coherent case (upper row); incoherent case (lower row); known signal (left column); and unknown signal (right column).

the cost-functions, and in particular, for estimating the signal matrix or for estimating the noise subspace, in this section it is assumed that the dimension of the signal subspace is known, i.e., it is equal 1 in the coherent case, and K in the incoherent case.

Since the main goal of acoustic tomography is the estimation of the temperature in the water column, the cost-functions were computed as a function of two EOF coefficients α_1 and α_2 in the EOF expansion of (2.4). Figure 5.1 shows the four possible cases using the BB Bartlett matched-field processor. The figure composition consists of four plots - 2 rows and 2 columns - with upper row and lower row respectively considering the coherent and the incoherent processor, and left and right column respectively considering known and unknown waveform. The processor used is always that obtained in (4.7), and in the cases where the

waveform is assumed unknown, (4.34) is used to estimate the signal matrix. Observing the figure it can be seen in general that the plots are very smooth as it is typical for the Bartlett processor. Looking in more detail it is very interesting to verify that

1. The coherent processor with known signal matrix has the narrowest main peak and lowest sidelobe structure.

2. The coherent processor with unknown signal matrix has a broader peak and increased sidelobe level, which is caused by the lack of knowledge on the signal matrix. Note that for each point of the surface an estimate of the signal matrix is produced using the corresponding field replica.

3. The incoherent processor with known signal has a sidelobe level that is comparable with the coherent processor with unknown signal. The peak does not attain 0 dB.

4. The incoherent processor with unknown signal matrix has its maximum value for wrong values of the parameters. To date this has not been well understood.

Next, the same series of ambiguity surfaces were computed for the broadband MV processor using (4.18). Figure 5.2 shows the behavior of this processor for the same four cases discussed above. As it is expected it can be seen that the performance of the MV processor in terms of sidelobe attenuation is superior to that of the Bartlett processor. In general, the main peak is narrower and the overall ambiguity level is lower as it can be seen by observing the colorbar, which has a wider range of variation. The coherent MV processor has a slightly lower sidelobe structure when the signal structure is known. The incoherent processor has a significantly higher sidelobe level in comparison to the coherent one.

Finally, the same plots were also computed for the MUSIC processor using (4.23). The
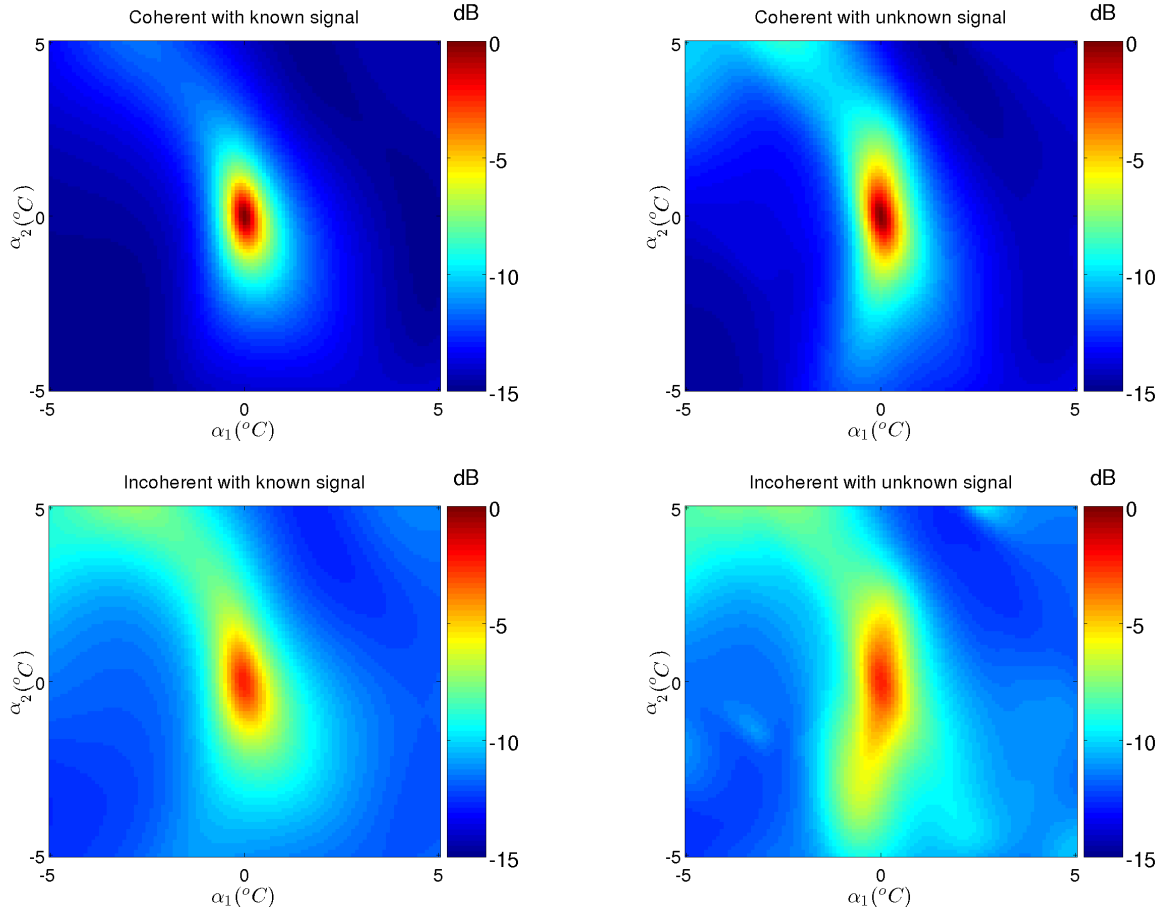
Figure 5.2: The behavior of the broadband MV processor for the coherent case (upper row); incoherent case (lower row); known signal (left column); and unknown signal (right column).

reader, might ask how this was done if this processor approaches ∞ when the parameter vector $\underline{\theta}$ approaches the true value, under the conditions used for generating the synthetic data. It is possible to portray the MUSIC processor such that its maximum has a finite value by

$$P_{\text{MUSIC,finite}} = \frac{1}{\gamma + \frac{1}{P_{\text{MUSIC}}}}. \tag{5.2}$$

It can be easily seen that $P_{\text{MUSIC,finite}} \to \frac{1}{\gamma}$ as $P_{\text{MUSIC}} \to \infty$. One positive side effect of this operation is that the experimenter has a reference value for the maximum value that can be attained. One can go further and scale the MUSIC processor such that it varies in the
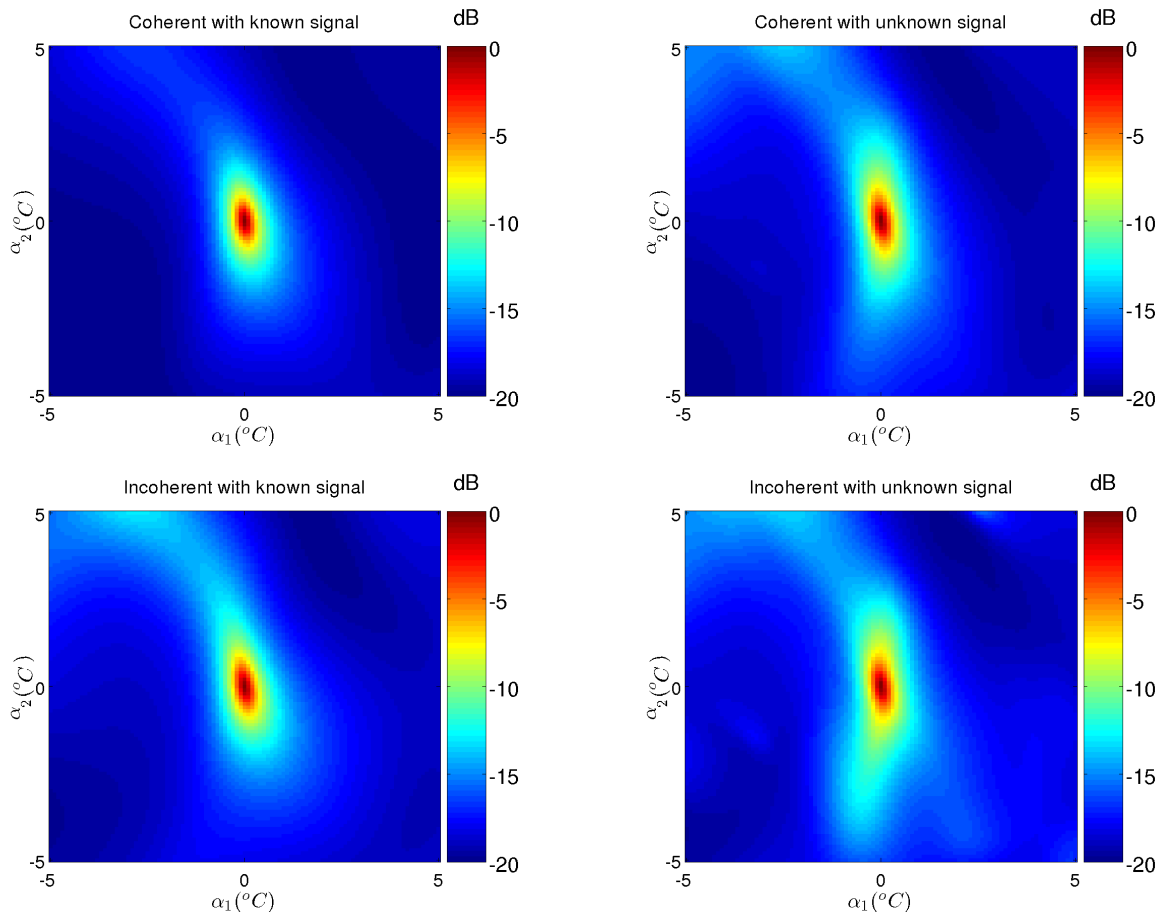
Figure 5.3: The behavior of the broadband MUSIC processor for the coherent case (upper row); incoherent case (lower row); known signal (left column); and unknown (right column).

interval $[0; 1]$, as the Bartlett and the MV processors do:

$$P_{\text{MUSIC},1} = \frac{\gamma}{\gamma + \frac{1}{P_{\text{MUSIC}}}}. \tag{5.3}$$

For the computer simulations reported in this study γ has been set to 0.01. Figure 5.3 shows

a series of plots computed for the MUSIC processor. It outperforms the MV processor in

terms of sidelobe structure. The maximum is always attained for the incoherent case. For

this setup there are no significant differences between the four cases, except that the coherent

processor with known signal has a slightly narrower peak, and the incoherent processors have

a slight tail coming from the main peak.

Table 5.1 summarizes the results obtained in this section in terms of peak-to-surface

	Coh. k.	Coh. unk.	Inc. k.	Inc. unk.
Bartlett	2.23	1.86	1.64	1.58
MV	17.9	14.5	6.08	5.41
MUSIC	53.0	41.9	41.9	37.2

Table 5.1: Peak-to-surface average ratio obtained for the different processors. *Coh.* and *Inc.* respectively stand for *coherent* and *incoherent*. *k.* and *unk.* respectively stand for *known signal* and *unknown signal*.

average ratio. This is the ratio between the surface maximum and the average MF response of the whole ambiguity surface. *Coh.* and *Inc.* respectively stand for *coherent* and *incoherent*. *k.* and *unk.* respectively stand for *known signal* and *unknown signal*. It is easy to conclude that there is an increasing discriminating potential when presenting the developed methods in that sequence. The MV processor shows the highest effectiveness when comparing coherent with incoherent processing. For the other two processors coherent processing with unknown signal gives similar performance to incoherent with known signal.

5.2 MFP with finite data observations

When it comes to produce inversions of experimental data some of the theoretical assumption cannot be reproduced by real data simply due to the finiteness of the observed data. For example, the model assumes that signal and noise are uncorrelated, but in the estimate of the SDM cross-terms between signal and noise will appear, where its significance decreases with the number of realizations of the received data. In general the variance of the SDM estimator will depend on N. This has certainly an impact on the parameter estimation performance, which varies from method to method. In order to compare the variability of the three proposed methods when the number of signal realizations is limited, another computer simulation study was performed. Ambiguity surfaces of α_1 and α_2 were computed in the baseline scenario for coherent signal components. The chosen frequencies (400, 450,
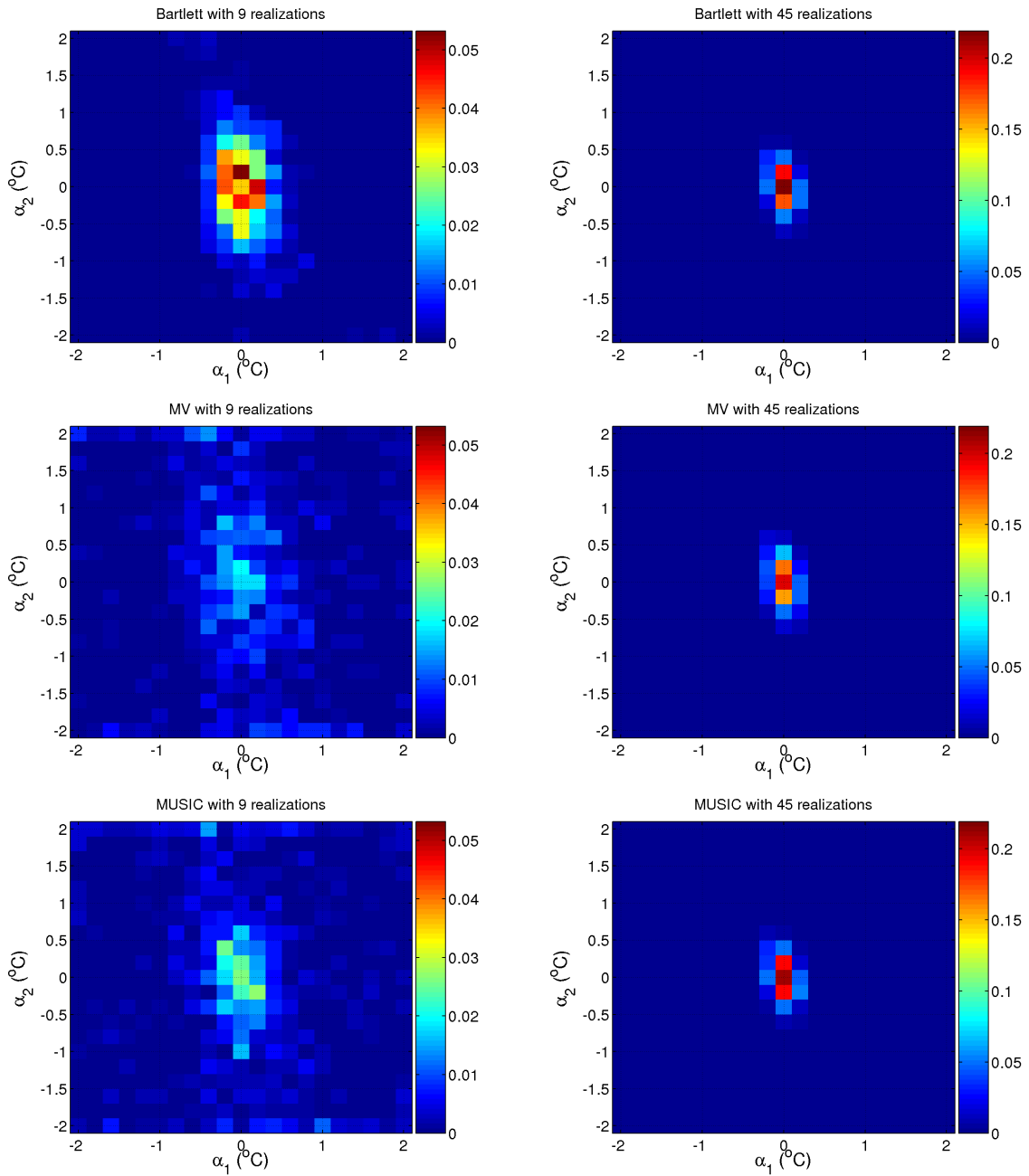
Figure 5.4: 2-dimensional histograms showing the dispersion of the estimates of the parameter vector $[\alpha_1\,\alpha_2]^T$: $N = 9$ in the left column; $N = 45$ in the right column.

and 500 Hz) and receiver depths (15, 60, and 75 m) are the same as those in section 5.1. The SNR was 0 dB. The experience was carried out 10^5 times for each processor, both using $N = 9$ and $N = 45$ for computing the sample SDMs (eq. (3.19)). Figure 5.4 shows 2-D histograms for the various processors and low and high number of signal realizations, showing the empirical joint probability density functions of the estimates of α_1 and α_2. For

	$N = 9$			$N = 45$		
	Bartlett	MV	MUSIC	Bartlett	MV	MUSIC
$\sigma_{\hat{\alpha}_1}$	0.27	0.72	0.74	0.11	0.12	0.11
$\sigma_{\hat{\alpha}_2}$	0.56	1.14	1.10	0.24	0.27	0.24

Table 5.2: Variances of the estimates of α_1 and α_2 obtained with the three proposed processors applied to synthetic data (see figure 5.4).

$N = 9$ it can be seen that the lowest variance is obtained when the Bartlett processor is used. The high-resolution methods show a significantly higher variance, in particular the MV processor. If $N = 45$, then the result of the comparison changes. The MUSIC and the Bartlett processor have similar performance with a slightly lower variance than the MV processor. Table 5.2 shows the variances obtained in each case for each processor.

The difficulties seen with the high-resolution methods come from the poor estimates of the eigenvalues λ_i. The datamodel assumes that the eigenvalues associated to the noise subspace are all equal. If N is finite, they will be different with probability 1. In the MV processor it is necessary to invert the SDM, whose accuracy depends on the eigenvalues' estimates. Concerning the MUSIC processor, the problem arises when the signal space is to be split into the signal and noise subspaces. This important issue is illustrated in figure 5.5 that shows in (a) the computed eigenvalues for two particular cases, one using 9 signal realizations, and the other using 11. The signal subspace dimension is estimated using the MDL criterion (see section 4.6). The former case yields a signal subspace with dimension 8, although a deterministic signal component is used for data generation - such dimension being caused by poorly estimating the eigenvalues, as it can be seen. Note that the smallest eigenvalue has a very high ratio to its predecessor. The latter case, $N = 11$, yielded a signal subspace with dimension 1 - it can be seen that the ratios between contiguous eigenvalues are reduced, except between the two first eigenvalues. Figure 5.5(b) shows the average eigenspectrum

when the number of realizations varies between 9 and 20. For each case 100 realizations of the eigenspectrum were computed and averaged. Considering the highest eigenvalue always 0 dB, it is interesting to observe the behavior of the remaining eigenvalues as the number of signal realizations increases: first, the 2nd and 3rd eigenvalues are decreasing with the number of signal realizations; second, the 5th through the 9th eigenvalues are increasing with the number of realizations; third, the 4th eigenvalue is almost steady, with a reduced non-monotonic variation. One can expect the remaining eigenvalues from 2 through 9 to approach eigenvalue 4 as $N \rightarrow \infty$. Finally, figure 5.5(c) shows the average order estimate obtained using the same data as in figure 5.5(b), applying the MDL information criterion. For the minimal number of signal realizations (9) the average order obtained is about 3; for 10 realizations it is about 2; for 11 realizations or more it estimates in average the correct value which is 1. The simulations carried out in this section clearly show that the impact of the number of signal realizations can be striking for some methods. Simultaneously, and according to the discussion in section 3.4.2, the observation time should be limited in order to maintain the channel coherence. In acoustic tomography, signals are usually emitted at maximum power, which implies that, due to technical limitations related to the instrumentation, the effective emission interval (duty cycle) will be only a small part of the total time (e.g. 25% during the MREA'03 sea trial [50]). Considering the present discussion, it is preferable to reduce the emitting power such that effective emission time approaches 100%. The MFP processors developed in this thesis use only discrete frequencies rather than the continuous spectral band. From this point of view it makes sense to design a signal consisting of sinusoids (multi-tones), with clear advantages in terms of signal-to-noise ratio in comparison to the LFM chirps, while simultaneously responding to the requirement of a
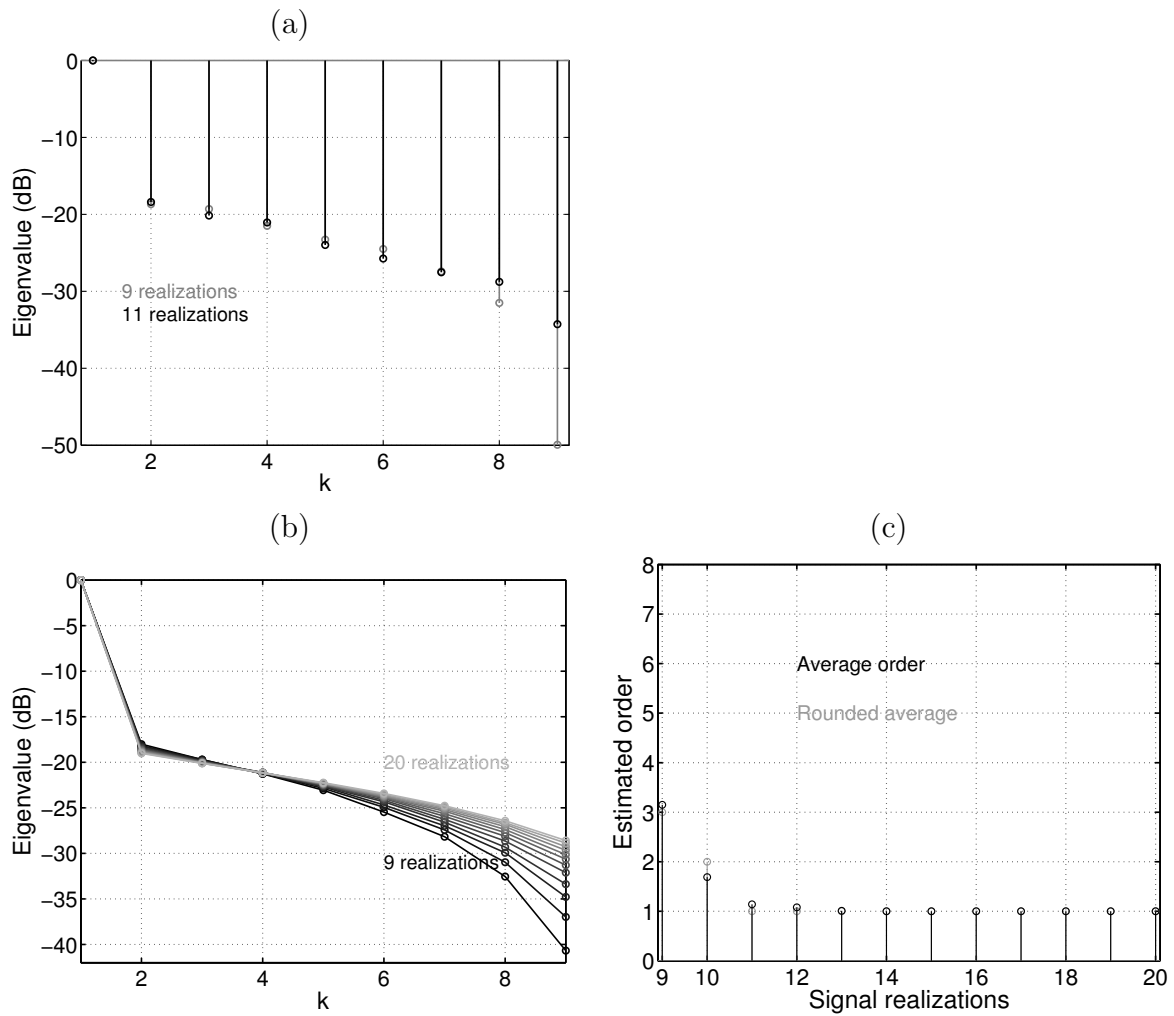
Figure 5.5: Eigenspectra for finite number of signal observations: comparison of two eigenspectra using $N = 9$ (gray) and $N = 11$ black (a); average eigenspectrum for a varying number of signal realizations (b); average order estimation for a varying number of signal realizations (c).

high number of signal realizations claimed above.

5.3 Local and global performance

In order to learn further on the potential of the proposed parameter estimation techniques, the CRLB both for the deterministic and random signal assumptions of the broadband data model are calculated for a numeric case, and root mean-square errors for the different processors under different assumptions are computed. The acoustic scenario is the same as that used in the previous sections of the current chapter. Figure 5.6(a) shows the CRLB
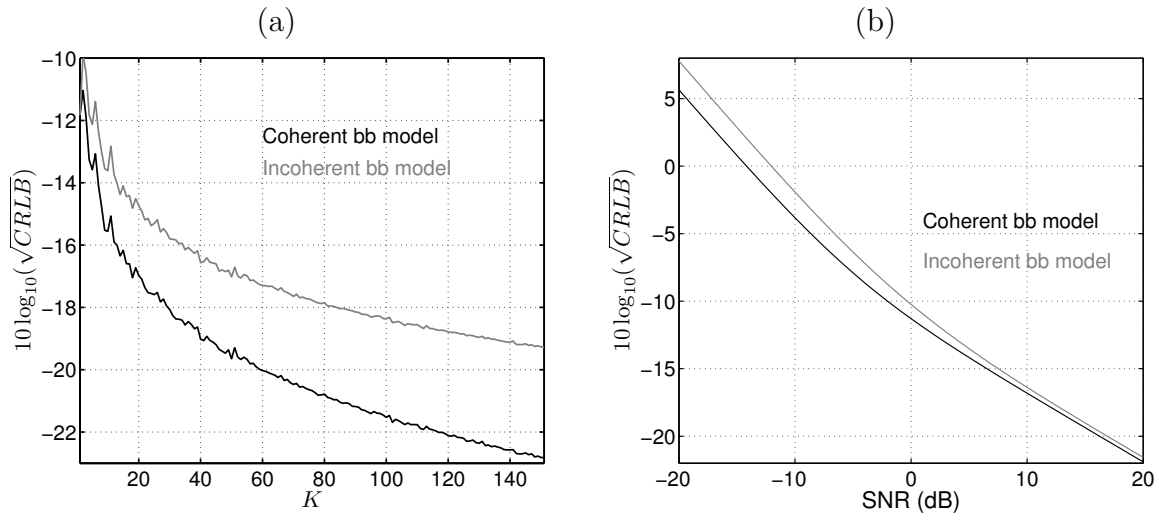
Figure 5.6: The Cramér-Rao Lower Bounds computed for coherent and incoherent data models: (a) CRLB as a function of K, the number of equispaced frequency bins in the band 900-1200 Hz; (b) CRLB as a function of SNR using frequencies 400, 450, and 500 Hz.

as a function of the number of equispaced frequency bins in the band 900-1200 Hz. It can be verified that for an increasing number of frequencies, and therefore an increment of the number of cross-pairs in the coherent case, the ratio between the CRLBs is always increasing. Figure 5.6(b) shows the CRLB as a function of the SNR. Here is seen the potential ability of the cross-frequencies to reject the noise and therefore improve the local performance in comparison to the incoherent model for a low SNR. Note that only 3 frequencies are used in order to emphasize the difference between the coherent and the incoherent case at low SNR and that this difference reduces with the SNR.

The next case is to investigate how the coherent processors perform against SNR and against the number of signal realizations N. Here the parameter subject to be estimated is α_1 whose true value is 0. Once again the 3-frequencies/3-receivers case is taken. Figure 5.7 shows four plots corresponding to the RMSE either as a function of SNR, or as a function of the number of snapshots N, assuming a known or an unknown signal matrix. It can be seen that in no case the CRLB is attained. For figures 5.7(a) and (b) the number of snapshots is
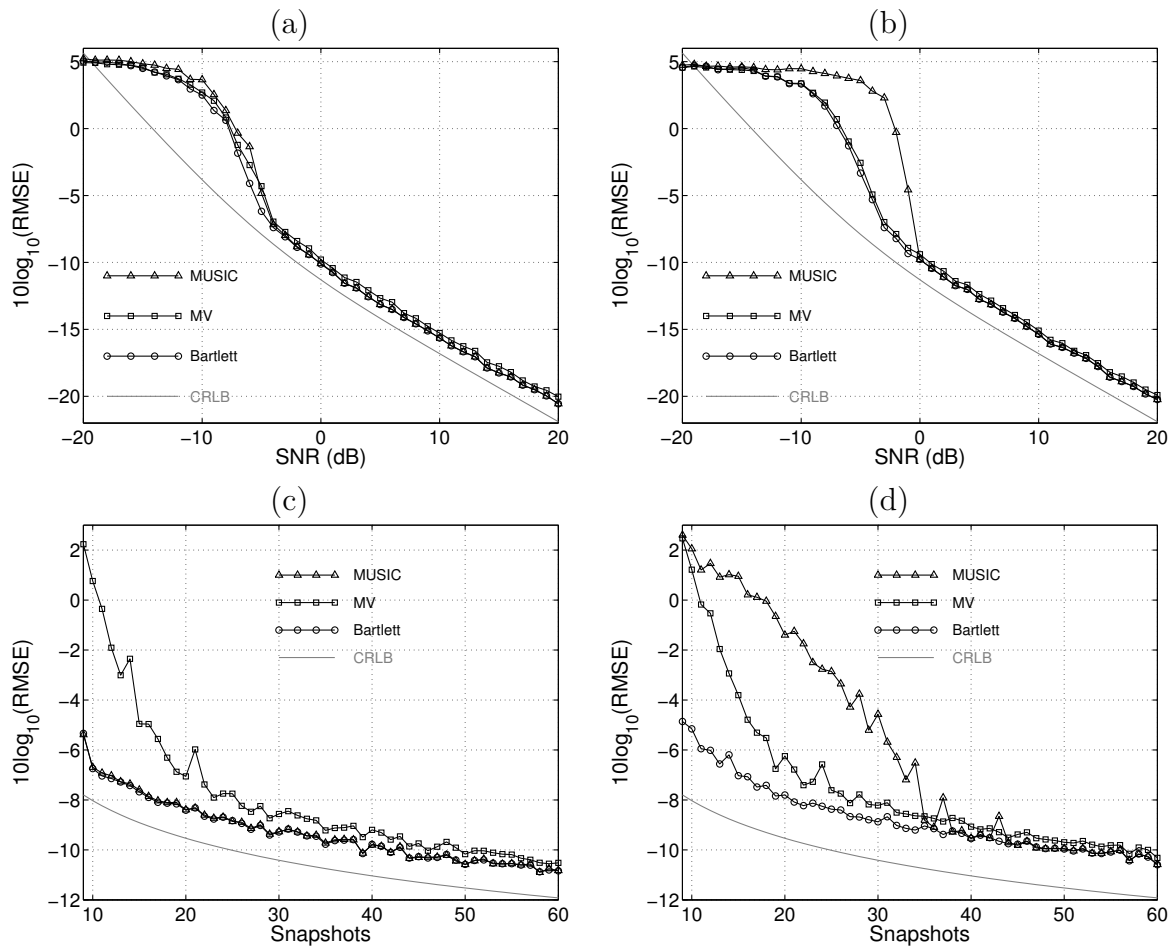
Figure 5.7: The RMSE for the three processors and the coherent model CRLB under comparison: (a) RMSE as a function of SNR with known signal matrix; (b) RMSE as a function of SNR with unknown signal matrix; (c) RMSE as a function of N with known signal matrix; (d) RMSE as a function of N with unknown signal matrix.

45. For figures 5.7(c) and (d) the SNR is 0 dB. The RMSE computed at each point is based on 100 estimates of parameter.

Figure 5.7(a) shows the RMSE of the three methods assuming known signal matrix and known dimension of the signal subspace. The performance is similar for all methods since the number of snapshots is relatively high in comparison to the dimensions of the SDM, and the signal structure is perfectly known. In figure 5.7(b) the signal structure and the signal subspace dimension are unknown, and must therefore be estimated together with the parameter. It can be seen that all methods performed worst than if the signal matrix was known, but the subspace based method in particular suffered a strong drawback. This is an

indication that it is fundamental to correctly separate the subspaces, since the signal subspace eigenvectors are used to estimate the signal matrix, and the noise subspace eigenvectors are used in the matched-field processor itself. In figure 5.7(c) the RMSE is computed against the number of signal realizations with SNR=0 dB, known signal matrix and signal subspace dimension. It is interesting to verify that the MUSIC processor and the Bartlett processor perform equally when the signal matrix is known, for any number of snapshots. On the other hand the minimum variance processor has poor performance when the number of snapshots is low and recovers comparatively to the others as the number of snapshots increases. This result is consistent with that obtained in section 5.2 (Figure 5.4), and further confirms that good estimates of the eigenvalues are required in order to accurately invert the SDM. Finally, in the case of unknown signal matrix and signal subspace dimension, it can be seen in Figure 5.7(d) how the low number of signal observations can impact on the performance of subspace based method, in particular the separation of the subspaces, in a conjunction of low SNR and low number of snapshots. The MV processor receives the same comments as in the previous case.

One of the fundaments of MFP is the degree of uniqueness of the acoustic field, i.e., how *different* a field generated for a given value of a physical parameter is to those fields generated with other values of the physical parameter. Such uniqueness will rule the sidelobe level of an ambiguity surface accounting for a certain search space. One common figure of merit is the peak-to-sidelobe ratio, which can be seen as a measure of global performance. Figure 5.8 shows a set of ambiguity surfaces of α_1 and α_2 calculated with the Bartlett processor. In the diagonal are the auto-frequency ambiguity surfaces, and off-diagonal are the cross-frequency ambiguity surfaces. It is seen that the ambiguity level in the auto-frequency surface is
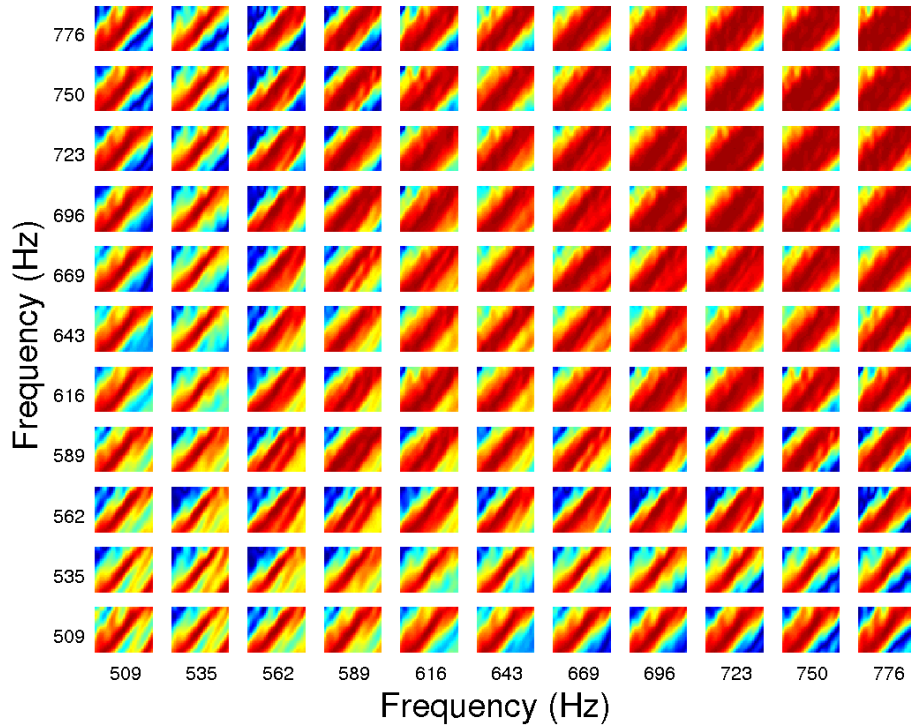
Figure 5.8: Ambiguity surfaces against α_1 and α_2 computed using cross-frequencies.

increasing with frequency, which is determined by the given physical conditions. The most relevant fact to be pointed out is that the off-diagonal ambiguity surfaces have less sidelobe structure than those in the diagonal, in particular, when the frequencies are well apart. The ability of cross-frequency processors in attenuating the sidelobe structure in comparison to conventional processing has been claimed in the literature in several occasions [75, 80]. This ability, generally observed for any set of free parameters, can be seen as a field uniqueness enhancement since the field at two frequencies is involved in the correlation.

5.4 Time-variant propagation channel

Time-invariance is one of the key assumptions in the modeling of signals in many parameter estimation problems. This assumption is usually made for the sake of simplicity in the development. This is, indeed, only an approximation of the reality. A careful observation

of the acoustic field can take the experimenter to the conclusion that in fact some features evolve during the observation time. In some experimental setups, such as those designed for the MREA experiments, the experimenter knows that, in particular, geometric parameters can evolve at a high rate. First, the ship towing the source is moving during part of the transmissions, where the speed projection in the 2-D plane containing the VLA and the source attained more than 100 m/min. Then, one should have into account that variations in absolute ship speed induce variations in the source depth. Second, the VLA was deployed in a free drifting configuration, with sea currents dragging the VLA away from the point of deployment. The average dragging speed of the VLA attained 4 m/min. Finally, environmental parameters are subject to vary during the observation time. As it can be seen, there is a great deal of possible change in the propagation channel during the observation time, specially due to changes in the geometric parameters.

The question is which impact such change in the channel parameters may have on the received signals, more precisely, considering the broadband data model under the assumption of time-invariance, which is the impact on the signal matrix $\mathbf{C}_{SS}$. Figure 5.9 shows a set of signal matrices estimates obtained with synthetic data. The data was generated assuming a source at 6 km range suffering a displacement during an observation time $T = 60$ s, with $\Delta T = 1$ s. The source displacements are respectively of 2, 7, 12, 16, 21, 26, 31, 35, and 40 m. The SDMs were generated as

$$\mathbf{C}_{YY} = \frac{1}{N} \sum_{n=1}^{N} \mathbf{H}(R_s^n) \mathbf{1} \mathbf{H}^H(R_s^n) \tag{5.4}$$

where R_s^n represents the source range at snapshot n. The data was generated in the frequency band 900-1200 Hz with a resolution of 10 Hz. For estimating the signal matrix, the channel matrix was filtered using the field obtained for $n = \frac{N}{2}$, which is midway between the initial
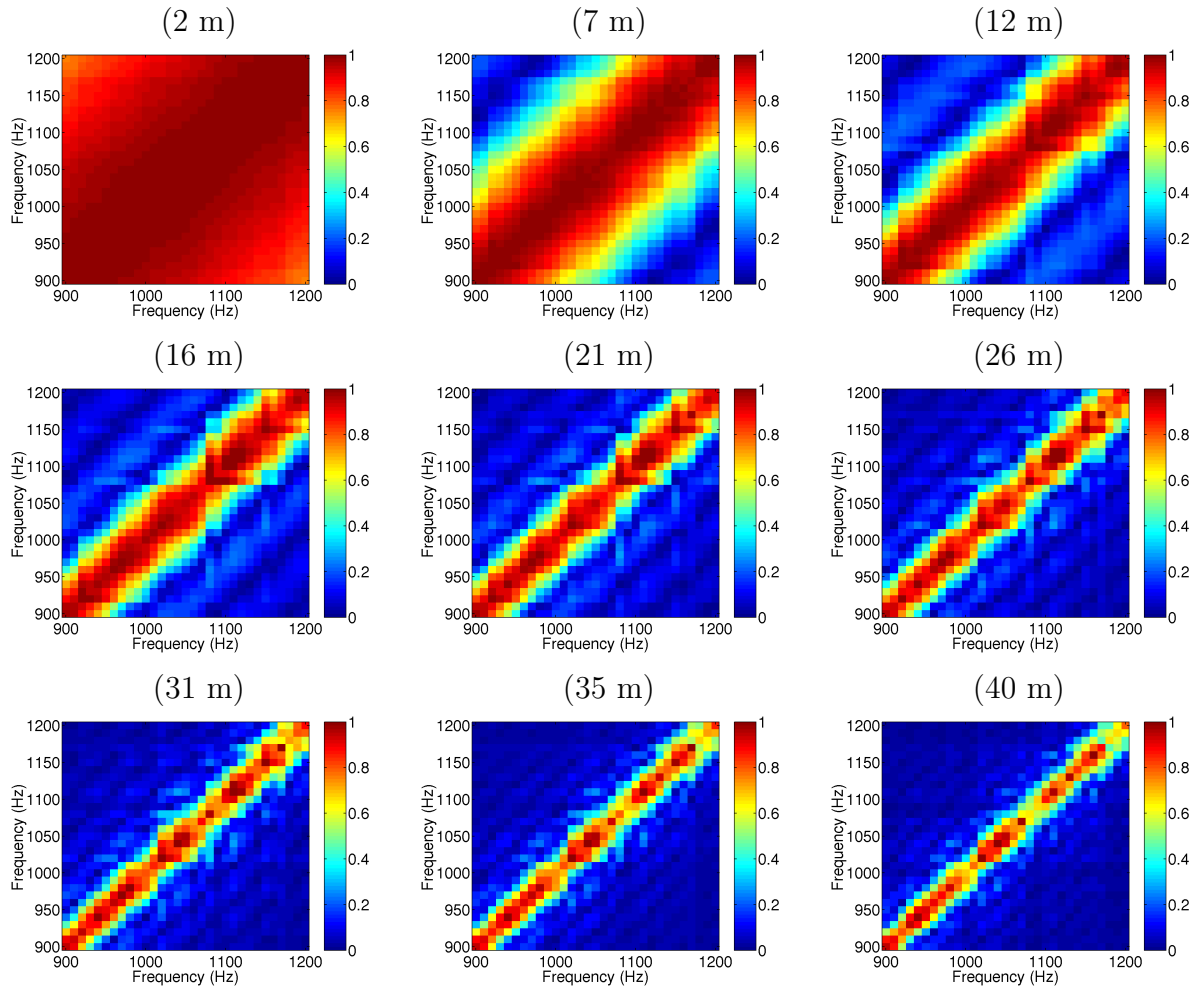
Figure 5.9: Signal matrix estimates obtained from synthetic data considering increasing source displacement during the observation interval.

and final position. It can be seen that the signal matrix suffers increasing diagonalization for increasing source displacement. For a displacement of 2 m it can already be noticed that the matrix values far from the diagonal already suffer some attenuation. For a displacement of 7 m it can be observed that cross-pairs with frequencies more than 100 Hz apart are significantly attenuated, and cross-pairs with frequencies more than 150 Hz apart almost completely vanished. For a displacement of 26 m even the auto-correlation terms degrade. It is indeed interesting to verify that for a certain amount of source displacement frequencies in a neighborhood preserve a degree of coherence/correlation.

Another exercise performed in the context of parameter variability was the application

of coherence restoration proposed in section 4.6. Figure 5.10 compares the computation of
the SDM $\mathbf{C}_{YY}$ without and with phase normalization. The initial range is 6 km and the
final range is 6.02 km in 36 steps. The SDM was computed for frequencies in the band
900 to 1300 Hz, with a resolution of 50 Hz, using 4 receivers - this results in $KL = 36$. To
perform the phase normalization, the correlation matrix in (4.44) was calculated for choosing
the receiver with best correlation with the remaining receivers as reference, as explained in
section 4.6. Figure 5.10 (a) shows the matrix computed as indicated by equation (5.4)
and that in figure 5.10 (b) uses identical calculation, however, with a phase normalization
using a reference receiver. While the former tends to have the energy concentrated on
the diagonal blocks, indicating that the energy in the cross-terms vanished due to loss in
spectral coherence, the latter shows energy well spread over the whole matrix. One can
think of the normalization scheme as an algorithm that freezes the phase at the reference
receiver and (a significant) part of the phase drift at the other receivers. This enables
the matrix computation to be carried out much more coherently preventing therefore loss
of cross-frequency energy. In terms of eigenvalues it can be seen that the normalization
scheme strongly enhances the dominance of the first eigenvalue, clearly reducing partitioning
of energy into different eigenvectors (see figures 5.10(c) and (d)). Finally, the broadband
Bartlett processor was applied in both cases. Plots in figures 5.10(e) and (f) differ not only
in the fit obtained for the maximum, but also in terms of sensitivity, demonstrating the
benefits that can be obtained by the phase normalization inducing high cross-correlation.
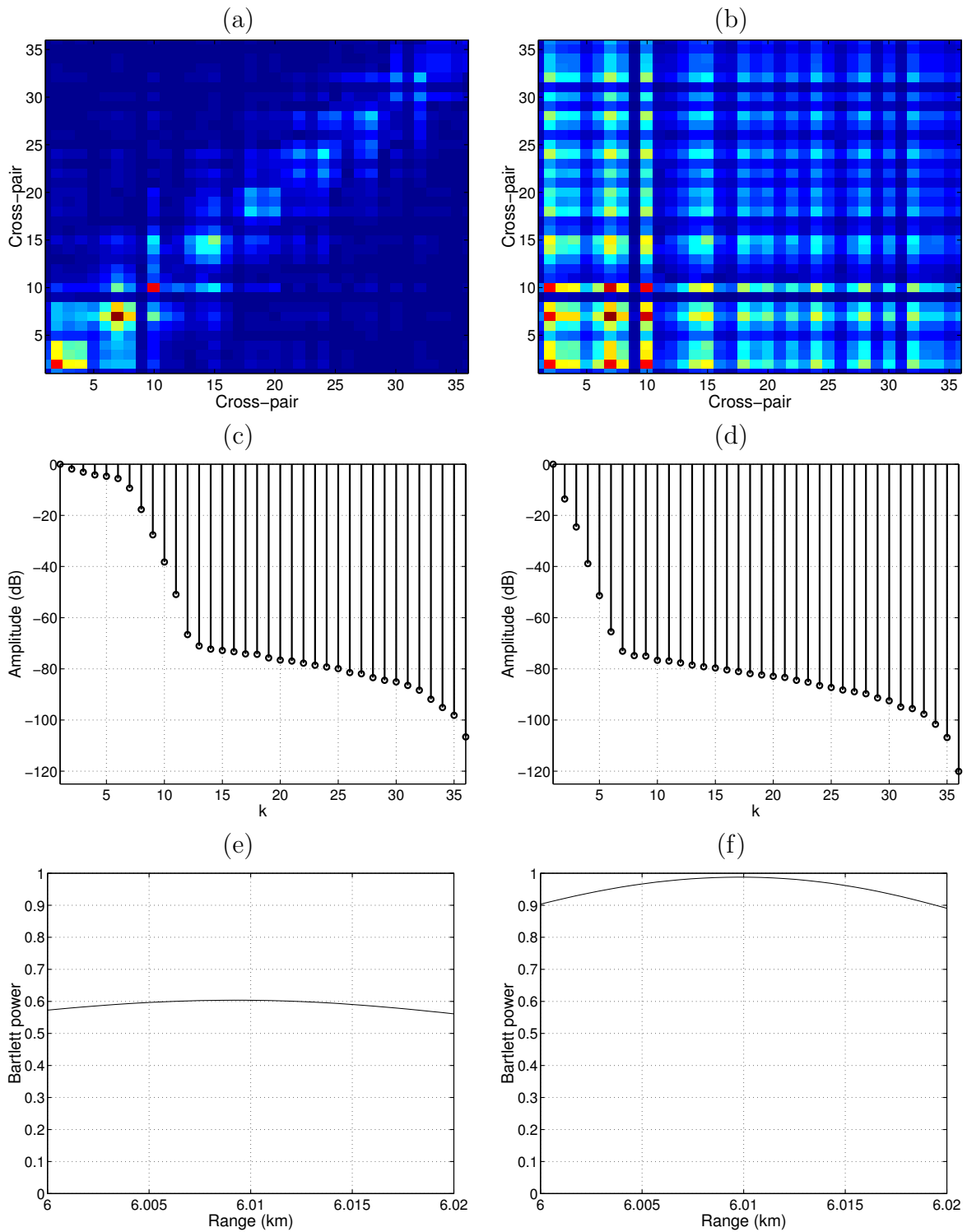
Figure 5.10: Comparison of standard computation of cross-frequency SDM (left column) and computation with phase normalization (right column): cross-frequency SDMs ((a) and (b)); eigenspectra ((c) and (d)); application with Bartlett processor ((e) and (f)).

5.5   A parameter sensitivity study

Performing a sensitivity study gives insight regarding the choice of the quantization and the

accuracy to which each parameter can be estimated. The sensitivity of the acoustic response

to variations of given parameters is case dependent. It will depend on the physical conditions and on the experimental setup, but also on the frequency band. The sensitivity to a given parameter rules its observability, i.e. the accuracy to which it can be determined, or if it can be determined. The sensitivity is also dependent on the cost-function being used.

This, in association with the degree of knowledge will condition the choice of the parameter search space - there is an important trade-off between *a priori* knowledge, sensitivity, ambiguity, and search space. Figure 5.11 shows the sensitivity plots corresponding to all parameters subject to enter the search space. The cost-functions correspond to the proposed processors: BB Bartlett (black); BB MV (darkgray); BB MUSIC (lightgray). They all are coherent and the signal matrix is known. The MUSIC processor is implemented in its altered fashion (equation (5.2)) with $\gamma = 0.01$. It can be noticed that the three processors have different abilities to discriminate the right value of each parameter. The Bartlett processor is comparatively weak, with particular difficulties for some of the seafloor parameters. Those parameters are likely to be erroneously estimated in the presence of a realistic noise level. The other two processors show a discrimination ability that can be judged to be sufficient for obtaining good quality estimates (provided that the physical model is sufficiently accurate). However, these simulations also indicate that, for example in a multi-parameter estimation problem, if some erroneous *a priori* information enters the inversion then it is likely that the data inversion process will miss to correctly find the true parameter vector, making it possibly mandatory to include every uncertain parameter.

In the next section it will be shown how the sensitivity can affect inversion quality when global methods are implemented in multi-parameter search problems.
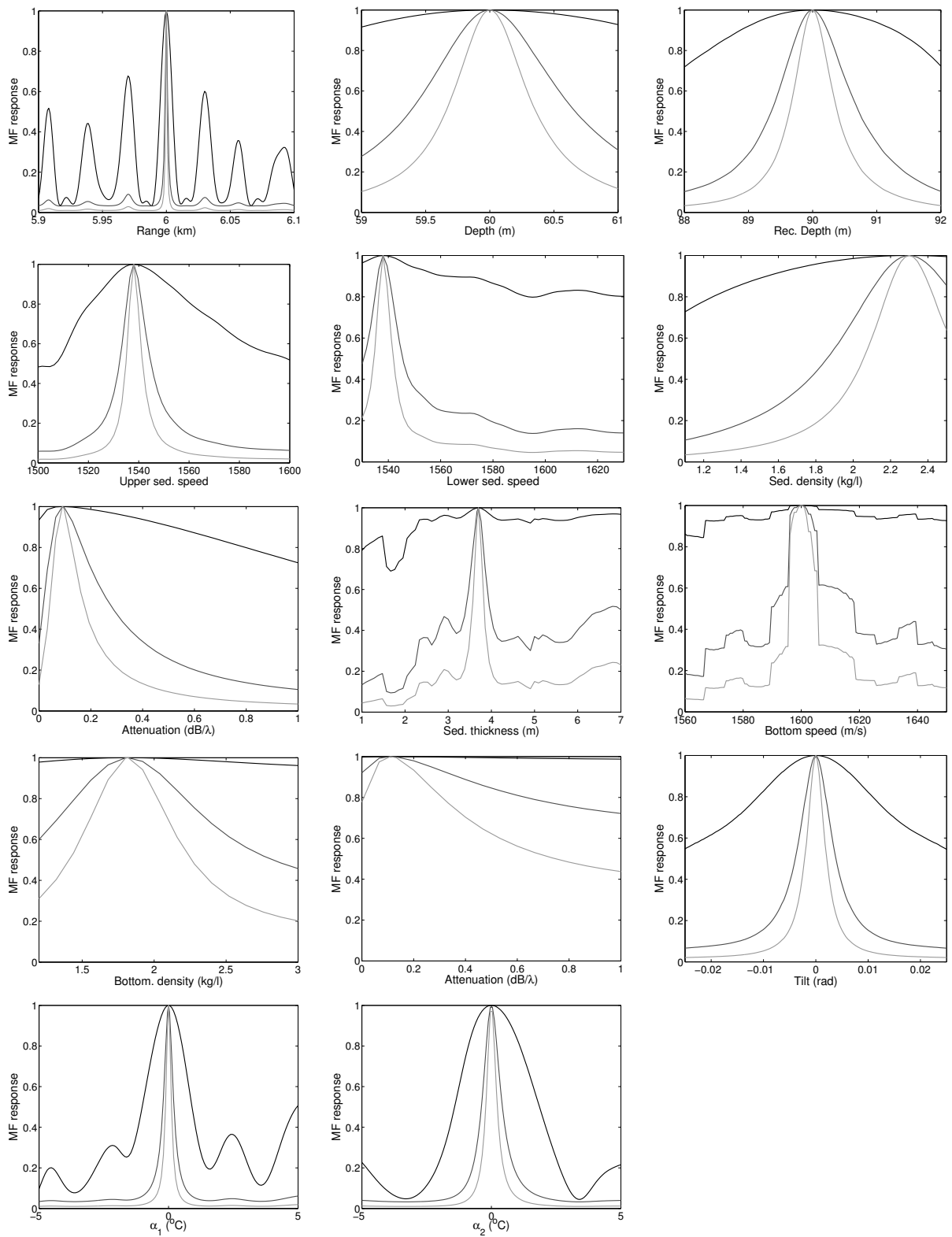
Figure 5.11: Sensitivity of the processors to the channel parameters: BB Bartlett (black); BB MV (darkgray); BB MUSIC (lightgray). The processors are all coherent with known signal matrix.

5.6   MFP and global search

In this chapter numerical characterization of the three proposed MF processors is carried out. They are compared in terms of sensitivity and in terms of error performance. The computer simulations in section 5.3 indicate how each processor performs under different signal assumptions, only in terms of local performance. The idea is to solve the most complicated problem, which is the estimation problem when multiple unknowns are present. The exercise is to conclude about the performance of each method when it is used in a global optimization problem using a global search method. A series of synthetic data inversions were carried out in order to make the comparison of the different methods with several choices of the number of snapshots N. Such choices are related to the number of signal realizations to be used with real data or with observations done during the local errors study (section 5.3). The idea is to complete section 5.3 in a more realistic scenario such as tomographic inversion. The general conditions for synthetic data generation are the same as those used in the sections above with an SNR of 0 dB. For each pair processor/N the data was generated and inverted 20 times. The inversion search space regarded the watercolumn and the seafloor properties, but array tilt was also included. The signal matrix and the subspaces' dimensions were known. Figure 5.12 shows several plots reporting the RMSE obtained for N equal 9, 12, and 45, and the three different processors, giving therefore 9 cells in each plot. The RMSE error is computed using the overall best individuals along independent populations. Ideally the RMSE should reduce with increasing number of snapshot and it would be expected that the methods with highest resolution would outperform those with lowest. However, this is not observed in all cases. First, the number of inversions performed for each case might not be sufficient to obtain a representative statistic, accompanied by the possibility
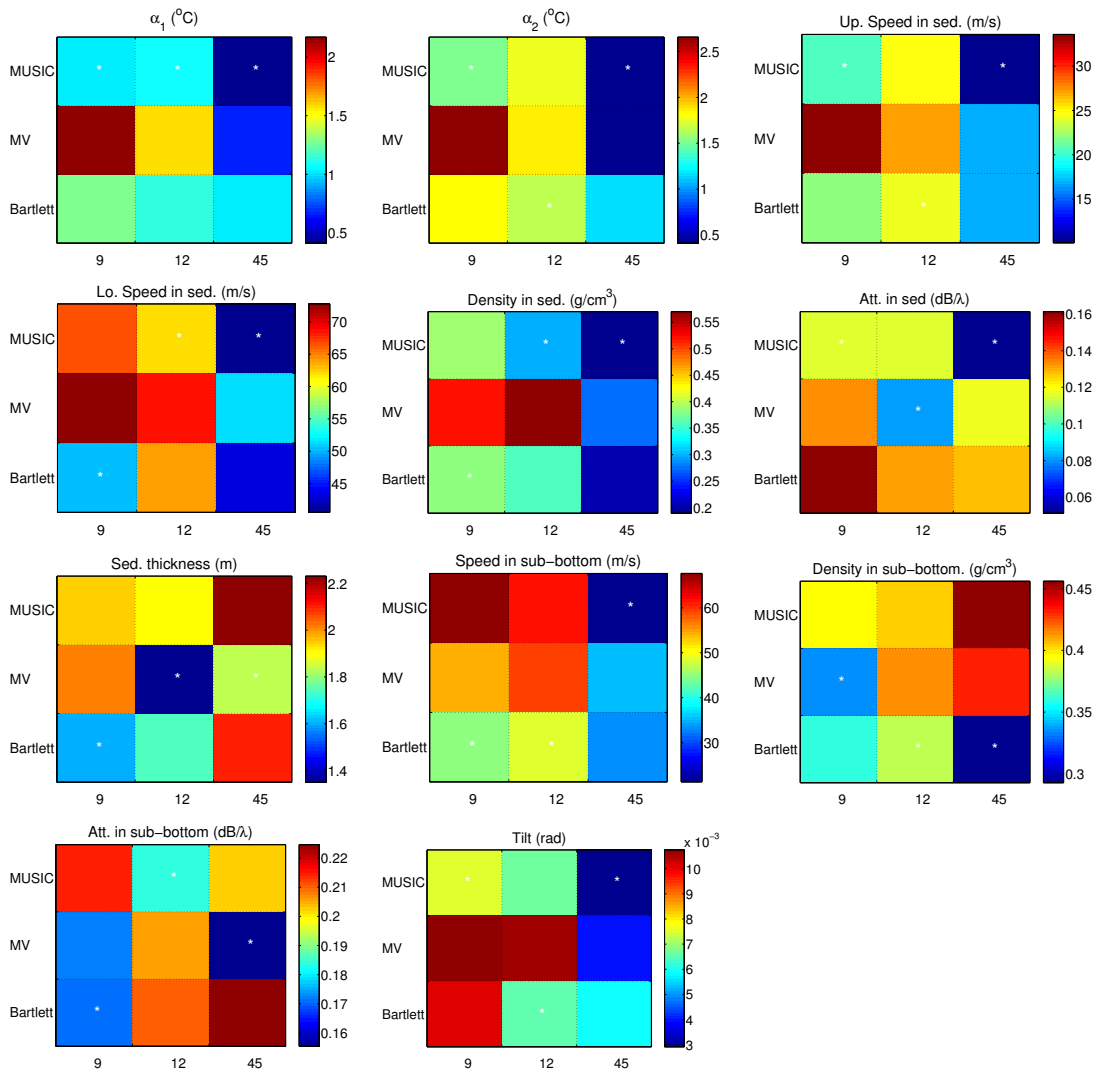
Figure 5.12: RMSE obtained during inversions with GA for the different parameters combining the three processors with three values of the number of signal realizations. A white asterisk indicates the processor with lowest RMSE for that number of signal realizations.

of the GA, which is a stochastic global search method, introducing additional uncertainty.

Important parameters such as speed in the seafloor, sediment density and attenuation, tilt, and temperature evolved regularly with N. It can also be observed that in general the MV processor performed worst for 9 or 12 snapshots, while the Bartlett processor often produced the best result. For 45 snapshots the MUSIC algorithm performed best for the most important parameters. This comparison is completed with table 5.3 which shows for how many parameters each processor obtained the lowest RMSE for a given number of signal realizations. The MUSIC processor clearly tends to be superior in an overall appreciation.

	$N = 9$	$N = 12$	$N = 45$
Bartlett	5	5	1
MV	1	2	2
MUSIC	5	4	8

Table 5.3: Number of parameters in which a processor obtained lowest RMSE for a given number of signal realizations (see figure 5.12).

In a direct comparison between the Bartlett and the MV processors, the MV processor is clearly superior for $N = 45$ (8 against 3).

Additional insight into the performance of the parameter inversion process can be obtained through the estimation of *a posteriori* distributions. These distributions emphasize the variability of each parameter over the search interval, which is intimately related to the ambiguity pattern of the cost-function used and the sensitivity to each parameter. The inversion problem has two main factors of complexity:

1. The size of the search space. A problem with a larger search space will yield solutions with higher uncertainty than a problem with a smaller search space.

2. The number of local maxima. A problem with a larger number of local maxima competing with the main maximum will yield solutions with higher uncertainty than a problem with less local maxima. Mitigation or attenuation of local maxima is one of the main motivations for studying the application of high-resolution methods in MFP.

Figure 5.13 shows the *a posteriori* distributions obtained using the individuals of the last GA generation of each independent population for the three methods. This corresponds to the case where the synthetic data was generated using 45 signal realizations. The first comment is that the MUSIC processor has clearly the narrowest distributions. In fact, the genetic algorithm could have a better convergence in that case, which confirms the discussion in section 2.5: the Bartlett processor has more false attractors, making convergence to the
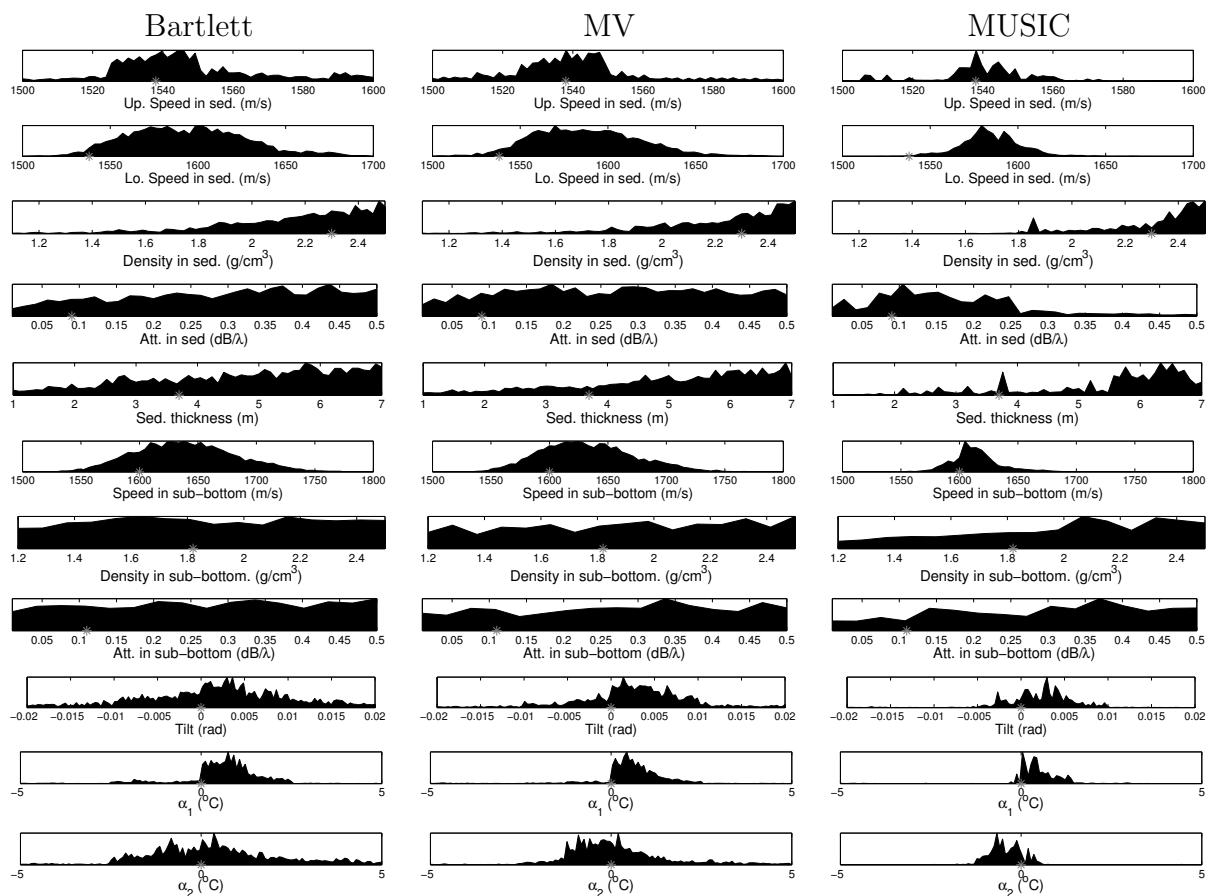
Figure 5.13: *A posteriori* probability distributions for each parameter based on the last genera-
tion of 20 independent populations. Each column respects to each of the processors entering the
comparison. The gray asterisks indicate the correct parameter value.

true solution more difficult. The second comment is that some bias relative to the true value

is seen in most distributions. This is particularly obvious for the distributions for tilt and

the EOF coefficients, which are high-ranking parameters. The suspicion is that the origin

for this bias is in the lower sediment sound-speed: upper and lower sediment sound-speeds

have a coupled parameterization in order to exclude models with a lower speed smaller than

the upper speed. However, both are 1538 m/s when the data is generated. Since the lower

sediment sound-speed is initialized uniformly in the interval 0 to 100 m/s a bias in the

distribution is induced. This could induce bias in cascade on the whole parameter space due

to the conditioning obtained at the first generation when the population is initialized. This

is an example where over-parameterization can create difficulties in the inversion process. In

terms of parameter hierarchy the sediment speed is of high rank. If the optimization process fails to converge to the correct value then other parameters will be conditioned to that. The MUSIC processor's *a posteriori* distributions have narrow peaks that for some parameters are very close to the right parameter value or at least allows to conclude that the genetic algorithm was able to converge to a solution close to the true solution. Convergence to the peak in the case of the MUSIC processor was a fundamental difficulty that could be overcome by implementing the MUSIC processor following equation (5.2). The MUSIC processor could in average determine particularly well sound speed in sediment and sub-bottom, EOF coefficients, and array tilt. Concerning the other two processors, these parameters have distribution peaks close to the true parameter with, however, a significantly higher spread.

5.7   Summary

In this chapter a collection of simulations was carried out with the main objective of comparing the three broadband processors and to test their performance under different working conditions.

First, in section 5.1, 2-D dimensional ambiguity surfaces of EOF coefficients were calculated for the three processors for combinations of coherent or incoherent signal assumptions with known or unknown signal, in order to become familiar with the expectable behavior of each processor. The coherent version with known signal provides always best peak-to-sidelobe ratio. However, the lack of knowledge on the signal clearly induces an increase of the sidelobe structure. The reason for this to happen is that the signal matrix must be jointly estimated with the physical parameters.

Sections 5.2 and 5.3 provide a comparison using finite data observations. In section 5.2

the evaluation is made in terms of the estimate standard deviations. In section 5.3 a local error analysis in terms of MSE is carried out. From this comparison the following conclusions can be made:

- The Bartlett processor performs always equal or better than the high-resolution methods, for any SNR or number of signal realizations.

- The MV processor performs as well as the Bartlett processor in the rich data case.

- The MUSIC processor performs as well as the Bartlett processor in the poor data case if the signal subspace dimension is known. If it is unknown it requires a high SNR or high number of data observations to perform as well as the Bartlett processor.

It was observed with synthetic data that the high-resolution methods are very sensitive to the quality of the SDM eigenvalues estimates, since these are used in an intermediate step before the MF response is calculated. A discrepancy between the assumed eigenspectrum and that estimated from the data is seen as statistical mismatch. These results were obtained by exhaustively searching for the solution with only 1 or 2 unknowns.

Sections 5.6 provides a comparison of the processors in an inversion problem with 11 unknown parameters. A genetic algorithm is applied to search for the solution. The test was carried out for the poor data case (9 and 12 snapshots), and for the rich data case (45 snapshots) at low SNR. The performance was evaluated in terms of MSE of the best individual independent populations, and in terms of *a posteriori* probability distributions using the last generation of each population. The following conclusions can be made:

- The MUSIC processor clearly tends to perform better than the others, and the MV processor tends to outperform the Bartlett processor in the rich data case.

- The MUSIC processor compares to the Bartlett processor in the poor data case.

This comparison indicates that although the high-resolution methods are not as robust in terms of statistical mismatch as the Bartlett processor, they may be very effective when the solution search has to be carried out via a global search method.

As a final remark on the comparison carried out in this chapter, it is understood that the difficulties encountered in the utilization of the MV and the MUSIC processor are mainly related to limitations in terms of SNR and number of data observation, with implications in the quality of the cross-frequency SDM eigenvalues estimates. In application to real data, the number of data observation might be an important source of difficulties.

Chapter 6

Experimental results I: Matched-field tomography on the MREA'03 data set

Environmental inversion of acoustic signals for water column and bottom properties has been proposed in the literature as an interesting concept for complementing direct hydrographic and oceanographic measurements for Rapid Environmental Assessment (REA) [93, 94]. REA is to provide environmental nowcasts and forecasts accurate and efficient enough to support operational activity in any arbitrary region of the global coastal ocean, and to respond to operational assessment requests effectively on very short notice.

MFT can bring interesting advances to REA as the result of acoustic inversions that can be assimilated into ocean circulation models tailored and calibrated to the scale of the area under observation [95]. Using sound in REA applications has been termed Acoustic REA (REA). Due to its high operationality requirements, traditional ocean tomography systems for their requirements of long and well populated receiving arrays and precise knowledge of the source/receiver geometries are not well adapted to operational Acoustic REA (AREA). The hardware involved in the reception of the acoustic signals must meet requirement of low-cost and easy deployment. AREA must also be able to assimilate *a priori* environmental knowledge such as seafloor properties, bathymetry and telemetry data like GPS positions

101

and acoustic source depth.

In order to respond to the above requirements, an innovative concept of AREA was proposed under a NATO Undersea Research Centre (NURC) Joint Research Project, named AOB-JRP, formally comprising the years from 2004 to 2006[1]. That concept included the development of water column and geoacoustic inversion methods being able to retrieve environmental true properties from signals received on a drifting network of Acoustic-Oceanographic Buoys (AOB). The AOB is a light acoustic receiving device that incorporates last generation technology for acquiring, storing and processing acoustic and non-acoustic signals received in various channels along a vertical line array. The physical characteristics of the AOB, in terms of size, weight and autonomy, will tend to those of a standard sonobuoy, with however the capability of local data storage, processing and online transmission [31, 96, 97]. There were only four acoustic channels in this first AOB prototype, AOB1. Using AOB1, a light receiving device, represents a challenge in terms of environmental parameter estimation. The number of receiving elements available is perhaps the most important factor determining the uniqueness of an inverse problem's solution in MFT. There is the inherent risk that the final model estimate might represent an acoustically equivalent but environmentally different model from the true model, leading to erroneous environmental parameter estimates. A difficulty associated to this is to validate model estimates when no concurrent ground truth measurements are available.

This chapter aims at analyzing and processing the experimental acoustic data collected during the Maritime Rapid Environmental Assessment 2003 (MREA'03) sea trial conducted in June 2003 off the west coast of Italy in an area at North of Elba Island [28, 50]. The

---

[1]the AOB-JRP was jointly submitted by the Université Libre de Bruxelles, Belgium, SiPLAB at University of Algarve and the Instituto Hidrográfico (IH), both from Portugal, and the Royal Netherlands Naval College (RNLNC), The Netherlands.

objectives of this chapter are the following:

- to provide an analysis of the received acoustic field regarding coherence across space and frequency, and observe the effects of source and array movement.

- to propose a frequency clustering algorithm, where highly coherent frequencies are clustered to form the cross-frequency spectral density matrix.

- to propose a data inversion procedure that includes a validation step by means of source localization in absence of ground truth measurements.

- to perform a comparison of the three BB processors applied to MFT, using field data collected on a sparse vertical line array.

The inverse problem will include watercolumn, geoacoustic, and array geometry parameters as unknowns. This will be regarded as active tomography since the knowledge on the source location will be used at all times.

6.1 The MREA'03 sea trial

In June 21st, the AOB was deployed on a free drift configuration with very favorable weather conditions in an area of mild bottom range-dependency. Fig. 6.1 shows the bathymetry at the experimental site together with the source-receiver geometry estimated from GPS recordings. The buoy was deployed at 11:01 local time and recovered at about 17:16. The bathymetric variability attained 20 m over some acoustic tracks, with 120 m waterdepth at buoy position and a maximum of 140 m waterdepth at source position. Source-receiver range varied between 500 up to 9 km (figure 6.2(a)). The acoustic source was deployed from the R/V Alliance at a variable depth between 54 and 106 m, depending on ship speed (figure
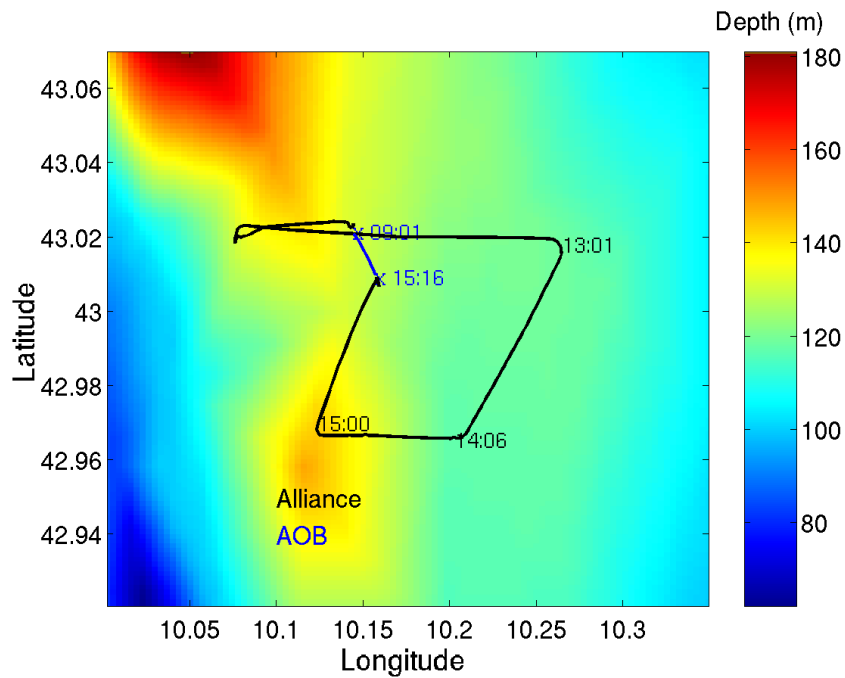
Figure 6.1: GPS estimated AOB and source ship navigation during the deployment of June 21st.
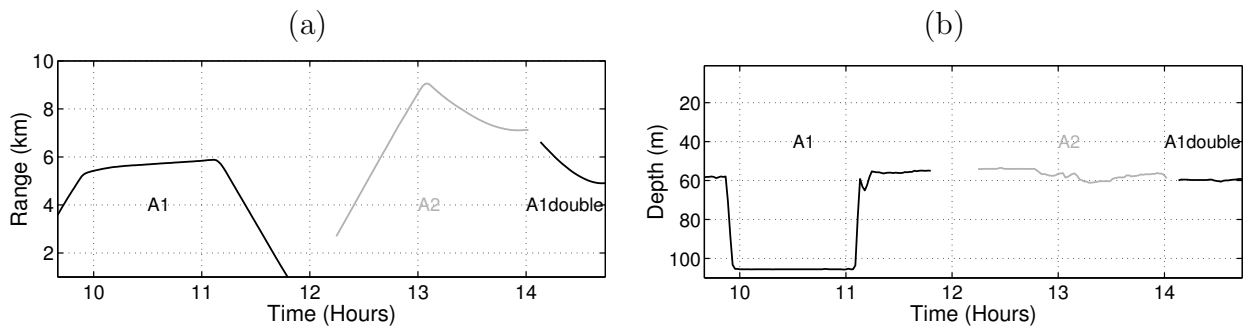
Figure 6.2: Source range (a) and depth (b) measured during the deployment of June 21st.

6.2(b)). The experimental setup consisted of a towed acoustic source and a free drifting VLA
with receivers at nominal depths of 15, 60, 75, and 90 m. However, the deepest receiver will
not be considered in this study due to extremely poor SNR during most of the experiment.

The data consists of LFM chirps of 2 seconds on two frequency bands. The signals
designated by "A1" and "A1double" are LFMs in the band 500 to 800 Hz; the signals
designated by "A2" are LFMs in the band 900 to 1200 Hz. Table 6.1 shows the emission
schedule.

	A1	A2	A1double
Start	09:40	12:14	14:07
End	11:47	14:01	14:44

Table 6.1: Signal emission schedule during June 21st. The times are in GMT.

6.2 The MREA'03 baseline model

One of the tasks with largest impact in the final result, is the choice of an adequate environmental model to represent the propagation conditions of the experiment. This choice is generally the result of a compromise between a detailed, accurate and parameter full model and a light model ensuring a rapid convergence during the processing. The baseline computer model adopted for the MREA'03 was built based on the segmentation of archival bathymetric information along the source-receiver cross sections at different times. Geoacoustic properties were drawn from a previous study in that area [13]. It consists of an ocean layer overlying a sediment layer and a bottom half space with the bathymetry assumed to be range-dependent, as shown in Fig. 6.3. The sound-speed profile was calculated using the Mackenzie formula in (2.1) with the mean temperature profile (figure 2.1(b)) and the mean salinity profile as inputs [50].

For the purposes of the inversion the forward model was divided into four parameter subsets: water column temperature, sediment, sub-bottom, and geometric parameters. Water column variability was characterized thanks to the CTD data acquired during the previous days as represented in Fig. 2.1(e) by a set of two EOFs.

6.3 Coherence and coherence restoration

Chapter 3 proposes a broadband data model defined in the frequency domain that provides the possibility of extending field coherence across the frequency band. In this context it
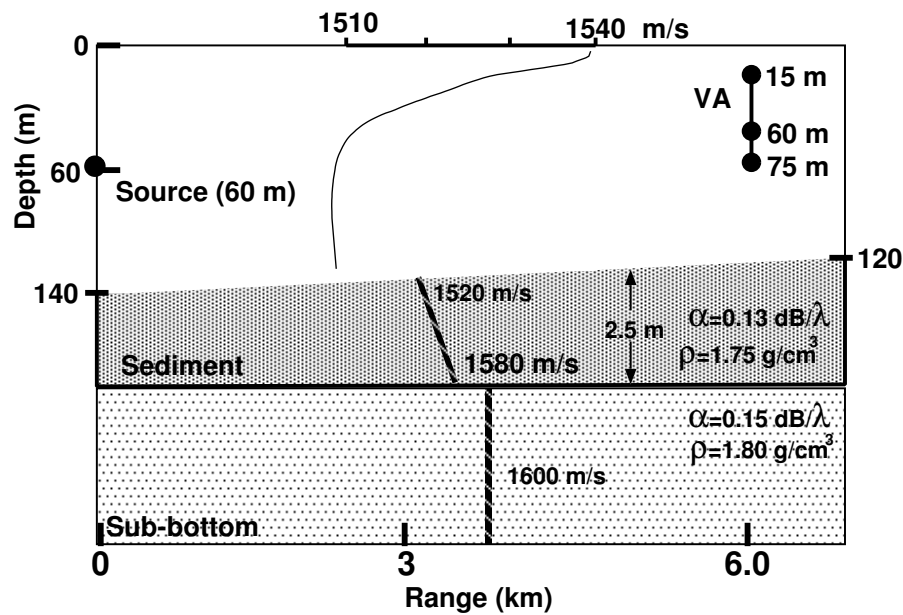
Figure 6.3: Baseline model for the MREA'03 sea trial. All parameters except waterdepth are range-independent.

is of interest to observe experimental data in the frequency domain. The analysis to be conducted in this section is essentially on the signal phases, since the main subject is on field coherence. The coherence is ruled by the signal phases at different points of space and frequency, and refer to the degree of correlation of their simultaneous evolution along time. For the broadband data model it makes sense to carry out this analysis both in space and frequency since it considers cross-relating data in space and in frequency. Figure 6.4 shows a set of plots with received signal phases for the receivers 1 to 3 at frequencies 910, 964, 1017, and 1071 Hz arbitrarily chosen. The phase at the first instant was set to zero for all receivers for better showing the perfect superposition of their variations. In fact, it is seen that in each frequency the signal phase perfectly superposes for the three available receivers, excluding the final part in frequency 910 Hz. This assures spatial coherence - the phases are highly coherent across space. For some time samples there are also common variations at different frequencies. Roughly, one can say that there is spectral incoherence and spatial coherence. The analysis above does not allow to learn on the frequency cross-correlations.
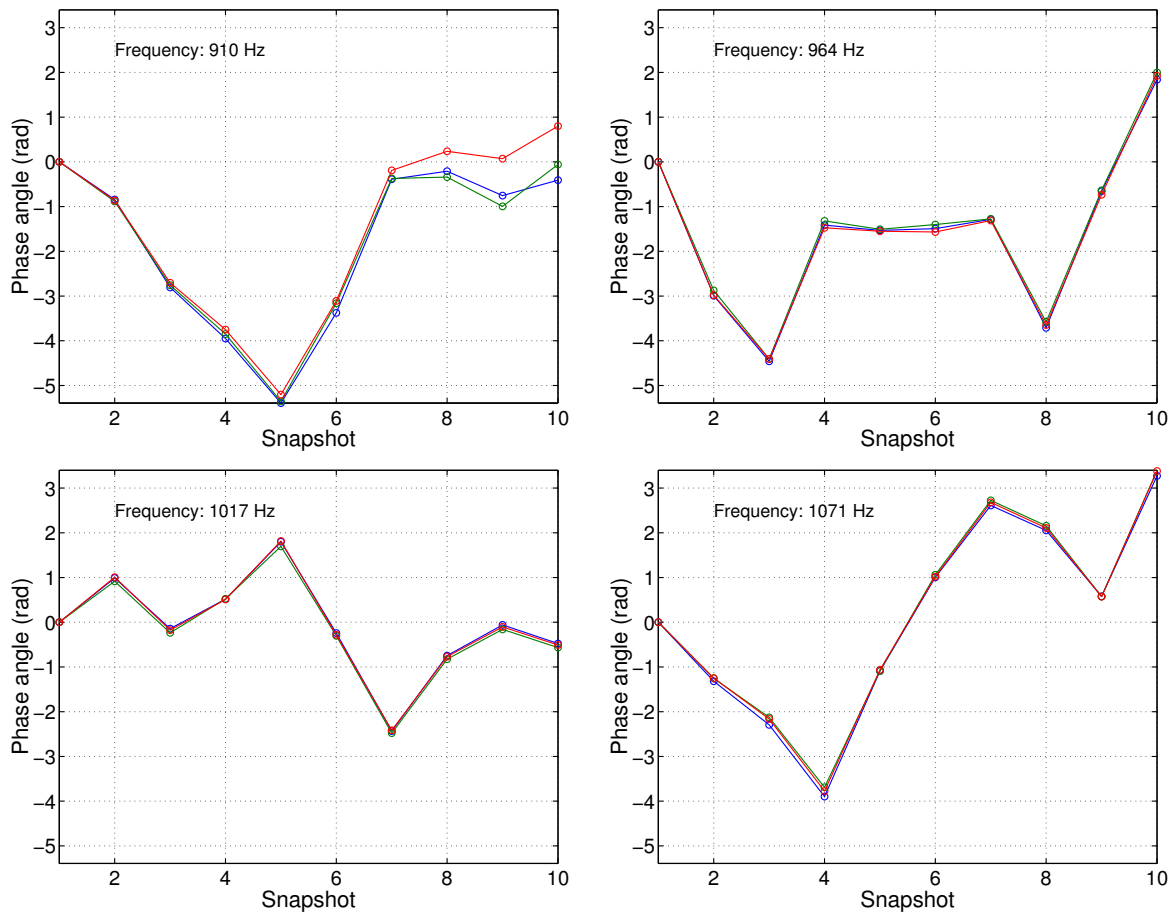
Figure 6.4: Observations of phases over time for receivers 1 to 3 at frequencies 910, 964, 1017, and 1071 Hz.

To support the proposed data model it is fundamental to observe the second-order behavior for space-frequency pairs. Figure 6.5 shows several correlation matrices chosen such that different correlation patterns were available for analysis. To avoid different powers at different receivers and frequencies all elements in the main diagonal are normalized to 1. It can be seen that all have a diagonal that diverges strongly in terms of width from case to case. It is interesting to verify that secondary diagonals rise significantly, showing the presence of strong cross-correlation between separated frequencies. It is also interesting to determine what is influencing the correlation pattern so significantly. The degree of correlation is related to the changes that occur in the received signals during the observation time interval. Table 6.2 shows times, ranges, and ship-speeds relative to the data shown above. The ship-speed is
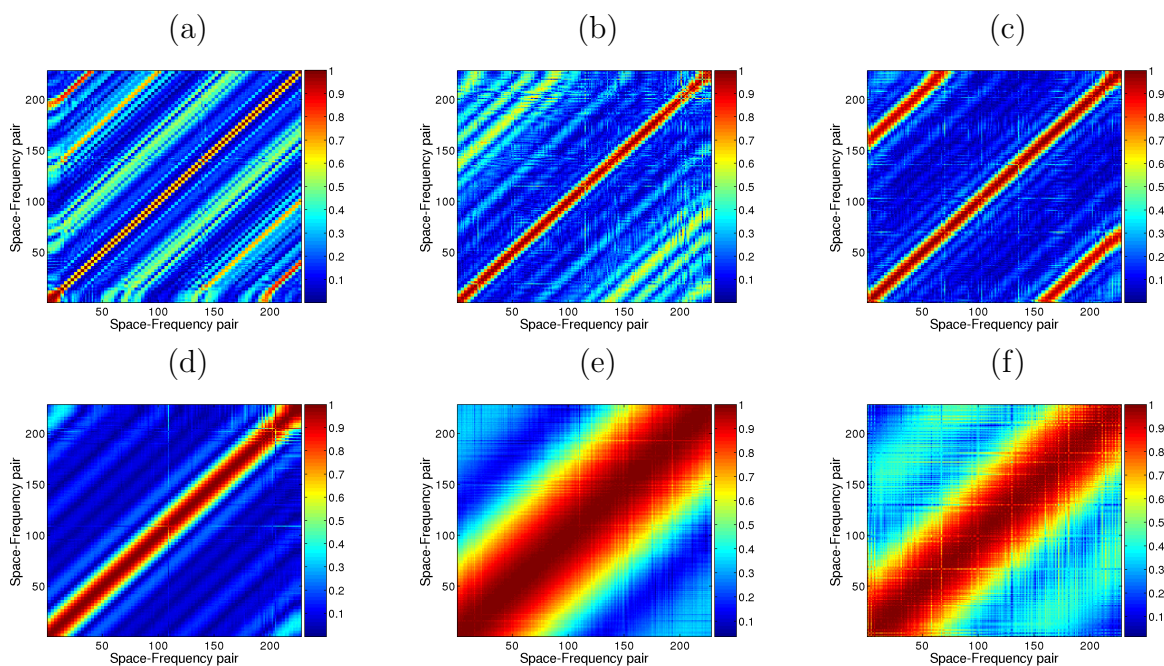
Figure 6.5: Diagonal normalized cross-frequency SDMs obtained for different source ranges and speeds (see table 6.2).

the projection of the absolute ship speed in the 2-dimensional propagation plane containing source and receiver array. It can clearly be seen that the speed has a strong impact on the correlation pattern. For case (a) a very narrow diagonal is obtained. It can be seen that a strong secondary diagonal far from the main diagonal is present. Then the speed drops to almost one third and a well pronounced diagonal is obtained (case (b)). Also several secondary diagonals are seen. During the following cases the speed keeps gradually dropping until it reaches the minimum speed yielding at the same time the widest diagonal (case (e)). Note that the diagonal is well bounded since beyond it, the correlations fall off to almost zero. Finally, in case (f), a slight rise in the ship speed causes the diagonal to narrow slightly together with a raise of the correlation at other points. It is important to note that the statistical properties of the received signals are imposing a bound on the maximum performance eventually attainable by any method to be applied. Thus, the coherence across frequencies is extremely important to promote the local performance and the ability of any

Plot	Time (H)	Range (km)	Speed (m/min)
(a)	12.36	3.58	134
(b)	13.32	8.26	53
(c)	13.46	7.81	46
(d)	13.70	7.28	23
(e)	13.90	7.11	4
(f)	13.99	7.13	12

Table 6.2: Times, source ranges and source speeds respective to the plots in figure 6.5.

matched-field processor to attenuate the sidelobes.

The spatial coherence can be used to restore the spectral coherence by normalizing the field through the phase of a reference receiver. The reference receiver is that with best average correlation with the other receivers as explained in section 4.6. Figure 6.6 shows the result of that normalization. Now it can be said that the spectral incoherence has almost completely vanished. In figure 6.3 are shown the results of such normalization. It is seen that all the matrices are nearly flat due to signals coherence restoration as it had been seen in section 5.4 with synthetic data.

6.4   Frequency clustering

The previous section has shown how the acoustic field is correlated across space and frequency, which justifies the use of the broadband SDM in (3.16). Emissions *A1* and *A2* consist of 2-second LFMs with a repetition rate of 8 s. The data recording interval is 80 s, which resulted in a number of snapshots $N = 9$ or $N = 10$. Emission *A1double* consists of double 2-second LFMs with a repetition rate of 10 s, which results in number of snapshots $N = 15$ or $N = 16$. Given the choice of using a number of receivers $L = 3$ and $K = 3$, i.e. $KL = 9$, and knowing of the existence of frequency-correlated frequencies, one can choose the frequency optimization scheme based on the ratio $\Lambda(\lambda_1, \lambda_2)$ (see equation 4.45). The
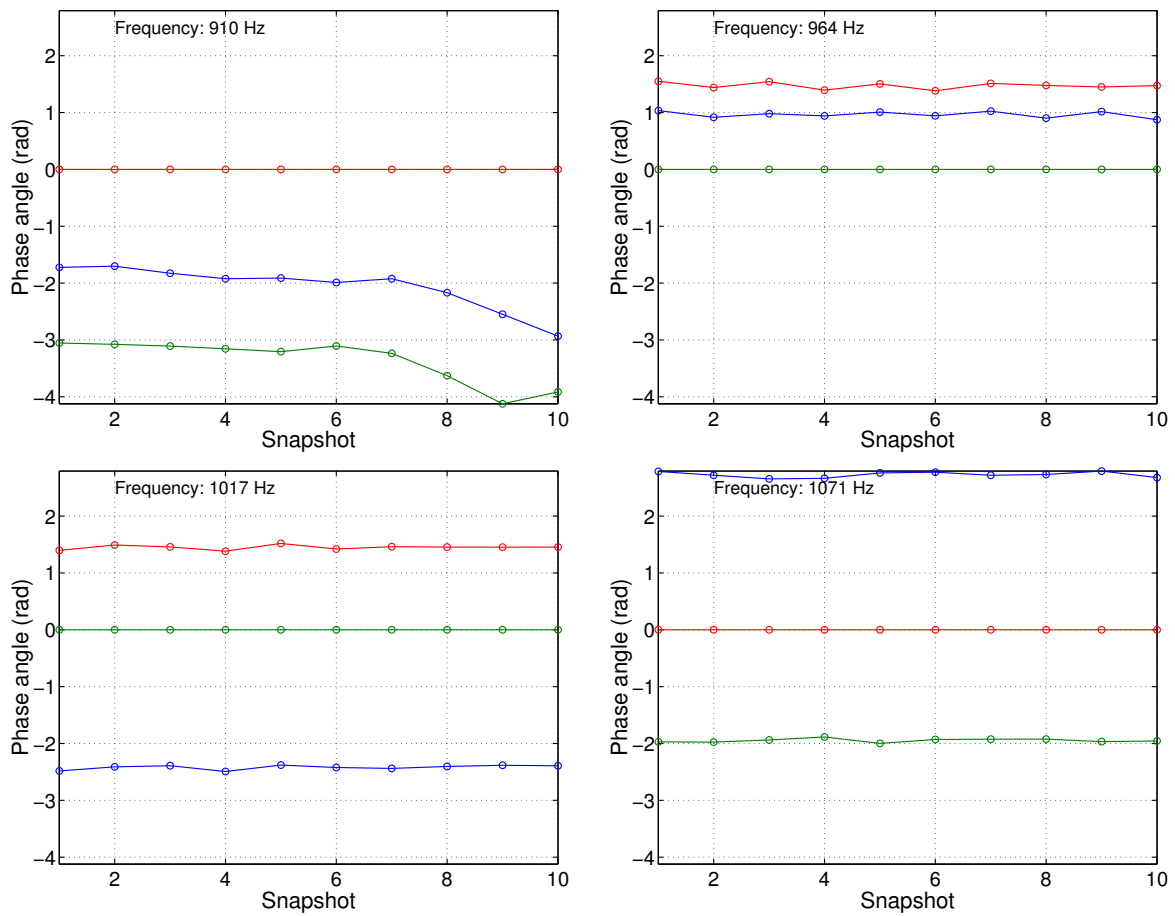
Figure 6.6: Resulting phases after applying phase normalization over time for receivers 1 to 3 at frequencies 910, 964, 1017, and 1071 Hz. The receiver with constant value of 0 is the reference receiver.
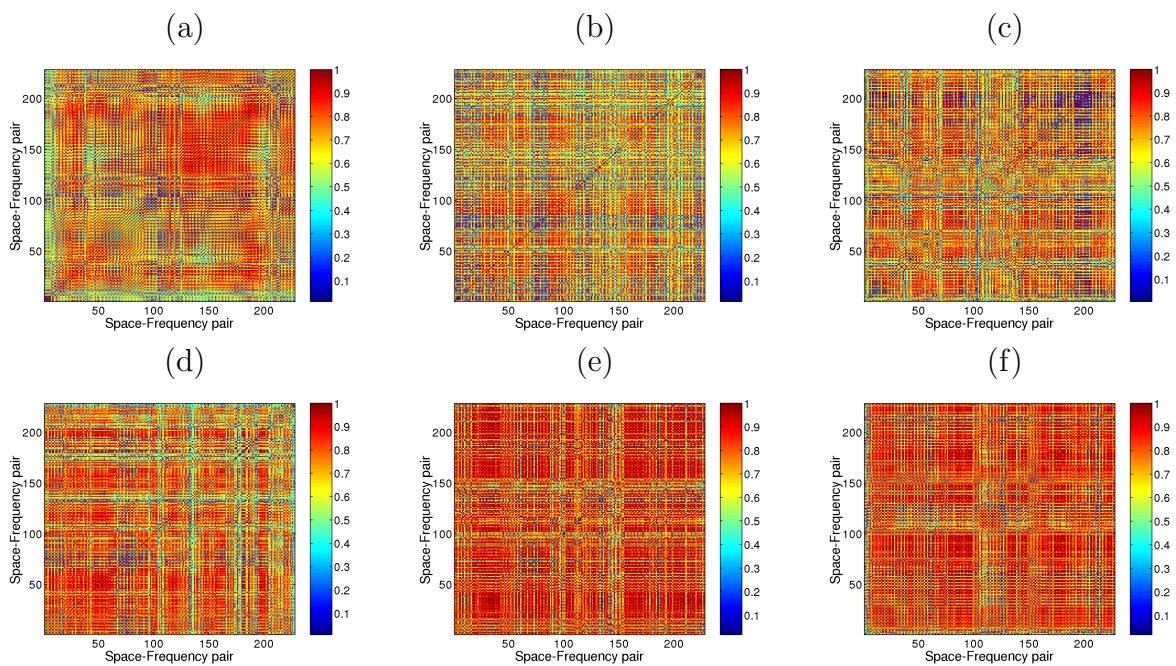
Figure 6.7: Cross-frequency SDMs with phase normalization obtained for different source ranges and speeds (see table 6.2).

reduced number of frequencies is linked to the low number of snapshots available, since it is required that the SDM must be full-rank. However, in order to overcome that limitation, it is possible to use $\mathcal{N}_g$ clusters of K frequencies. An alternative matched-field processor output is then given as

$$P^{\mathcal{N}_g}(\underline{\theta}) = \frac{1}{\mathcal{N}_g} \sum_{n=1}^{\mathcal{N}_g} P(\underline{\theta}, \underline{\omega}_n), \tag{6.1}$$

where $\underline{\omega}_n$ is the nth cluster of frequencies. Since $\Lambda(\lambda_1, \lambda_2)$ is a measure of the signals' coherence, $\underline{\omega}_1$ will be the frequency cluster with highest coherence, since the frequencies will be sorted decreasingly during the optimization, and only the $\mathcal{N}_g$ best ratios will be saved. The optimization algorithm included frequencies in the respective bands with a frequency resolution of 4 Hz. The optimization algorithm can be summarized as follows:

1. Compute $\hat{\mathbf{C}}_{YY}$ for $\underline{\omega} = [\omega_1, \ldots, \omega_k, \ldots, \omega_K]$;

2. Compute the λ_i;

3. Compute $\Lambda(\lambda_1, \lambda_2)$;

4. if $\Lambda(\lambda_1, \lambda_2)$ falls among the $\mathcal{N}_g$ best ratios then save $\underline{\omega}$;

5. Step $\underline{\omega}$;

6. Goto 1.

The effect of this algorithm is to cluster frequencies such that the maximum coherence is obtained between frequencies to be processed together. There is also a tacit assumption that frequencies in different clusters are uncorrelated. For the current data an additional constraint was added: in order to assure frequency diversity, frequencies were separated by at least 52 Hz. Figure 6.8 shows histograms along time for the frequencies belonging to the

$$f_1$$

$$f_2$$

$$f_3$$
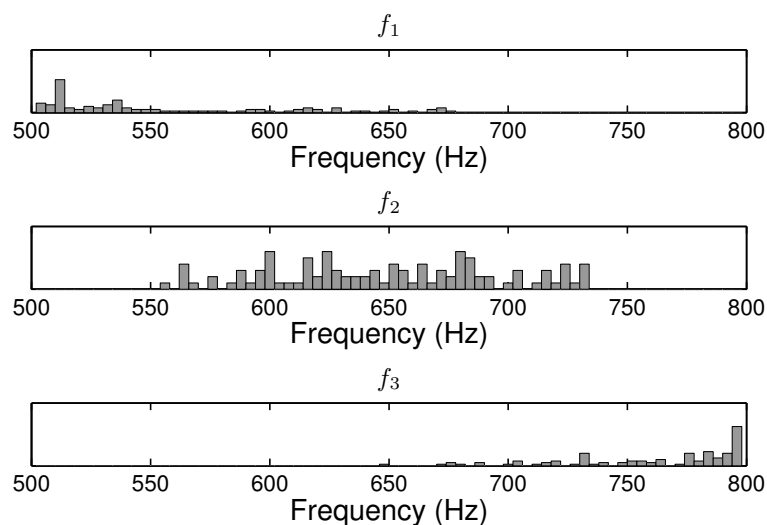
Figure 6.8: Histograms showing how the components of the optimized frequency vector are distributed.

best cluster. The effect of the constraint on the frequency selection along the band is clearly visible. For example f_1 cannot assume values in last third of the interval. Apart from the constraint, the optimization procedure tends to choose frequencies close to the lower bound of the frequency band for f_1. f_2 is close to a uniform distribution, and f_3 has a peak close to the upper bound. In theory, a higher degree of coherence at lower frequencies is expectable due higher wavelengths. However, in practice, lower frequencies are more corrupted by noise than higher frequencies, which might explain the histogram obtained for f_3.

6.5   Data processing procedure

This section explains the general procedure applied for the processing of the data collected during the MREA'03 experiment. Several steps are performed until the MFT procedure is complete:

1. Frequency selection by optimization criteria based on the eigenvalues of the SDM, or direct frequency selection with coherence restoration if necessary.

2. Acoustic field inversion by means of environmental focalization for all unknown envi-

ronmental parameters and nuisance parameters such as geometric parameters related to the array (e.g. tilt and receiver depth).

3. Inversion validation by means of source localization with large bounds using estimated environmental models.

4. Reconstruction of physical parameters of interest using only environmental estimates validated in step 3.

These steps will be explained in detail in the following. For the MREA'03 data set the frequencies were optimized using the $\Lambda(\lambda_1, \lambda_2)$ cost-function (see section 6.4).

For the inversions to be performed it will be assumed that all parameters of the three-layer environmental model are unknown. Table 6.3 shows the parameters to be searched as free unknowns, with their search bounds and number of quantization steps. They are divided into watercolumn, sediment, sub-bottom and geometric parameters. The geometric parameters are simply regarded as nuisance parameters, since there is absolutely no interest in their values once the MFT procedure is finished. The parameter vector is coded in 68 bits which results in a search space size approximately equal to 2.95×10^{20}. To perform the search, a GA has been used [98]. The GA settings are summarized in table 6.4. Given the density of the processed data along time and the nature of this study only a single population is used for each inversion. Also the number of generations is quite conservative.

Step 3 is to validate the model estimates obtained in Step 2. The true values of the environmental parameters are unknown. But the source location is known and is held fixed during step 2. The source location is at the top of the parameter hierarchy and is known with very high accuracy, which is a fortunate conjunction. Since MFP has been credited to

Model parameter	Lower bound	Upper bound	Quantization steps
Water column			
$\alpha_1(°C)$	-15	15	128
$\alpha_2(°C)$	-7	7	128
Sediment			
Up. sediment speed (m/s)	1470	1560	64
Lo. sediment speed (m/s)	0	100	64
Sediment density (g/cm³)	1.2	2.5	64
Sediment wave att. (dB/λ)	0.01	0.5	32
Sediment thickness (m)	2	6	64
Sub-bottom			
Sub-bottom speed (m/s)	1	100	64
Sub-bottom density (g/cm³)	1.2	2.5	16
Sub-bottom wave att. (dB/λ)	0.01	0.5	16
Geometric			
Receiver depth (m)	74.5	76.0	16
Tilt (rad)	-0.025	0.025	64

Table 6.3: GA forward model parameters with search bounds and quantization steps for MFT.

Parameter	Setting
Generations	30
Population size	200
Independent populations	1
Mutation probability	0.004
Crossover probability	0.9
Number of crossover points	4

Table 6.4: GA settings for MFT.

be extremely dependent on the environmental knowledge and therefore sensitive to environmental mismatch, the result of a source localization step with large search bounds should be a good indication on the quality of the estimated environmental model. If significant environmental mismatch is present then it is very likely that the maximum of the ambiguity surface appears at the wrong location.

Finally, in step 4, the environmental estimates corresponding to correct source localizations are used for providing environmental estimates along time.

The next section will apply MFT on the data collected during the MREA'03 sea trial.

6.6 MFT on the MREA'03 data set: performance comparison of three processors

In chapter 5 computer simulations aiming at characterizing the three MF processors were performed. Good indications were given regarding the processors' performance, in particular, the high-resolution methods. On one hand the computer simulations have shown that the high resolution methods perform poorly in the presence of noise when the number of signal realizations is low. On the other hand they seem to enable the GA to perform better in converging to the true solution.

For inverting the data, signal matrix $\mathbf{C}_{SS}$ is assumed unknown. But since the frequencies were optimized in the sense of clustering those with highest coherence, it was decided to assume that the signal subspace dimension M is equal to 1, although the source is moving most of the time, and the total observation time is about 80 s, which can be considered long when the source speed is high (see figure 6.5). That choice is also related to the fact that a low number of signal realizations disables an Information Criterion (e.g. the MDL criterion, eq. (4.47)) to properly estimate M. Thus, the processing performed with each method was broadband coherent, assuming an unknown waveform.

The only tool available for evaluating the performance of each processor on the different emission periods is the performance of step 3. The source localization results are reported in first place, since the main goal is to quantitatively compare the three processors. After performing MFT, source localization along time was performed within ranges from 1 to 10 km, and depths from 1 to 110 m. Figure 6.9 shows the localization results based on the MFT inversions performed. The plots correspond to the three proposed matched-field processors, with range estimates on the left, and depth estimates on the right (see figure 6.2
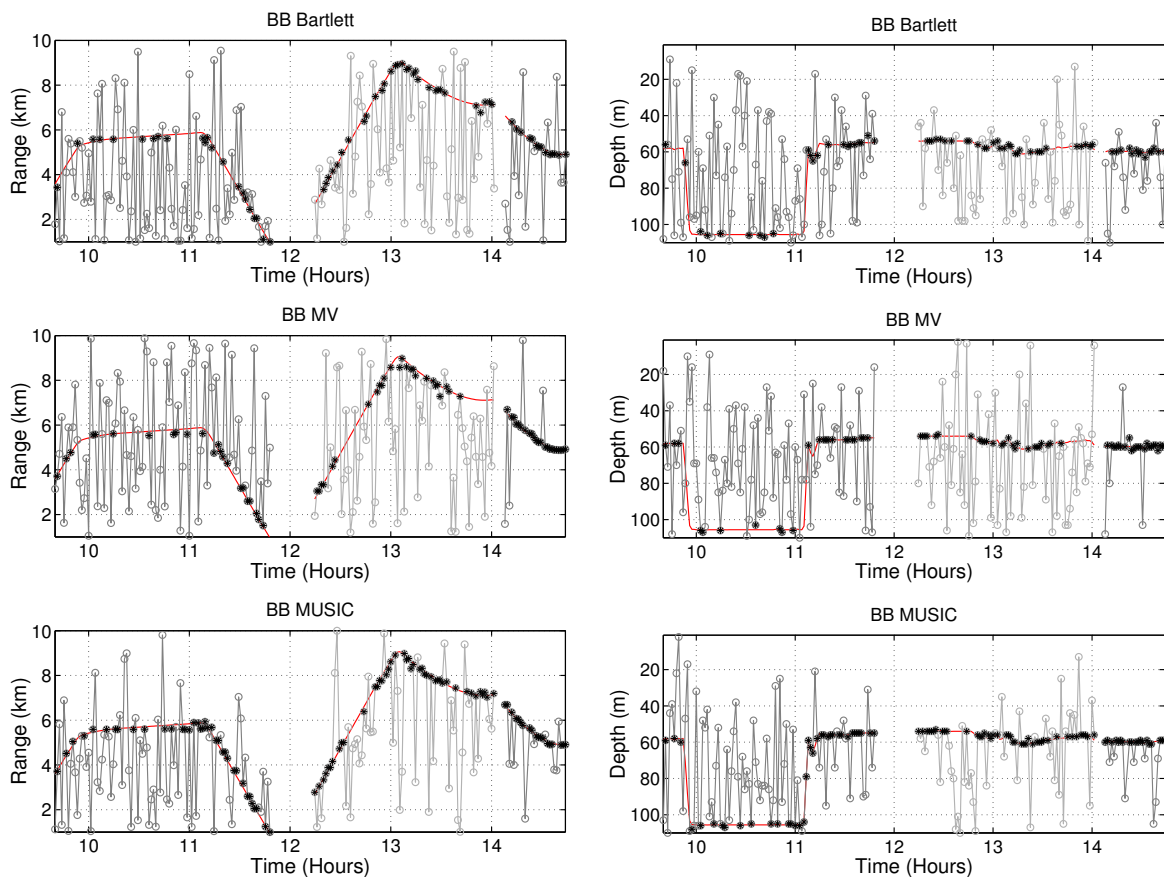
Figure 6.9: Source localization as a MFT validation step. Source range (left column) and source depth (right column). True location is given by the red curve in the background. The gray curve with circles are the source localization results. The black asterisks indicate the successful localizations.

for true values). The red curve in the background indicates the true location of the source.

The gray curves with circles are the source localization results. Successful localizations are

marked with a black asterisk. The source is admitted as correctly localized if the error both

on range and depth is less than 5% of the search interval amplitude. In other words the

maximum must fall in a rectangle centered on the true location, with a length of 0.9 km

and a width of 11 m. The degree of stationarity of the gray curve, the density of asterisks,

and the degree of visibility of the reference curve, are all visual indicators of the localization

performance. It can be seen that all processors achieved their best performances in the last

interval corresponding to the *A1double* emissions. The interval corresponding to the *A1*

emissions, were most difficult, although the source was held fixed during more than half of

Processor	A1	A2	A1double	Overall
Bartlett	22.7%	38.3%	51.9%	32.7%
MV	22.7%	29.6%	85.2%	35.1%
MUSIC	39.0%	53.1%	70.4%	48.3%

Table 6.5: Rates of successful localization for the different processors and different signals.

that emission period. The generic interpretation on the resulting performance is intimately linked to the signal design. The *A1* signal is located in a mid frequency range with a high repetition time. The *A2* signal is similar to *A1* but is in a frequency range higher than that typically used for tomographic applications. *A1double* is also in a middle frequency range but allows the collection of a higher number of signal realizations than *A1*. Measurements of noise power in this data set indicate that it falls off 7 dB in the band 400 to 1600 Hz. From that point of view one can expect better inversion performace for the *A2* interval in comparison to the *A1* interval, and that the number of 16 signal snapshots provides a better balance in terms of signal variance than *A2*. By observing the localization during the *A1* emissions interval one can see that the rate of success is clearly lower during the time the source is stalled. During that time it is at a depth of 105 m. Recalling the temperature profiles collected during days prior the acoustic experiment (see figure 2.1(b)) one can see that the thermocline is extremely strong. This will strongly refract the acoustic field downwards causing very low energy to be received at the top receiver. With the source close to the seafloor it is almost like considering only receivers 2 and 3. Table 6.5 shows the rate of successful localization for each processor in percent. The rate of localization was computed for each emission interval due to the different signal characteristics, and then summarized on the rightmost column as an overall appreciation. It can be seen that the performance is in general in agreement with the resolution of each processor and the balance in terms of signal variance provided by each signal type.

Figure 6.10 shows the MFT inversion obtained using the MUSIC processor. The reason for showing the run performed with the MUSIC processor was its overall superiority in terms of source localization, and the belief that this means that the environmental estimations are also of superior quality in comparison with those obtained with the other processors. The empty circles correspond to inversions where the source was not correctly localized during the validation step, while the circles filled with an asterisk correspond inversions with successful localization. The interpretation of the results is difficult since the observation period is more than 5 hours, and the source is moving most of the time.

It can be seen in plot (a) that from time 10:00 to time 11:00 the estimate of the α_1 EOF coefficient follows the poor performance of the source localization. The reason for the poor source localization performance during the period where the source is stalled is explained by the high variability in the estimates of α_1. At the same time it is observed that the model fit suddenly increases during that interval, which results from the fact that only receivers 2 and 3 are contributing to the matched-field process due to strong refraction in the thermocline. When the source moves and goes up to approximately mid-watercolumn, the variability substantially reduces, with the estimates becoming confined in the interval -10 to 10. During *A2* the estimates continue in the interval -10 to 10 at the beginning but then during the remaining part the estimates are in the upper half of the search interval between 0 and 15. Finally, the α_1 estimates in the *A1double* period are clearly in the interval -10 to 10. The second EOF coefficient was searched in an interval with amplitude less than half of that chosen for the first one. At some periods it appears to be concentrated in subintervals, but the stability is in general relatively low.

Concerning the seafloor parameters, their estimates over time are not consistent, but
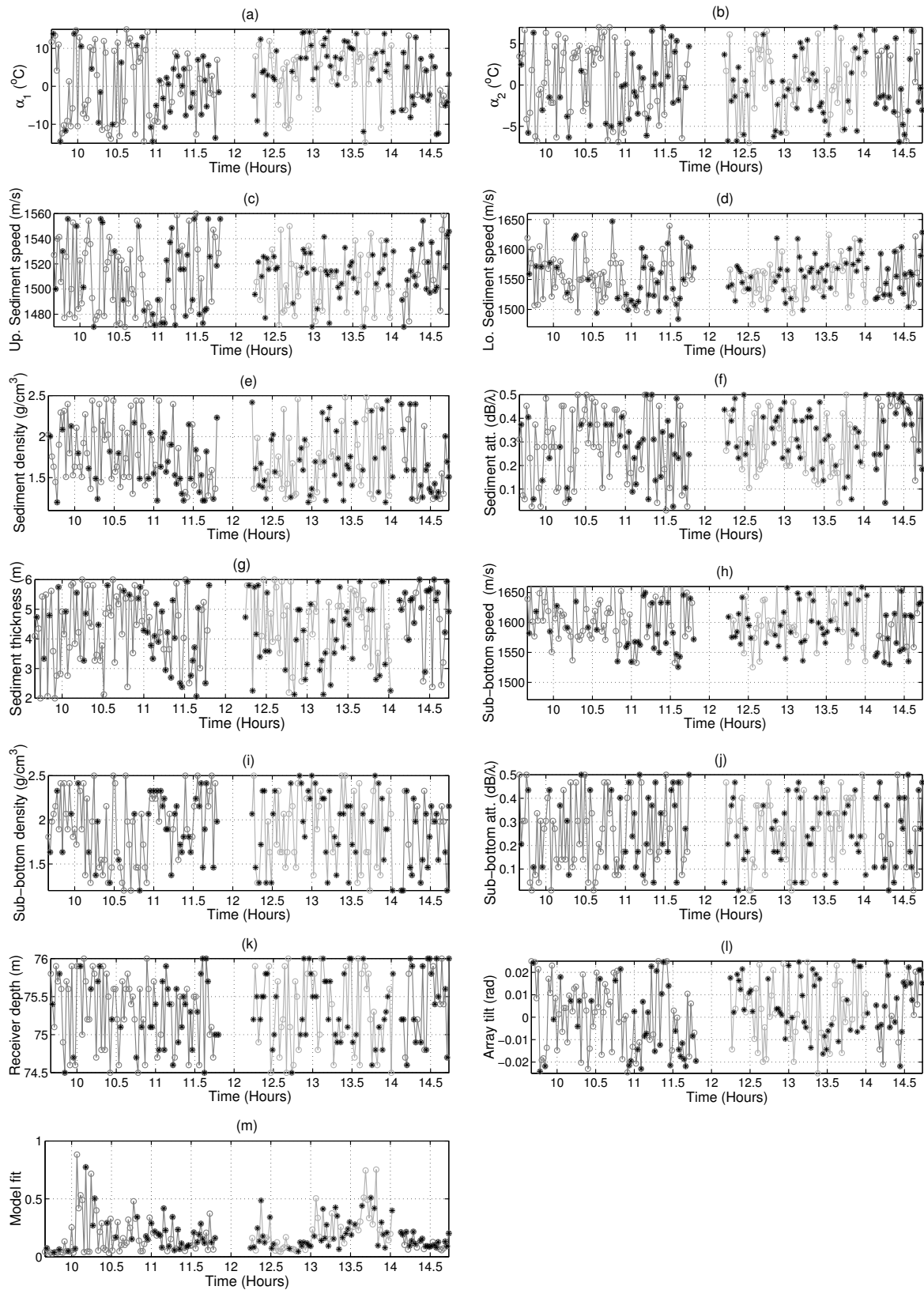
Figure 6.10: Model parameters estimates obtained via MFT using the BB MUSIC processor.
Water column ((a)-(b)); sediment ((c)-(g)); sub-bottom ((h)-(j)); geometric ((k)-(l)); MF response
((m)). The black asterisks indicate model estimates allowing for successful source localization in
the validation step.
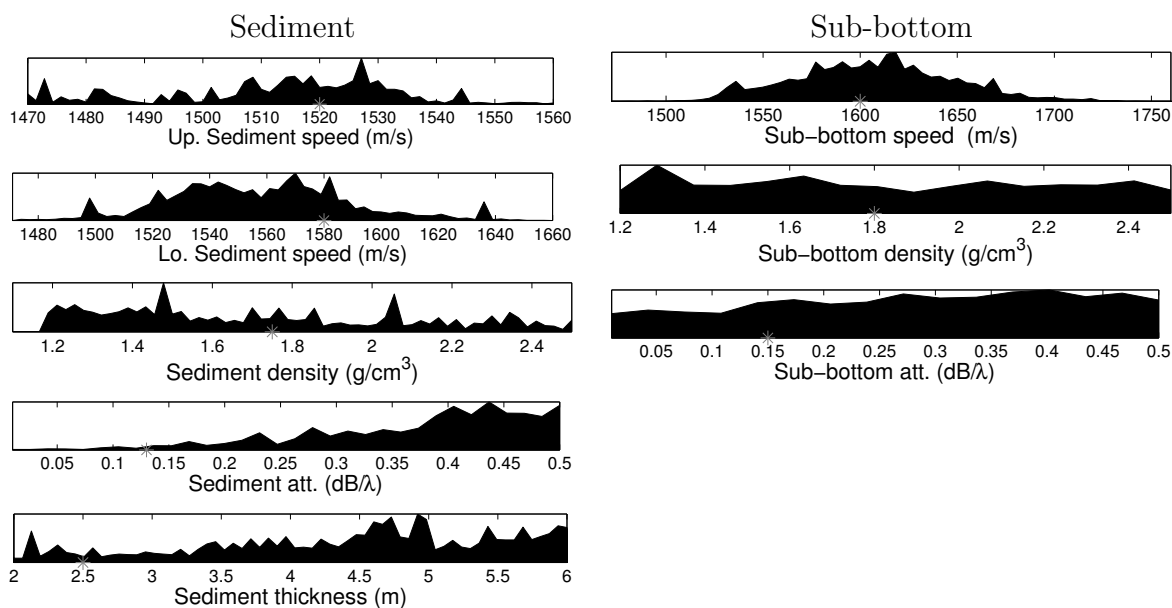
Figure 6.11: *A posteriori* probability distributions for the seafloor parameters based on the last generation of the GA. Only inversions validated by means of source localization during the *A2* period are considered. The gray asterisk indicates the baseline value of the parameter.

some are fairly restricted to sub-intervals if only those upon successful source localization are considered. Specially the sediment and bottom compressional speeds seem to be relatively well determined over some time periods. In order to obtain a single estimate for each of the seafloor parameters, *a posteriori* distributions based on the last generation of each inversion with correct source localization (43 inversions out of 81), were computed (see fig. 6.11). Only the *A2* emission period was considered for this purpose. These distributions provide additional insight into the parameter inversion process and emphasize the variability over the search interval. Sediment and sub-bottom compressional speeds, and sediment attenuation are relatively compact with a peak indicating that the inversion was fairly successful at finding a good fit for these parameters. From the *a posteriori* distributions model estimates based both on the distribution peak and distribution mean are available. Table 6.6 contains the values of the distribution peak and the distribution mean of the seafloor. It also contains the baseline values and a measure of the estimation reliability, which is simply the standard

Model Parameter	Baseline	MAP	GA mean	Reliability
Up. Sediment speed (m/s)	1520	1527	1513	0.22
Lo. Sediment speed (m/s)	1580	1570	1557	0.17
Sediment density (g/cm^3)	1.75	1.48	1.72	0.27
Sediment att. (dB/λ)	0.13	0.44	0.38	0.20
Sediment thickness (m)	3.7	4.92	4.4	0.27
Sub-bottom speed (m/s)	1600	1618	1607	0.14
Sub-bottom density (g/cm^3)	1.80	1.29	1.83	0.31
Sub-bottom att. (dB/λ)	0.15	0.40	0.28	0.29

Table 6.6: Baseline seafloor parameters, two parameter distributions based on 43 GA populations, and a reliability measure.

deviation of the *a posteriori* distribution divided by the search interval length. It is not obvious which of the two available estimators yield more appropriate estimates, but the distribution mean appears to be very dependent on the *a priori* knowledge of the parameter. For example the sub-bottom density distribution mean is coincident with its baseline value, however, its estimation reliability is the lowest of all. According to the estimation reliability measure, the sediment and sub-bottom compressional speeds and the sediment attenuation have fairly consistent estimates compatible with the baseline values, while the other seafloor parameters were not consistently estimated. It should be remarked that during the *A2* emission period, the source was steadily moving, covering a significant area, and therefore possibly with varying seafloor properties (see figs. 6.1 and 6.2).

Finally, some attention is paid to the temperature profiles' estimates, under the belief that those have most influence on the acoustic propagation and therefore the model fit should strongly rely on them. In figure 6.10 it was seen that the EOF coefficients could not be uniquely determined. But such observation is not sufficient to evaluate the temperature estimation because the EOFs are symmetric below 30 m depth (see figure 2.1(e)), and might largely be compensated by each other, which is a source of solution ambiguity as shown in Ref. [28]. Other factors such as physical model mismatch, the reduced number

of receivers, and the size of the search space might have contributed for the difficulty in uniquely determining the EOF coefficients and all the other parameters. Figure 6.12 shows the reconstruction of the temperature profiles along time. Only profiles corresponding to successful source localization were taken into consideration and gaps in between were filled by linear interpolation in time. The gaps seen in the plot are due to acoustic source shut off and change of emitted waveform. It is seen that significant difficulties are found in dealing with the strong thermocline. This may be the result of strong refraction that prevents the top receiver to receive a significant level of acoustic power. Although low precision was attained in estimating the first layer, it should be remarked that the source localization has filtered profiles with unlikely temperature estimates. The maximum estimated surface temperature is 28 °C for few time points, most of the time it is about 27 °C which is in agreement with the measurements.
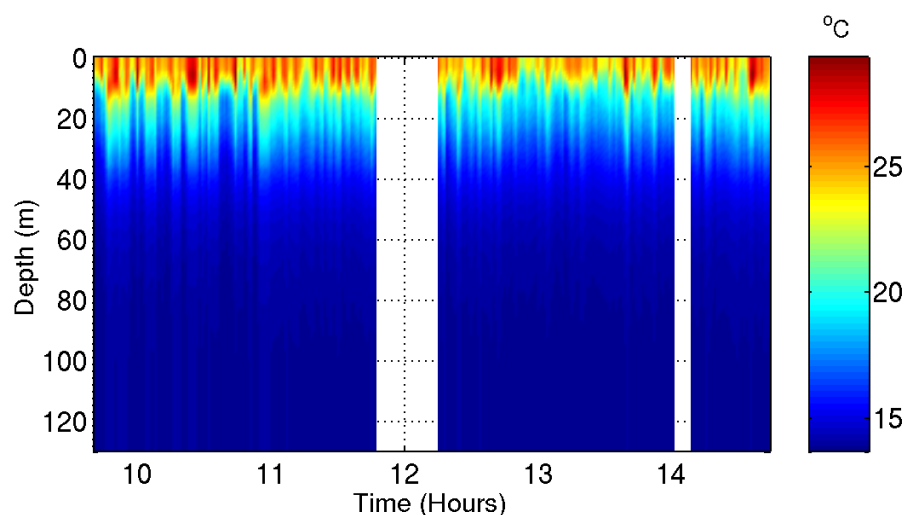
Figure 6.12: Reconstruction of the temperature profiles estimated using the BB MUSIC processor. Only profiles corresponding to successful source localization are taken into consideration (see figures 6.10(a) and (b)). The gaps in between were filled by linear interpolation in time.

6.7 Summary

This chapter was dedicated to MFT applied to the MREA'03 data set using only AOB1 receivers 1 through 3. The broad objective of this chapter was to verify the achievable performance under the present circumstances of data collection applying the processing methods proposed in this thesis. Some of the characteristics of the MREA'03 data set are: 1) reduced number of receivers; 2) moving source and free drifting receiver array; 3) signal frequency band from 500 to 1200 Hz; 4) relatively low number of signal realizations available.

The data processing consisted of three steps: first, a pre-processing step for frequency clustering was carried out. Then the inversion of the whole data was performed. Finally, range-depth source localization with large search bounds for model validation was performed. The whole process was repeated for the three broadband processors in order to produce a performance comparison. Since no ground truth measurements were made during the acoustic transmissions, the estimation performance had to be measured in terms of successful localization.

Section 6.3 provides an analysis of real data giving insight on spatial and spectral coherence. The main conclusions on this topic are:

- spatial coherence is in general high, and the signals are far less coherent across the spectral band than across space.

- source-receiver relative displacement has clearly a negative impact on the spectral coherence, leading to the diagonalization of the cross-frequency SDM, and to much lesser extent on spatial coherence.

Clustering of frequencies was proposed with the objective of optimizing the spectral

coherence. A side-effect of this optimization is the enhancement of the SNR of the cross-frequency SDM. The frequency clustering led to the use of multiple frequency clusters in the processing, resulting in a superposition of several MF responses, as an attempt to increase the amount of information available in the acoustic field.

MFT was applied on the whole MREA'03 data set collected on 3 receivers, performing one run for each of the three BB processors with application of the proposed frequency clustering. The inversion was followed by range-depth source localization with large search bounds for model validation. A strong relation between the degree of parameter estimates variability and correct localization rate can be perceived, suggesting that source localization may provide a mean for model validation. It is remarkable that the source was correctly localized at ranges up to 9 km (about 80 waterdepths). This should, in principle, give high confidence in the model parameter estimates. However, even during time intervals with less estimation variability, high-ranking parameters such as the EOF coefficients could not be uniquely determined. In Ref. [28] it is shown that for this data set the EOF coefficients, to large extent, tend to compensate each other. Nevertheless, the reconstructed temperature profile, using only validated models, shows a good stability. The seafloor parameters were estimated via *a posteriori* distributions, in order to obtain a single estimate for each. Seafloor compressional velocities in both sediment and sub-bottom, and sediment attenuation could be relatively well determined.

Concerning the comparison of the processors:

- the MUSIC processor achieved the overall best performance.

- the MV processor achieved the best performance in the rich data case (*A1double* emissions), and had poor performance in the poor data case.

The comparison result obtained here is consistent with that obtained with synthetic data in section 5.6, such as the difficulties encountered over chapter 5 with the MV processor. Note also that in the case of the MUSIC processor, the optimization carried out for the frequency clustering allowed for assuming that the signal subspace dimension was 1, avoiding risk of erroneous estimation, and possibly relaxing the requirement of a high number of signal realizations.

As a final appreciation, it can be said that the high-resolution processors performed surprisingly well in application to real data MFT, and the processor comparison result met the expectations. Moreover, the application of these high-resolution methods can be noted as being a novelty in terms of application.

Chapter 7

Experimental results II: Matched-field tomography on the MREA'04 data set

The three BB matched-field processors proposed in this thesis were applied to the MREA'03 data set in chapter 6. The MUSIC processor resulted in an overall performance superiority in comparison to the Bartlett and the MV processors.

In the present chapter the data processing procedure of the previous chapter will be applied on the MREA'04 using only the MUSIC processor. One reason is its good performance in the previous chapter, and the other is the high number of signal realizations this data set can provide. Besides seeking for further demonstrating the MUSIC processor's applicability to inverse problems such as MFT and geoacoustic inversion, two more objectives are contemplated in this chapter. One is studying the possible benefits of increasing the size of frequency clusters to the parameter estimation accuracy, as an attempt to compensate for the reduced number of receiving elements. The other objective it to quantify the impact of model validation via source localization. The evaluation of these issues is made by means of standard deviations on the estimates, assuming that part of the variability observed is due to errors in the estimation of the parameters.
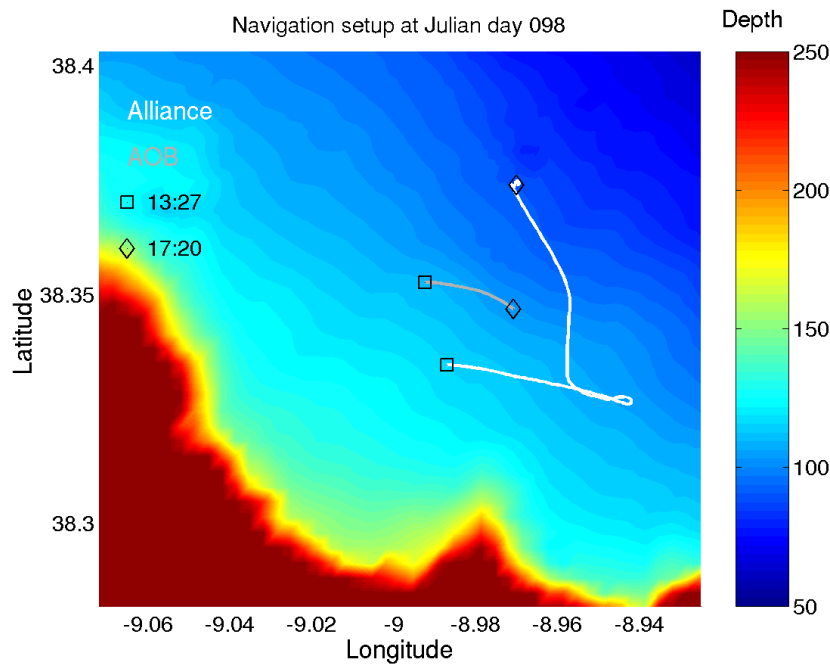
Figure 7.1: GPS estimated AOB and source ship navigation during the deployment of April 8.

7.1   The MREA'04 sea trial

The MREA'04 sea trial was the second sea trial carried out in the framework of the AOB-JRP
and took place from 29 March to 19 April 2004 off the west coast of Portugal, south of Lisbon
[51]. The research vessel used was the R/V Alliance. The main objectives of this sea trial
were testing an improved version of the AOB and its functionality in a simple network, and
environmental inversion of acoustic signals for bottom and water column properties for REA,
denominated as Acoustic REA (AREA). The former objective could not be accomplished
due to technical problems in one of the buoys, leaving only one buoy available.

The acoustic experiments took place during four days, from April 7 to 10, where de-
ployment configurations included both range-dependent and range independent tracks. The
data processed in this study is that collected during April 8 (Julian day 98), when the AOB
was deployed in a free drifting configuration in an area of mild bottom range dependency
with favorable weather conditions. Figure 7.1 shows a bathymetric map with both the AOB
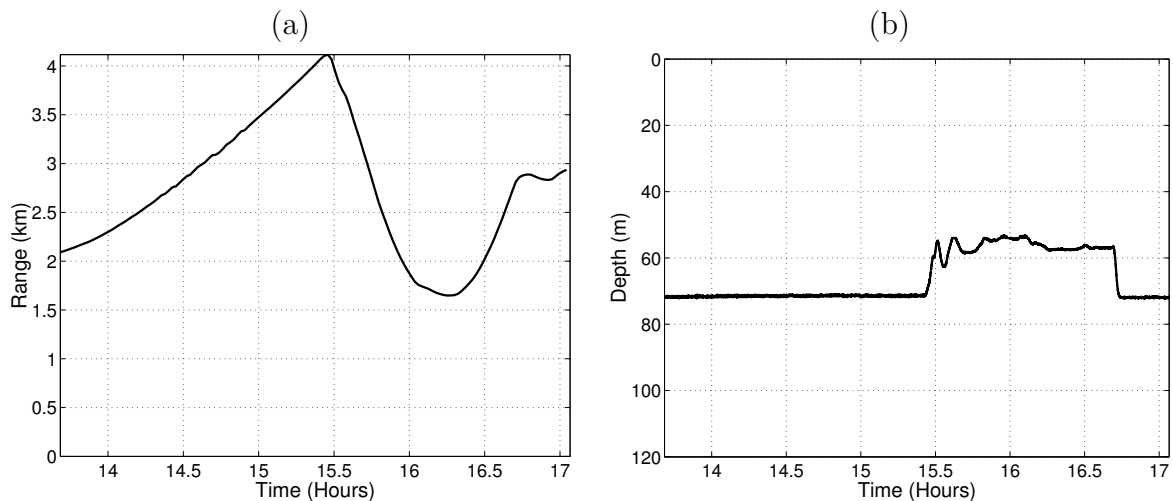
Figure 7.2: Source range (a) and depth (b) measured during the deployment of April 8.

drift and the Alliance navigation obtained from GPS recordings, and AOB deployment and recovery times. The waterdepth at the AOB position varied between 103 and 108 m, and the waterdepth at the ship position varied between 90 and 114 m. Source-receiver range varied between 1.6 and 4 km (figure 7.2(a)). The acoustic source was deployed from the R/V Alliance at a variable depth between 54 and 72 m, depending on the ship speed (figure 7.2(b)).

The emitted sequence consisted of multi-tones and LFMs in the bands 900 to 1200 Hz, and 1200 to 1500 Hz, giving 4 different combinations. The sequence chosen for the present study was the LFMs-sequence in the band 900 to 1200 Hz. The AOB-version used during the MREA'04 sea trial had an array consisting of 8 acoustic receivers, but for this study only 3 receivers were used, with depths of 15, 60, and 75 m, which are the same depths used in the previous chapter, for the MREA'03 data inversions. The reason for such choice is to study how MFT performs when the array is sparse, since one of the requirements of AREA is the usage of light receiving devices.

Extensive ground truth measurements were performed before, during and after the target

week, including CTD, XBT, vessel mounted ADCP, one SEPTR buoy, two bottom mounted

ADCPs, two thermistor chains, one meteo buoy and one wave rider buoy. The actual pro-

cessing includes CTD measurements performed during April 7 and 8 (see figure 2.1(c) and

(f)), where the temperature profiles will be modeled as an expansion using the mean profile

and the first EOF (eq. (2.4)).

7.2   The MREA'04 baseline model

The baseline computer model adopted for the MREA'03 was built from the segmentation

of archival bathymetric information along the source-receiver cross sections at the instant

when the waterdepth at the ship coordinates was minimum, which is 90 m, and 104 m

at the AOB coordinates. The geoacoustic properties are typical values of continental shelf

environments [99, 100, 1]. It consists of an ocean layer overlying a sediment layer and a

bottom half space with the bathymetry assumed to be range-dependent, as shown in Fig.

7.3. The sound-speed profile was calculated using the Mackenzie formula in (2.1) with the

mean temperature profile (figure 2.1(c)) and the mean salinity profile as inputs [51].

For the purposes of the inversion the forward model was divided into four parameter

subsets: water column temperature, sediment, sub-bottom, and geometric parameters.

7.3   Data processing procedure

Although the goal of the current chapter is different regarding that of the previous chapter,

the data processing remains basically the same. Steps 1 through 4 given at the beginning of

section 6.5 will be followed.

There is a particular remark to be made regarding step 1: the frequency optimization
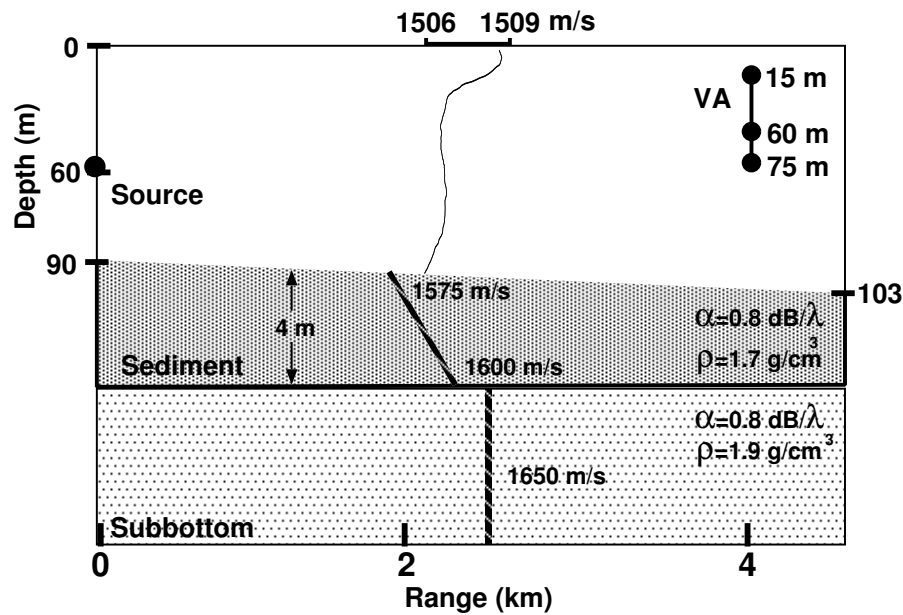
Figure 7.3: Baseline model for the MREA'04 sea trial. All parameters except waterdepth are range-independent.

was carried out using as cost-function the $\Lambda(\lambda_1, \lambda_2)$ ratio (see eq. (4.45)), aiming at making the first eigenvector as most dominant as possible, under the belief that that criterion will result in grouping most coherent frequencies. In principle, one could guess that if that ratio was as high as e.g. 15 dB, then the signal subspace would have dimension 1. One would also believe that under a good SNR an information criterion such as the MDL would be in principle able to estimate "correctly" the signal subspace dimension. In fact it has been observed that even if λ_1 is far from the remaining eigenvalues it just happens that M is estimated up to 4 or 5. Thorough inspection has shown that the information criterion is rather sensitive to the *constancy* of the eigenspectrum than to the dominance of individual eigenvalues. It has also been observed that cases where the dominance of the first eigenvector is not very pronounced can yield signal subspace dimension equal 1. The main conclusion is that optimizing for $\Lambda(\lambda_1, \lambda_2)$ does not guarantee that the estimate of M will be equal 1 even if very high values for that criterion are found. Thus, it was decided, once again, to use $M = 1$ throughout the processing.

Model parameter	Lower bound	Upper bound	Quantization steps
Water column			
α_1 (°C)	-12	12	128
Sediment			
Up. sediment speed (m/s)	1450	1700	128
Lo. sediment speed (m/s)	0	100	64
Sediment density (g/cm³)	1.0	2.5	64
Sediment wave att. (dB/λ)	0.01	1	32
Sediment thickness (m)	1	8	64
Sub-bottom			
only 3 Sub-bottom speed (m/s)	1	100	64
Sub-bottom density (g/cm³)	1.5	3.0	16
Sub-bottom wave att. (dB/λ)	0.01	1	16
Geometric			
Receiver depth (m)	74	77.0	16
Tilt (rad)	-0.050	0.050	64

Table 7.1: GA forward model parameters with search bounds and quantization steps for MFT.

Another important aspect is the search space for optimization. Table 7.1 shows the unknowns with their search bounds and quantization steps. Some intervals were slightly extended in comparison to those chosen for the MREA'03 data set reflecting a lower *a priori* knowledge on the environmental properties. Concerning the water column only one EOF coefficient was optimized, since the criterion in eq. (2.5) yielded $\hat{\mathcal{N}} = 1$. The size of the search space is approximately 2.3×10^{18}. The GA settings remained equal to those used for the MREA'03 data set (see table 6.4)

Finally, it remains to say that in the source localization step, the search bounds are between 1 and 10 km in range, and 1 and 90 m in depth.

7.4 High-resolution MFT using the MUSIC MF processor

It is found in the literature that the performance of subspace based methods is highly dependent on the amount of observations and SNR. Although the data set collected during

the MREA'03 sea trial allowed only $N = 10$ or $N = 16$ realizations in a observation window of 80 s, the MUSIC processor could outperform the Bartlett and the MV processors in terms of source localization, which is intended to evaluate the quality of the environmental inversion. The signals emitted during the MREA'04 sea trial were designed such that a much higher number of signal realizations could be extracted. In this case 46 signal realizations in 46 s could be taken. This should in principle provide data with higher quality since there are more signal realizations in shorter time, which would allow reducing field decorrelation during the observation time. Having a high number of signal realizations is particularly important when subspace based methods are applied, since it is required that $N \geq KL$.

This section aims at studying the MFT performance with a sparse array with the main objective of finding out whether increasing the number of frequencies can compensate the lack of spatial information that could eventually be earned by using a larger number of receivers. Thus the inversion process was repeated for a number of frequencies from 3 to 6, which was the maximum number of frequencies allowing the exhaustive search to be performed in a reasonable computation time. Note that the frequencies were optimized by searching exhaustively for the matrices with highest $\Lambda(\lambda_1, \lambda_2)$. The number of frequency groups $\mathcal{N}_g$ was set to 7. The inversion performance is measured in terms of the estimates' standard deviation, under the belief that part of the variability is inherent to the estimation algorithm, and part of the variability is inherent to the parameters' evolution with time and space. Table 7.2 shows the standard deviations of the estimated unknowns with increasing K, together with the rate of successful source localization. The expectancy is that the variability of the parameter estimates decreases with K. It can be seen that the standard deviation does not monotonically decrease with K, giving the idea that there is not a significant difference

Parameter	K=3	K=4	K=5	K=6
α_1 (^{o}C)	6.60	7.61	6.67	**5.59**
Up. Speed in sed. (m/s)	61.5	71.1	68.2	**59.3**
Lo. Speed in sed. (m/s)	73.1	83.4	75.0	**67.7**
Density in sed. (g/cm³)	0.436	0.466	**0.426**	0.442
Att. in sed (dB/λ)	0.306	0.291	0.305	**0.280**
Sed. thickness (m)	1.95	2.05	**1.82**	2.15
Speed in sub-bottom (m/s)	77.2	92.0	76.8	**71.8**
Density in sub-bottom. (g/cm³)	0.439	0.396	0.465	**0.396**
Att. in sub-bottom (dB/λ)	0.266	0.289	0.289	**0.261**
Receiver depth (m)	1.03	0.94	1.01	**0.93**
Tilt (rad)	0.031	0.033	**0.026**	0.027
Localization rate (%)	40.4	48.1	**53.8**	50.0

Table 7.2: Standard deviations of the parameter estimates as the number of frequencies K increases. In the bottom line source localization rate.

when K has a small increment. Nevertheless most minima are found for $K = 6$ and some

for $K = 5$, leaving a slight impression that increasing the number frequencies can be useful

for coping with variability in the parameter estimates. Some seafloor parameters have a low

rank in the inversion process and can just not be inverted for with those frequencies and

only 3 receivers - measuring their standard deviation has no meaning. Interesting is the

result obtained in the source localization step. The rate of successful source localization is

increasing until $K = 5$, which further confirms the benefit of increasing K. The difficulty in

continuing this test for larger values of K is in the computation load required for optimizing

the frequencies by exhaustive search. This test could be repeated for higher values of K if a

GA algorithm was employed in that step.

An interesting exercise is to compute the estimates' standard deviations excluding the

time points where correct localization did not succeeded as an attempt to filter out model

estimates of weak quality. The idea is based on the requirement of a valid environmen-

tal estimate to properly localize the acoustic source with large search bounds. Table 7.3

compares both cases, and it clearly shows that choosing upon successful source localization

Parameter	(a)	(b)
α_1 (^{o}C)	5.59	**4.91**
Up. Speed in sed. (m/s)	59.3	**36.6**
Lo. Speed in sed. (m/s)	67.7	**36.7**
Density in sed. (g/cm^3)	0.44	0.44
Att. in sed (dB/λ)	**0.280**	0.283
Sed. thickness (m)	2.15	**1.86**
Speed in sub-bottom (m/s)	71.8	**43.0**
Density in sub-bottom. (g/cm^3)	0.396	**0.371**
Att. in sub-bottom (dB/λ)	**0.261**	0.270
Receiver depth (m)	**0.93**	1.02
Tilt (rad)	0.027	**0.026**

Table 7.3: Comparing standard deviations of the parameter estimates at all times (a) with standard deviations considering only times on successful source localization (validation step) (b).

clearly reduces the standard deviation of the most important parameters. The compressional speeds in the seafloor had significant reductions in their standard deviations. But note that the seafloor compressional speeds are coupled, and that part of that reduction is induced by the upper speed in the sediment. The seafloor parameters whose standard deviations could not be reduced through source localization are parameters to whom the acoustic field is insensitive.

Finally, figure 7.4 shows the parameter estimates obtained for $K = 6$, with asterisks marking the time points with successful source localization. The first comment is relative to the stability of the parameter estimates, in particular, concerning the EOF coefficient α_1, which is the most important parameter. It can be seen that during the time interval from 13.75 to 14.25 hours its estimates lie restricted in the interval from -10 to 0. But then suddenly the dispersion increases since estimates of α_1 are found over the whole search interval until time 16.25. Then, during the remaining part of the run the estimates are again restricted in the interval -5 to 0, with a high rate of successful source localization. The other interesting aspect is to inspect which is the impact of the model selection (rejection) pro-
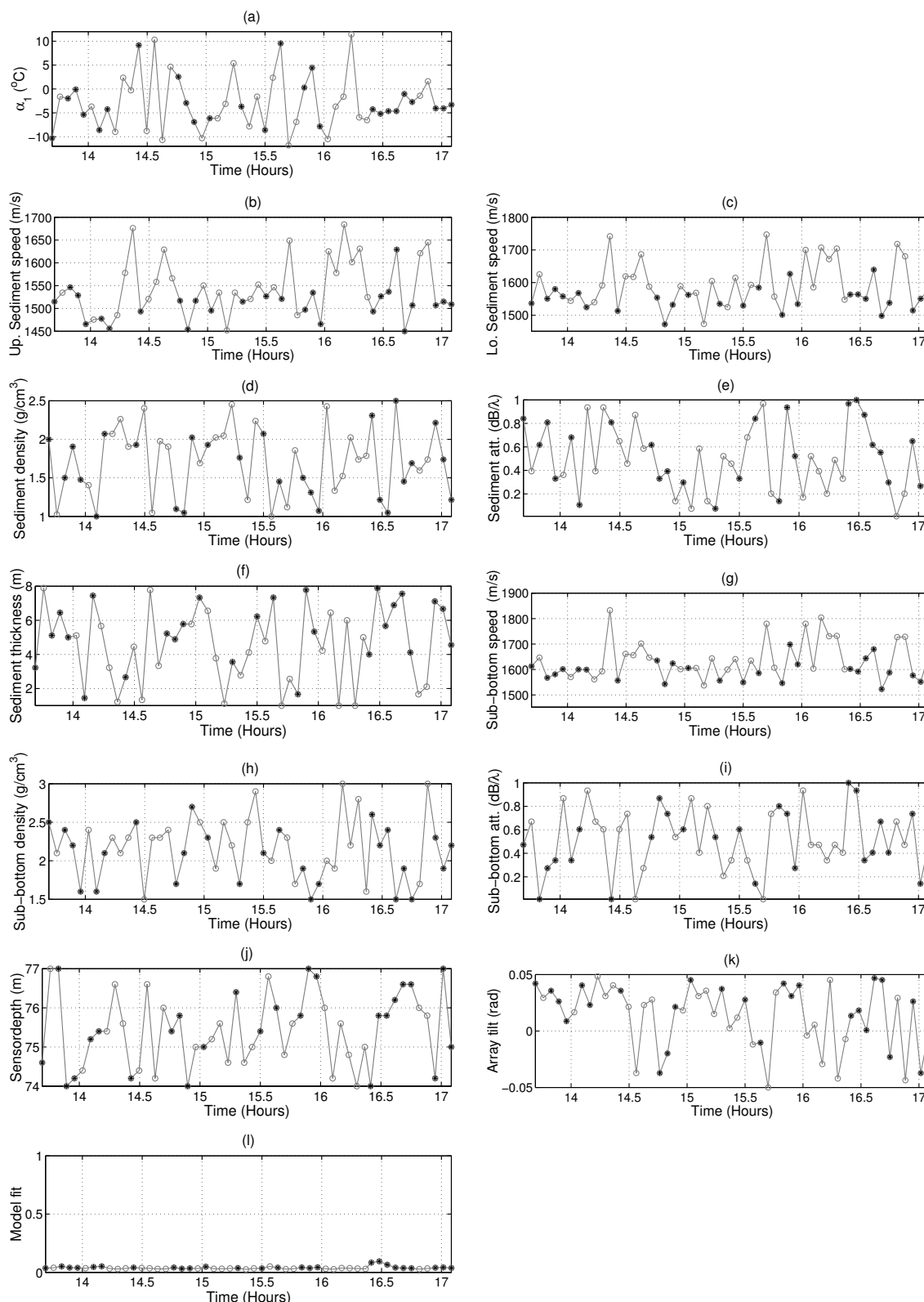
Figure 7.4: Model parameters estimates obtained via MFT using the BB MUSIC processor. Water column ((a)); sediment ((b)-(f)); sub-bottom ((g)-(i)); geometric ((j)-(k)); MF response ((l)). The black asterisks indicate model estimates allowing for successful source localization in the validation step.
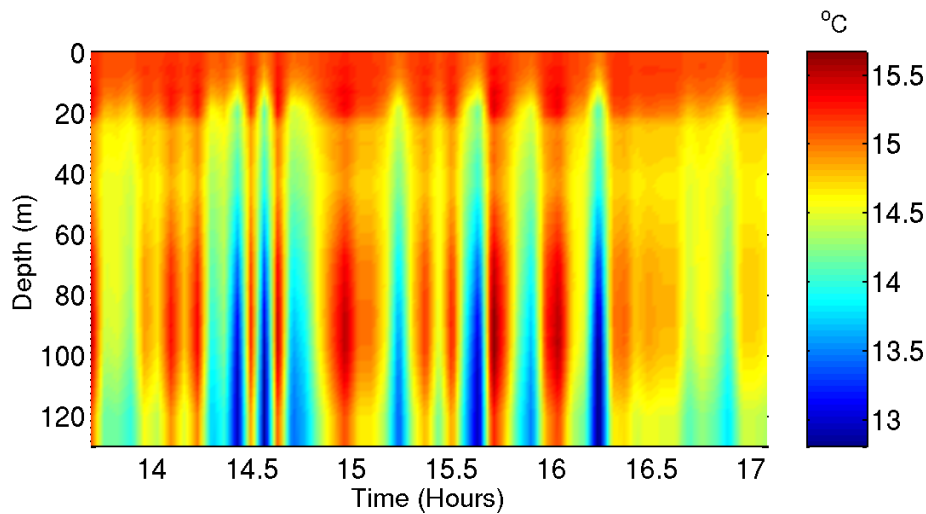
Figure 7.5: Reconstruction of the temperature profiles estimated using the BB MUSIC processor with $K = 6$. Only profiles corresponding to successful source localization are taken into consideration (see figures 7.4(a)). The gaps in between were filled by linear interpolation in time.

vided by the source localization step. For example it can be verified that the upper sediment compressional speed estimates above 1550 m/s were in general rejected, such as lower sediment compressional speed estimates above 1600 m/s, and sub-bottom speed estimates above 1700 m/s. Correct values for the sediment thickness seem to lie in the interval 3 to 8 m. As a generic appreciation it can be said that the uncertainty in the environmental model estimates is quite large although a satisfactory rate of source localization was achieved. Finally, note the low model fit obtained with the BB MUSIC processor which has a mean value of 1.5×10^{-3}.

The processing is completed by reconstructing the estimated temperature profile using the α_1 estimates corresponding to successful source localization. The actual problem is almost isovelocity which causes the interval between minimum and maximum temperature to be very short. The plot in figure 7.5 shows the reconstructed temperature profile, which reflects the variability seen in the parameter estimates. Above 20 m depth it is quite stationary, but below it shows an unlikely variability.

7.5   Summary

The present chapter was completely dedicated to further application of the MUSIC processor to MFT using the MREA'04 data set, due to its surprising success in the previous chapter, and due to the high number of signal realizations available in this data set. Although 8 receivers were available only receivers 2, 4, and 7 were used in order to keep the study in the line of sparse receiver arrays. There were two main objectives in this chapter:

- to study the possible benefits of increasing the size of frequency clusters to the parameter estimation accuracy, as an attempt to compensate for the reduced number of receiving elements.

- to quantify the impact of model validation via source localization on the overall estimation accuracy.

Concerning the first objective, MFT inversions were carried out for clusters with 3 to 6 frequencies, since this number was limited by the computational burden required to optimize the frequencies. The performance was measured in terms of standard deviations of the parameter estimates and rate of correct source localization. The minimum standard deviations and the maximum source localization rate were found for clusters with 5 or 6 frequencies. Although the result is not unequivocal, increasing the size of the cluster, hence the dimension of the cross-frequency SDM, clearly contributes for improving the estimation stability.

Concerning the second objective, it simply consisted in comparing the standard deviations on the parameter estimates with those obtained when parameter estimates corresponding to incorrect source localizations were discarded. The result was a significant drop on the

standard deviation of the EOF coefficient, sound velocities in the seafloor, and sediment
thickness. The standard deviation of the remaining parameters remained practically un-
changed, which indicates that the field is not sensitive to those parameters.

Chapter 8

Experimental results III: Passive tomography on the INTIMATE'00 data set

Chapters 6 and 7 presented experimental results on acoustic tomography using a light array with Rapid Environmental Assessment as an application example. In this chapter the simplification occurs at the emitter end where a ship is used as the emitting sound source, with passive acoustic tomography as an application example. This chapter aims at summarizing the experimental results on passive acoustic tomography obtained with the INTIFANTE'00 data set reported in [34], which constitutes a first attempt on using the noise radiated from a ship for ocean tomography.

8.1   The INTIFANTE'00 sea trial

The INTIFANTE'00 sea trial [49, 101, 102] was a joint experiment carried out by Instituto Hidrográfico and the University of Algarve, with the collaboration and support of several other institutions[1] in the fall of 2000, in a shallow-water area close to Setúbal, Portugal. A detailed and complete description of the experiment and of the various data sets acquired

---

[1] Insituto Superior Técnico (IST), Lisboa, Portugal, Ente per l'Energia ed l'Ambiente (ENEA) and SACLANT Undersea Research Centre, both in La Spezia, Italy

during the INTIFANTE'00 sea trial can be found in [101] while here only a brief description will be given. The experiment area was a rectangular box situated within the continental shelf with depths varying from 60 to 140 m. There was a broad range of objectives pursued by this experiment, among which the testing of the ability of inverting ocean properties with both known and unknown, active and passive, stationary and moving acoustic source signals in various environments, both range independent and range dependent using a standard receiving device [103, 104, 105]. Experimental results have been reported on several occasions, both in international conferences [101, 106, 107, 29] and in reports written in the framework of the TOMPACO project [102, 108, 109]. The INTIMATE'00 sea trial consisted of a series of experiments (denoted as *Events*) aiming at studying the feasibility of Passive Acoustic Tomography, where working conditions were progressively relaxed at each *Event* until the most realistic scenario was reached:

1. *Event 2* was carried out in a range-independent propagation track, where the source moved during 2 hours from a range of 0.7 to 5.7 km away from the receiver array (see figure 8.1). The emitted waveform was deterministic.

2. *Event 5* included two factors of difficulty in comparison to *Event 2*: one was concerning the emitted waveform, now of random nature, and the other was concerning the bathymetry, which now is clearly range-dependent (see figure 8.1). During *Event 5* the sound source was emitting a pseudo-random noise (PRN) sequence in the band 150 - 1100 Hz, supposed unknown at the receiver. At maximum range of 5.2 km the bathymetry varied approximately linearly from 60 to 118 m depth.

3. Finally, in *Event 6* the acoustic source was replaced by the research vessel NRP D. Carlos I. This represents the real challenge since the acoustic source is emitting a real

unknown and stochastic signal at unknown location and moving in a poorly known environment. In order to maximize the probabilities of successful inversion and get close to the cruising speeds of "normal" ship traffic, NRP D. Carlos was set to steam at her full speed along a series of three concentric portions of circle as shown in figure 8.1 (gray line). Figure 8.2 shows that the the ship maintained a speed of approximately 9 kn with several speed drops during sharp turns.

The actual acoustic runs were performed over three distinct paths on whose intersection a vertical line array (VLA) was moored. The path directed to the NW, parallel to the continental platform, is approximately range-independent, while the NE path, oriented towards the coastline, is range-dependent with water depths varying from 120 m at the VLA location to 70 m at the path end. In between these two paths, the environment is progressively and slowly changing from range-independent to range-dependent when going from NW to NE. In this thesis only the results obtained for the Event 6 data are reported.

As an overview of the technical aspects involved in the experiment, it can be referred that acoustic signals were transmitted with an acoustic transducer suspended from the research vessel NRP D. Carlos I, a Portuguese Navy oceanographic research ship managed by Instituto Hidrográfico (IH), and received on a 16 hydrophone-4m spacing VLA. The acoustic aperture of the VLA was located between the nominal depths of 30 and 90 m in a 120 m depth water column. The acoustic signals received in the VLA were transmitted via an RF link to onboard ship, processed, monitored and stored. The acoustic portion of the VLA was hanging from the sea surface and attached through a 70 m long umbilical to the radio buoy that was itself bottom moored.
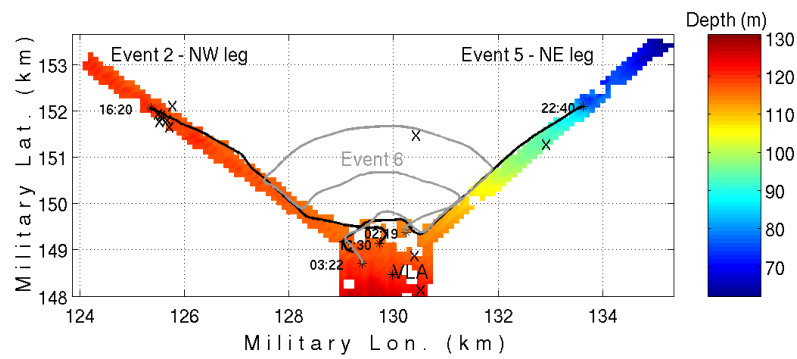
Figure 8.1: INTIFANTE'00 sea trial: acoustic runs and bathymetry during Events 2, 5 and 6, X signs mark the XBT locations and VLA indicates the vertical line array location.
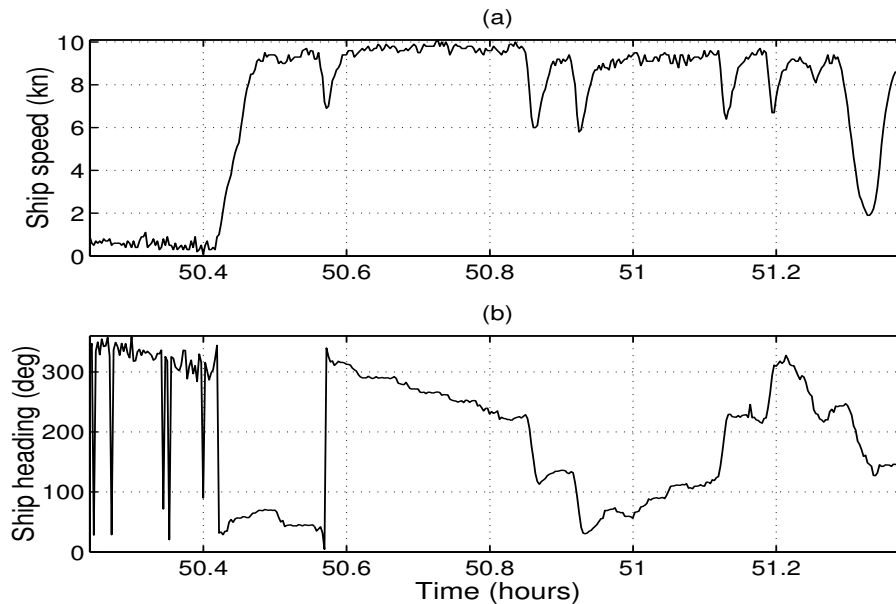
Figure 8.2: GPS estimated ship speed (a) and ship heading (b) during Event 6

8.2   Ship radiated noise

Research vessel NRP D. Carlos I is a 2800 ton relatively recent ship. Her main propulsion system is formed by two diesel-electric engines developing 800 HP attaining a maximum speed of 11 kn. According to her characteristics NRP D. Carlos I can be considered as an acoustically quiet ship. Hence, her use for the purpose of passive tomography can be considered as providing conservative results when compared with full length cargo ships or tankers traveling at cruising speed. As an example, figure 8.3 shows a time-frequency plot

(a) (b)
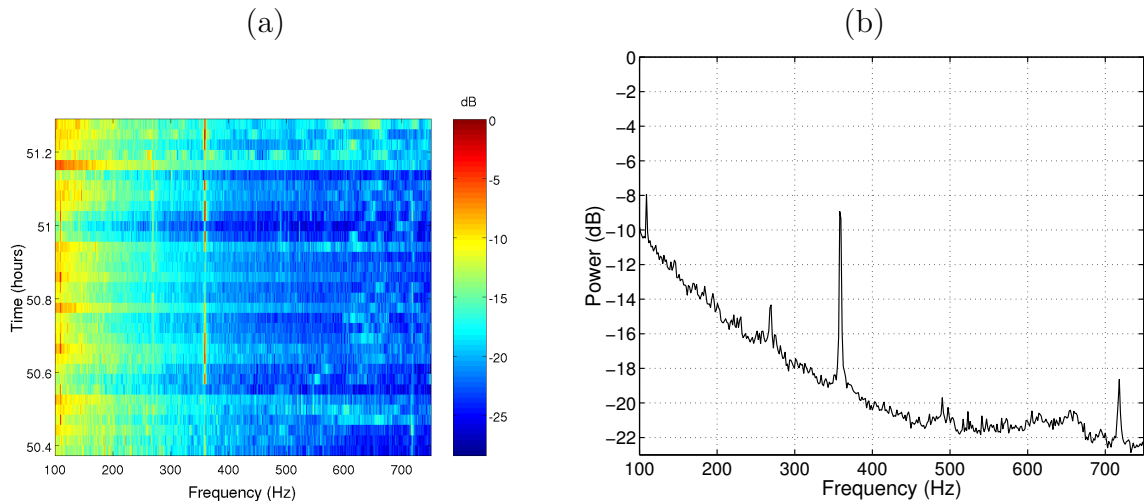
Figure 8.3: NRP D. Carlos I ship radiated noise received on hydrophone 8, relative power scale on a time-frequency plot (a) and mean power spectrum (b).

of the relative power spectrum received on hydrophone 8 at 60 m depth (a), and a mean power spectrum over the whole *Event* (b). There are clearly a few characteristic frequencies emerging from the background noise between 250 and 260 and a strong single tone at 359 Hz. There is also a colored noise spectra in the band 500 to 700 Hz with, however, a much lower power.

8.3 Environmental model

During this experiment several difficulties are present: i) the source is moving fast, ii) the environment is a mixture of range dependent and range independent propagation, and iii) the source signal is ship noise with unknown and presumably time-varying characteristics. On top of those difficulties, the actual processing adds also a further problem which is that it is not possible to decide during the processing to switch between range-independent and range-dependent environmental models. In theory, a range-dependent model is also applicable to the range-independent case, allowing water depth at the source end to change along the ship track. Due to the well known source range vs. water depth interrelation
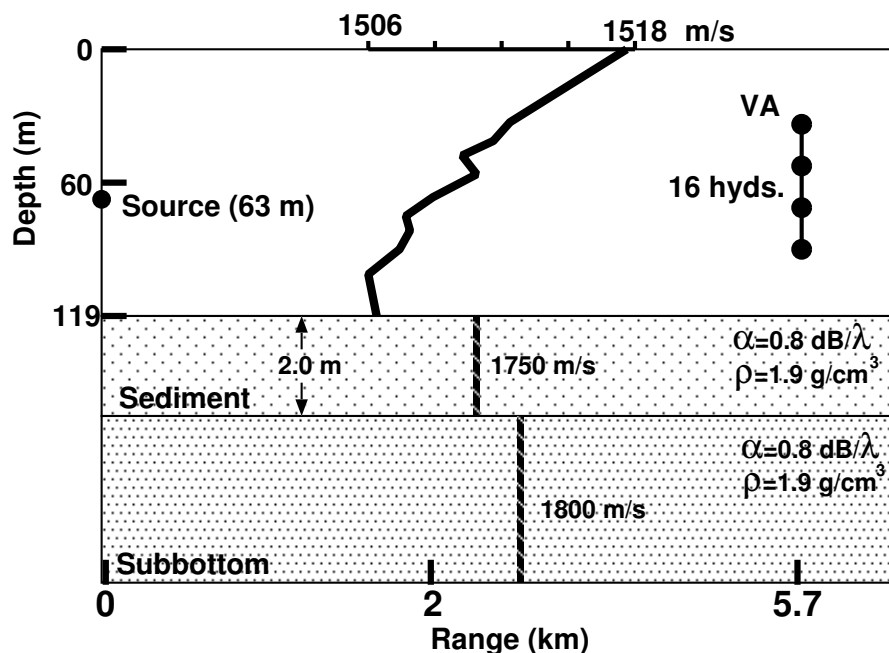
Figure 8.4: Range-independent baseline model for the INTIFANTE'00 sea trial.

and parameter hierarchy, it is impossible, or at least extremely difficult, to simultaneously estimate source range and water depth as well as other low dependence parameters. In this analysis it was decided to use a range independent model for reducing the computation and inversion burden (Fig. 8.4). As it will be seen in the following section, the usage of a range-independent model, even in a slightly range-dependent environment will add a significant source range mismatch, at some well defined points during the processing.

8.4 Inversion results with a coherence-based frequency selection

The inversion methodology was based on a three step procedure: i) preliminary search of the outstanding frequencies in a given time slot, ii) the usual parameter focalization, based on an incoherent broadband Bartlett processor, a C-SNAP [52] forward acoustic model and a GA based optimization and iii) inversion result validation based on model fitness and coherent source range and depth estimates through time. There are a number of possibilities for

implementing the frequency selection procedure for the first step. A first attempt using

a simple periodogram based spectral estimator for frequency selection was shown in [33]

and a similar estimator coupled with an amplitude estimator for frequency selection and

weighting in [107]. In the present study a coherence-based approach is proposed, where the

time coherence of a given frequency ω is evaluated according to

$$\Gamma(\omega) = \frac{1}{N-1} \sum_{n=1}^{N-1} \frac{\underline{Y}^H(\omega, t_{n+1})\underline{Y}(\omega, t_n)}{\|\underline{Y}(\omega, t_{n+1})\|\|\underline{Y}(\omega, t_n)\|} \geq \gamma_0, \tag{8.1}$$

where $\underline{Y}(\omega, t_n)$ is a L-dimensional complex vector with the L array sensor output at frequency

ω in time snapshot t_n, N is the total number of time realizations in a given window and

γ_0 is a constant detection threshold depending on the actual SNR and signal / ambient

noise level. The idea is that if a signal is present in a given frequency bin, a slow change

of the channel structure would allow to make the signal to maintain its coherence from one

snapshot to the other while there is a good chance that ambient noise will have a lower time

coherence. Figure 8.5 shows the plots of the phases taken at frequencies 359 and 718 Hz.

These are credited as being the most powerful frequencies radiated by the research vessel.

Time 50:24 h is when the vessel is steaming at her maximum speed on the NW-leg away from

the receiver array, while time 50:57 h is when it is performing the 2.2 km bow. The phases

shown correspond to receivers 4, 8, 12, 16. It is difficult to explain why in one case it is the

359 Hz frequency that is almost perfectly linear with time, and in the other case it is the

718 Hz frequency. There is a complex conjunction between the speed, the maneuvering, and

even ambient noise that might differently corrupt the signals at different frequencies. The

observed coherence can be detected by (8.1) for selecting the frequencies to be processed.

Basically, it combines the data received in two consecutive instants and coherently sums

the receivers. For the data of Event 6, 16 seconds of data were divided into 0.5 seconds
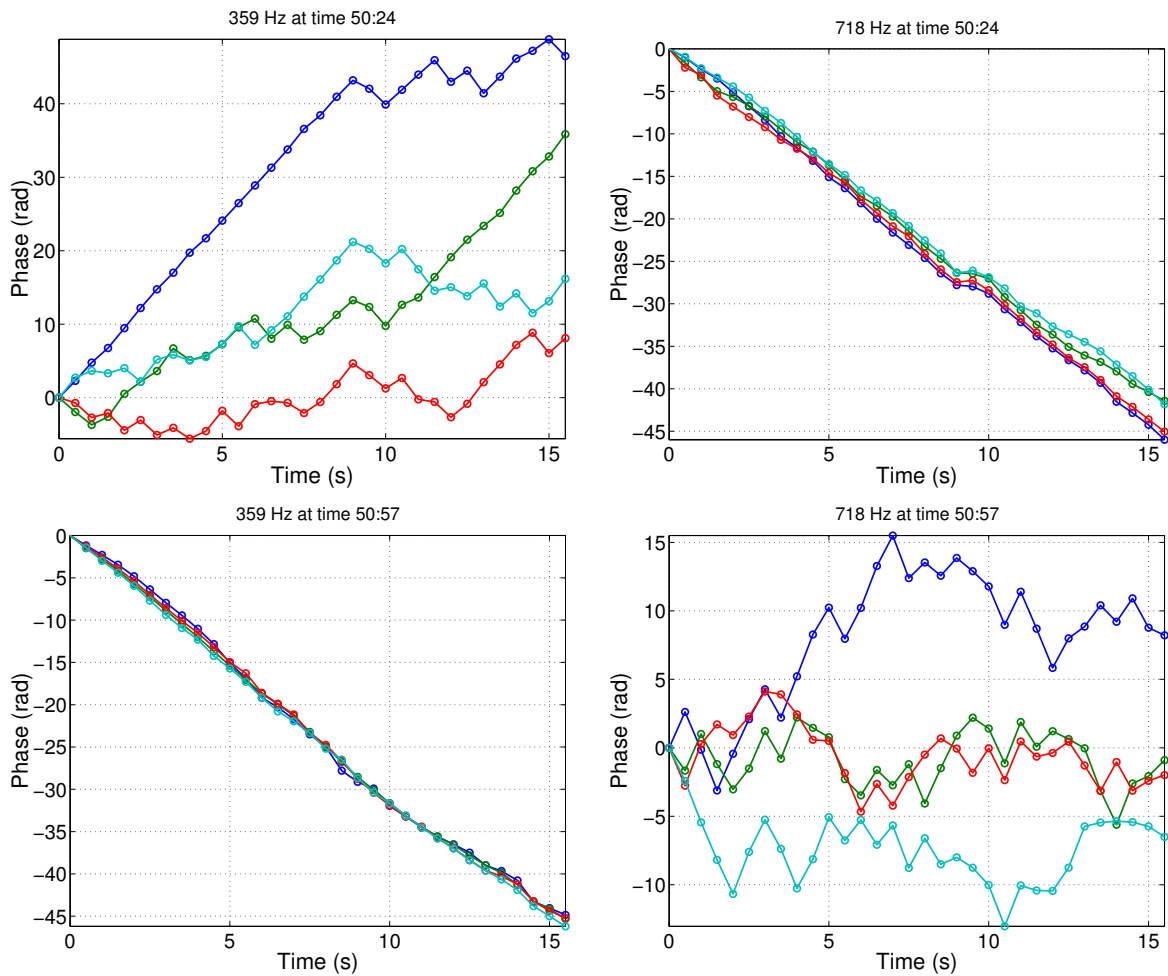
Figure 8.5: Examples of phases measured during Event 6 at frequencies 359 and 718 Hz.

duration snapshots, thus giving a frequency resolution of 2 Hz, and a number of realizations $N = 32$. The result of applying equation (8.1) in the frequency band 350 to 750 Hz gave the results shown in figure 8.6. This figure shows which bins were selected for processing - the third axis is 1 upon selection, and 0 otherwise. Note that there are a couple of frequencies almost constantly present throughout the run at 359 and 719 Hz, where one might be a harmonic of the other as well as other high coherence bins with some persistence at 490, 498 and 542 Hz. Actually, instead of setting γ_0, and in order to limit the computational complexity of the problem, a fixed number of frequency bins were selected at each time slot according to the maximum values of (8.1). The inversion results are shown in figure 8.7, from (a) to (j) are individual parameter estimates while plot (k) shows the water column
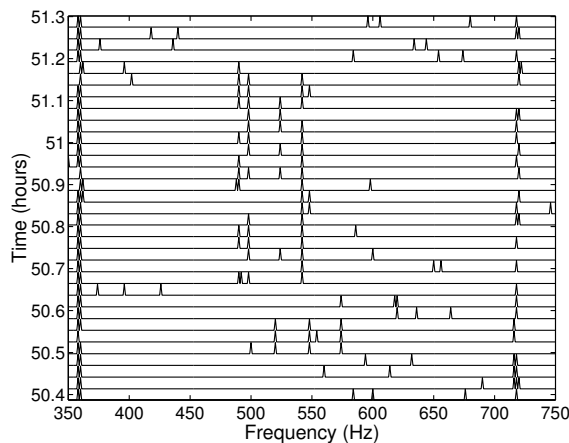
Figure 8.6: INTIFANTE'00 sea trial, Event 6 frequency selection: 1 - selection and 0 - no selection based on contiguous snapshot mean signal coherence along time (eq. (8.1)).

temperature reconstruction based on the EOF linear combination of parameter estimates (i) and (j). Plot (b) shows the estimated source range together with the GPS measured source range (continuous line). At first glance from the model fit indicator (Bartlett power) the result is poor, since it is always below 0.8; however, source range, which is one of the leading parameters, shows values in coincidence with the GPS measured source range while source depth is highly incoherent within the 0-6 m depth interval; and finally the reconstructed temperature (plot (k)) appears to be too variable for such a small time interval (slightly over 45 min). Looking more in detail, and comparing plot (a) of figure 8.2 with plots (a)-(c) of figure 8.7 the following conclusions can be drawn: i) for $50.42 \leq$ time ≤ 50.57, ship speed increases steeply to 9 kn, while heading off from the VLA. Range variation is about 4.6 m/s which, may cause a violation of the stationarity assumption during the averaging time. Source range estimation error progressively increases as the ship reaches the longest range point and then continues high during part of the first loop trajectory at an approximate constant range of 3.2 km; this erroneous source range estimate is almost certainly due to the environmental water depth mismatch in this portion of the track. After the end of the first loop the estimated source range perfectly matches the GPS curve. As mentioned above,
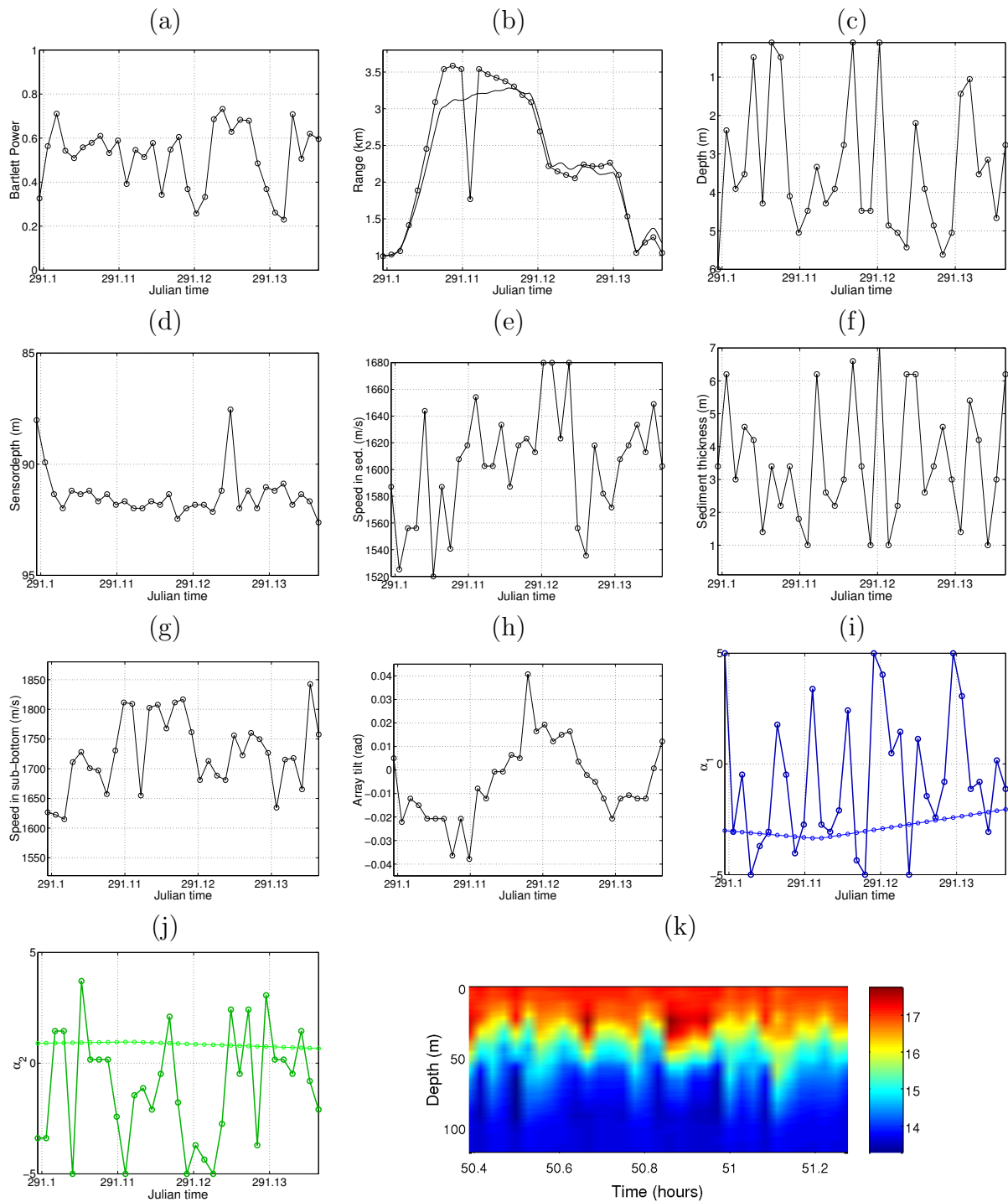
Figure 8.7: Focalization results for Event 6: Bartlett power (a), source range (b)[the continuous line is the GPS measured source-receiver range], source depth (c), receiver depth (d), sediment compressional speed (e), sediment thickness (f), sub-bottom compressional speed (g), VLA tilt (h), EOF coefficient α_1 (i), EOF coefficient α_2 (j) [filled dotted lines are the XBT measured data projected onto the respective EOFs] and reconstructed temperature (k).

source depth (plot (c)) is highly variable in the interval 0 - 6 m depth which is understood to

be due to the nature of the emitted signal (ship noise) radiated from a structure extending

below but also on or above the sea surface. Receiving array estimates shown in plots (d) and (h) for array depth and tilt respectively, are in agreement with the expected values. Notice the interesting behavior of array tilt that varies from -0.03 to +0.03 almost linearly during the side looking view 45 degree change when running from the NE to the NW leg and then back to the NE leg at the end of the run. Concerning the seafloor properties, one can say, that their estimates are confined to relatively short time intervals at periods when the vessel is steaming at her maximum speed, what somehow justifies for their high variability as seen on plots (e) to (g). EOF coefficients α_1 and α_2 are shown in plots (i) and (j), respectively. The estimated values are highly variable within the search interval, which is believed to be due to the highly variable and extremely low number of frequencies available in the ship radiated noise spectrum, associated with ship's acceleration and deceleration during maneuvering.

As a final comment on figure 8.7, the reconstructed water temperature - plot (k) - suffers both from poor estimation and ship variability. A different way of looking at the results is to plot histograms of the estimates as shown in figure 8.8, where it can be seen that α_1 most frequent estimate is -3 and that of α_2 is 0, which are values compatible with those measured with the XBT during that period of time (filled dots curve on plots (i) and (j)).

8.5   Summary

The objective of this chapter was to process acoustic data where the simplification was operated at the emitting end. The application considered herein was Passive Acoustic Tomography (PAT) using ship radiated noise collected during the INTIFANTE'00 sea trial, whose feasibility was to be proven. The variant of PAT considered was termed Blind Ocean Acoustic Tomography (BOAT), since it was assumed that the knowledge on the source po-
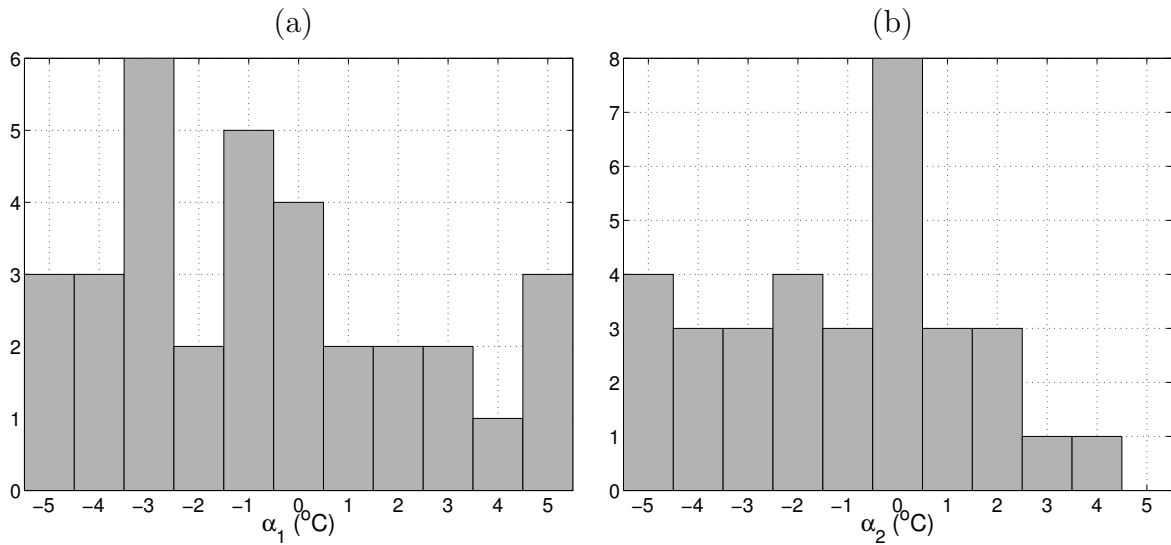
Figure 8.8: INTIFANTE'00 sea trial, Event 6: histograms of the EOF coefficients estimates for α_1 (a) and α_2 (b).

sition was limited, the emitted waveform was unknown, such as the seafloor properties.

The challenge was represented by the fact that during the various phases of the processing the *a priori* knowledge about the source was progressively relaxed leading to a situation close to that encountered in plain passive tomography, culminating with the replacement of the controlled source by the ship itself moving at high speed in a series of concentric loops around the receiving array. Several conclusions can be drawn:

- the ship range could be accurately estimated at times with range-independent bathymetry, and with an offset that is in agreement with the model mismatch at times with range-dependent bathymetry. Estimating the source depth appears to be more difficult than source range.

- the watercolumn parameters represented by the EOF coefficients vary over the entire search interval.

- given the short duration of the experiment (ca. 45 minutes) and the relatively reduced area, the parameter estimates can be looked in terms of *a posteriori* distributions. The

maximum of these distributions is coincident with the ground truth measurement of coefficients α_1 and α_2 .

One of the key difficulties in this study was dealing with the ship emitted waveform. The ship emitted waveform was completely unknown and possibly changing over time. This required application of a detector able to find out which frequencies contained ship radiated noise. This detector is sensitive to signals with high spatial and time coherence. There were two frequencies that were consistently detected over the whole period, and other were detected over shorter time intervals or on an occasional basis. There is the belief that this detector proved to effective in estimating which spectral component were being radiated by the ship.

One concern relates to the useful bandwidth of the radiated ship noise for environmental inversion. Although that concern was partially mitigated by the frequency selection based on the signal's short time coherence, a doubt remains whether real cargo ships at cruising speeds do radiate enough bandwidth sufficiently loud for the purpose of BOAT.

Chapter 9

Conclusions

Objective of this thesis

The present thesis deals with the possibility of using simplified acoustic systems to be used in ocean acoustic tomography and geoacoustic inversion. The motivations for simplifying an acoustic system are related to equipment and operational costs, and the difficulties associated with the operation of standard tomographic equipment. Such simplifications can be operated either on the emitting end, or on the receiving end. On the emitting end, one can reduce the size of the acoustic source, at the cost of decreasing the wavelength of the emitted waveforms, or use sources of opportunity such as ships or marine mammals instead a controlled source. Simplifications on the receiving end may consist in reducing the array length or the number of receiver elements, and therefore minimizing the overall size of the receiving equipment.

Operating simplifications on one end may imply an increase of the complexity on the other end, since the proposed simplifications may represent a loss or a reduction of the amount of information contained in the acoustic field, possibly conducting to degradation in the inversion results.

The objective of this thesis was to adapt existing array processing methods to be used in acoustic tomography and geoacoustic inversion taking into account the challenges posed

by the simplifications considered herein, and to cope with the loss of available information they may represent. Considering those challenges and their underlying relaxation in terms of working conditions, a Matched-Field (MF) based approach such as Matched-Field Tomography (MFT) appears to be more suitable than approaches based on travel-times for the reasons presented in chapter 1.

The contributions of the present thesis

Two aspects are exploited with the objective of coping with the reduction of information: one is the development of a broadband data model (proposed in Ref. [75]), and the other is the development of MF processors based on that broadband (BB) data model, with particular emphasis on high-resolution processors. Note that the experimental data used in the present work was collected under experimental scenarios considering the proposed simplifications.

The idea of proposing a linear broadband data model in the frequency domain is twofold: one is to compensate the loss of information induced by the reduction of the number of receivers by efficiently using the spectral components of the acoustic field; the other is to exploit field coherence across the spectral band, which has been seen in the literature as a mean of exploiting additional information contained in the acoustic field. The proposed data model also includes a random perturbation factor, which is frequency dependent and space independent. The introduction of this random perturbation factor is clearly justified by real data observations: it can be observed that the phases of the pressure field are in fact random, which may be due to unmodeled ocean inhomogeneities or parameter variability, and that they are generally perfectly coherent across space. The field coherence in the frequency domain is lower than in the space domain, and clearly depends on the degree of parameter variation and the frequencies involved. The random perturbation factor also

provides a mean to handle parameter variability under the assumption of a constant channel matrix, since such parameter variability will at least induce phase variability over the field observation time. This conducted to the most significant result of the broadband data model formulation, which was the generalization in terms of the degree of field coherence across frequencies by allowing assumptions from fully coherent signals to incoherent signals. An important by-product of this generalization was the representation of the data in signal and noise subspaces, where the dimension of the signal subspace intimately related to the degree of spectral coherence.

The other aspect of this thesis was the derivation of various matched-field processors based on the broadband data model. Formally using the broadband data model allows for obtaining true broadband matched-field processors, rather than a superposition of multiple narrowband processors. The main focus was in the derivation of coherent processors and high-resolution processors. The processors developed herein were a Bartlett processor, the minimum-variance (MV) and MUSIC processors, all broadband and coherent, with the latter two processors considered as high-resolution methods. Since the received signals are generally random with a certain degree of spectral coherence, the emitted signal is assumed unknown and it is represented in terms of second order statistics by a correlation matrix. This correlation matrix is unknown and jointly estimated with the physical parameters of interest, by means of a subspace based estimator adapted to the present data model.

Bartlett processors, based on correlations and of straightforward application, have been widely used in underwater acoustics, including acoustic tomography. The proposed high-resolution methods, involve computations that go beyond simple correlations, and so far were not used in acoustic tomography. The idea of using these processors is not to estimate

ocean environmental parameters with high resolution, but in fact to take advantage of their capability in attenuating sidelobes and therefore cope with solution ambiguity. This is particularly important when a processor is coupled with a meta-heuristic search method such as a genetic algorithm. Chapter 5 constitutes a synthetic study that was crucial for inferring on the applicability of high-resolution to matched-field tomography on experimental data by leading to the following conclusions:

- the performances of both the MV and MUSIC processors are much more dependent on the number of signal realizations than that of the Bartlett processor.

- in the case of the MUSIC processor, *a priori* knowledge on the signal subspace dimension clearly improves its average performance to a point where the requirement of a high number of observations can be relaxed.

- in practical applications, when searching for a full parameter set using a genetic algorithm, indications that high-resolution methods can significantly improve the search performance were obtained, since their increased ability in attenuating the sidelobes allows for improved convergence to the problem's solution.

This thesis includes experimental results on active and passive tomography obtained with several data sets, with application of incoherent and coherent, conventional and high-resolution processors. Both watercolumn and seafloor properties were included as unknown parameters throughout this study.

Active tomography via MFT was carried out assuming accurate knowledge on the source location, where source location parameters were either included in the search space only for allowing fit improvement, or were not included at all. The accurate knowledge on the source

location was used after the inversion in a source localization step with large search bounds aiming at validating model estimates in the absence of concurrent ground truth measurement. It was shown that this step allowed for discarding erroneous model estimates since a relevant relation between the estimation stability and the rate of correct source localization was found (see Chapter 6). It was also found that the standard deviation of the estimates of relevant model parameters clearly decreased with this validation step (Chapter 7).

Concerning the performance of the proposed matched-field processors in experimental data it was shown that:

- the proposed pre-processing schemes, aiming at improving the spectral coherence and/or the SNR, can significantly contribute to the increase of the estimation performance of a coherent processor over its incoherent counterpart (see Ref. [29]).

- the high-resolution methods clearly allowed for improving the convergence of the GA to the solution in comparison to the Bartlett processor (see Chapter 6).

Note that the performance comparison of the proposed MF processors was primarily based on the rate of successful source localizations. In terms of processor comparison in different working scenarios, the experimental results were consistent with the synthetic data results.

The inversion results obtained with simplified receiving arrays, considering only 3 or 4 hydrophones, demonstrate that it is possible to invert both watercolumn and seafloor properties, although a high degree of estimation variability is anticipated. The validation step via source localization is a very important aid in reducing the uncertainty of model estimates over time. It was possible to correctly localize the source at ranges up to 9 km (see Chapter 6 and Ref. [28]), which gives high confidence in the quality of the model estimates:

- the temperature in the watercolumn could be consistently estimated, although in some cases considerable ambiguity between EOF coefficients was noticed (see Chapters 6 7, and Ref. [29]).

- concerning the compressional speeds in the sediment and sub-bottom layers could generally be consistently estimated via *a posteriori* probabilities (see Chapters 6 and 7).

Finally, there is a remark to be made on the experimental setup: in the three data sets using a controlled source, the source was towed by the research vessel, moving in range and varying in depth. By inspection of the several inversion results the following could be found:

- source-receiver range variation rate (source speed projected in the source-receiver plane) impacts on the data structure but did not play a noticeable role in the quality of the inversion results. During the MREA'03 the source-receiver range variation attained a rate of up to 130 m/min (see Chapter 6).

- a conjugation of the receiving array design and environmental conditions (water temperature) with source depth played an important role in the quality of the inversion results (see Chapter 6). Variation in source depth due to research vessel acceleration/deceleration had a relevant impact in the data structure (see Ref. [29]).

The experimental results also include a case where the simplification in terms of acoustic system occurs at the emitting end by replacing the controlled source with a ship. MFT was applied to this data set aiming at inferring on the applicability of this technique in passive acoustic tomography with reduced knowledge on the source position (see Chapter 8 and Ref. [34]). This concept was termed Blind Ocean Acoustic Tomography (BOAT) for

this assumption. The acoustic data used for this purpose was radiated from the research vessel ranging up to 3.2 km away from the receiver array. The experimental results aiming at proving the feasibility of passive tomography are encouraging:

- although the EOF coefficients were estimated with considerable uncertainty, the maxima of the *a posteriori* distributions on these parameter estimates are compatible with concurrent ground truth measurements.

- source range can be accurately estimated.

It should be remarked that the research vessel was designed to be quite, and therefore these can be considered conservative results. A doubt remains whether real cargo ships at cruising speeds do radiate enough bandwidth sufficiently loud for the purpose of BOAT.

Recommendation for developing simplified acoustic systems

The conclusions made on the synthetic and experimental results of this thesis allows for making recommendations on the characteristics of simplified acoustic systems both for active and passive tomography able to work in conjunction with the proposed processing techniques. There are several components that can be setup in an acoustic system for acoustic tomography:

1. acoustic source experimental setup (range, depth, motion speed);

2. signal design and emitting band;

3. receiving array design (receiver density, array length) and deployment;

4. processing techniques.

First, an **acoustic system for active tomography** in shallow-water, taking into account the experimental results achieved in this thesis, is described. This system consists of a controlled acoustic source and a receiving array, and the following recommendations are made:

- the **source** may be deployed at a range up to 9 km from the receiver array, and may move with a speed up to tens of m/min, although it is desirable to minimize the source speed. The source depth, according to the experimental results, should be at mid-waterdepth or shallower, and should not vary during the collection of the acoustic data.

- there are also some hints on the **signal design**: so far successful results on environmental focalization were obtained at frequencies up to 1.5 kHz [68], which allows for using light and easy deployable acoustic sources; it is desirable to transmit deterministic signals with 100% duty cycle, i.e., transmit signals with no silence intervals during the observation window, in order to maximize the number of signal realizations which is an important aspect when applying high-resolution processors. Simultaneously, minimizing the length of the observation window, allows for reducing the parameter variability. Multi-tones allow for concentrating the emitted energy on discrete frequencies, and can be easily divided into snapshots. LFMs on the other hand provide a high number of frequencies.

- the **receiving array** may consist of 4 receivers, which is certainly the minimum allowing for MF methods to produce environmental estimates with an acceptable performance. Using a low number of receivers may contribute for reducing the cost and complexity of the receiving systems. Using the MUSIC processor in acoustic inversions

would, theoretically, allow for significantly reducing the length of the array.

- the experimental results obtained throughout this study have demonstrated that MF based **processing techniques** are very appropriate to be applied in ocean acoustic tomography and geoacoustic inversions with relaxed instrumentation deployment conditions. Specifically, it was proved that coherent and high-resolution MF processors can be used with simplified receiving systems in experimental scenarios.

An **acoustic system for passive tomography** in shallow-water, will consist of an uncontrolled acoustic source, a source of opportunity, and a receiving array. In this case it is more difficult to assert on the minimal requirements of the receiving system since it is uncertain what signals sources of opportunity will be emitting. Nevertheless, based on the experimental results presented in this thesis, the following recommendations can be made:

- The **receiving array** should be deployed in an area with regular traffic of cargo ships, since these should in principle be loud enough in order to provide sufficient bandwidth with sufficient signal-to-noise ratio.

- The **receiving array** may consist of 16 receivers or more, in order to increase the detection ability of radiated spectral components, and to compensate for the possibly reduced number of detectable spectral components.

- Concerning the **processing methods**, in this thesis the incoherent Bartlett processor was successfully applied to ship radiated noise, but also the incoherent MV and MUSIC processors may be applicable. Regarding the possibility for applying coherent methods, observations made on the spectral components most consistently detected during the INTIFANTE'00 data set, suggest that these are deterministic.

Future work

The simplification of acoustic systems for acoustic tomography and geoacoustic inversion together with processing techniques is worth further investigation, since several questions subsist.

Coherent high-resolution processors were applied to experimental data with a pre-processing step aiming at selecting highly coherent frequencies. The disadvantage of this scheme is the computational burden required in the frequency optimization step. Simulations demonstrate that the incoherent high-resolution processors still have a remarkable ability for attenuating sidelobes. Thus, it would be interesting to compare the incoherent high-resolution processors with their coherent counterparts in application to experimental data.

Concerning specifically the inversion, the experimental results have demonstrated the potential for the joint estimation of both watercolumn and seafloor parameters using an active source and a sparse array. However, low-ranking seafloor parameters were not consistently determined. Besides their low influence on the acoustic field, another factor causing difficulties was the huge size of the search space, which possibly increased the uncertainty in the parameter estimates in general. The implementation of a multi-stage inversion strategy would be a natural step for ameliorating the estimation of both high-ranking and low-ranking parameters, since this would significantly reduce the size of the search space at each stage.

Finally, there are also some questions regarding passive acoustic tomography. In order to consolidate the concept it would be necessary to conduct a sea trial with the main goal of recording noise radiated by loud cargo ships. A new data set collected in an area with regular traffic would allow for, first, answering to the question whether real cargo ships at cruising speeds do radiate enough bandwidth sufficiently loud for the purpose of BOAT;

second, allow to further infer on the characteristics of ship radiated noise.

Bibliography

[1] F. Jensen, W. Kuperman, M. Porter, and H. Schmidt. *Computational Ocean Acoustics.* AIP Series in Modern Acoustics and Signal Processing, New York, 1994.

[2] Ocean surface topography from space. *http://sealevel.jpl.nasa.gov/mission/topex.html.*

[3] W. Munk and C. Wunsch. Ocean acoustic tomography: A scheme for large scale monitoring. *Deep Sea Research*, 26(A):123–161, 1979.

[4] W. Munk, P. Worcester, and C. Wunsch. *Ocean acoustic tomography.* Monographs on mechanics. University Press, Cambridge, 1995.

[5] M. J. Hinich. Maximum-likelihood signal processing for a vertical array. *J. Acoust. Soc. Am.*, 54:499–503, 1973.

[6] H. P. Bucker. Use of calculated sound fields and matched-detection to locate sound source in shallow water. *J. Acoust. Soc. Am.*, 59:368–373, 1976.

[7] A. B. Baggeroer, W. A. Kuperman, and P. N. Mikhalevsky. An overview of matched field methods in ocean acoustics. *IEEE J. Ocean Eng.*, 18:401–424, 1993.

[8] A. Tolstoy, O. Diachok, and N. L. Frazer. Acoustic tomography via matched field processing. *J. Acoust. Soc. America*, 89(3):1119–1127, March 1991.

[9] I. A. Tolstoy. Low-frequency acoustic tomography using matched field processing (part i). *J. Acoust. Soc. America*, 85(S1):S7, November 1989.

[10] A. Tolstoy. Low-frequency acoustic tomography using matched field processing (part ii). *J. Acoust. Soc. America*, 85(S1):S7, November 1989.

[11] A. Tolstoy. Acoustic tomography using widely distributed vertical arrays and matched-field processing. *J. Acoust. Soc. America*, 88(S1):S117, November 1990.

[12] P. Gerstoft. Inversion of acoustic data using a combination of genetic algorithms and the gauss-newton approach. *J. Acoust. Soc. America*, 97(4):2181–2190, 1995.

[13] D. F. Gingras and P. Gerstoft. Inversion for geometric parameters in shallow water: Experimental results. *J. Acoust. Soc. America*, 97:3589–3598, 1995.

[14] P. Gerstoft and D. Gingras. Parameter estimation using multi-frequency range-dependent acoustic data in shallow water. *J. Acoust. Soc. America*, 99(5):2839–2850, 1996.

[15] M. Siderius and J.-P. Hermand. Yellow shark spring 1995: inversion results from sparse broadband acoustic measurements over a highly range-dependent soft clay layer. *J. Acoust. Soc. America*, 106(2):637–651, August 1999.

[16] M. Snellen, D. G. Simons, M. Siderius, J. Sellschopp, and P. L. Nielsen. An evaluation of the accuracy of shallow water matched field inversion results. *J. Acoust. Soc. America*, 109:514–527, 2001.

[17] M. D. Collins and W. A. Kuperman. Focalization: Environmental focusing and source localization. *J. Acoust. Soc. America*, 90:1410–1422, 1991.

[18] J. Capon. High-resolution frequency-wavenumber spectrum analysis. In *Proc. IEEE*, volume 57(8), pages 1408–1418, August 1969.

[19] R. O. Schmidt. *A signal subspace approach to multiple emmiter location and spectral estimation*. Phd. dissertation, Stanford University, 1982.

[20] Z.-H. Michalopoulou. Matched-field processing for broad-band source localization. *IEEE J. Ocean Eng.*, 21:384–392, 1996.

[21] Z.-H. Michalopoulou. Source tracking in the Hudson Canyon experiment. *J. Comput. Acoust.*, 4:371–383, 1996.

[22] S. Jesus, M. Porter, Y. Stephan, X. Démoulin, O. C. Rodríguez, and E. Coelho. Single hydrophone source localization. *IEEE Journal of Oceanic Engineering*, 25(3):337–346, July 2000.

[23] W. H.Munk, R. C. Spindel, A. B. Baggeroer, and T. G. Birdsall. The Heard Island Feasibility Test. *J. Acoust. Soc. Am.*, 96:2330–2342, 1994.

[24] P. F. Worcester and R. C. Spindel. North pacific acoustic laboratory. *J. Acoust. Soc. Am.*, 117:1499–1510, 2005.

[25] P. F. Worcester, W. H. Munk, and R. C. Spindel. Acoustic remote sensing of ocean gyres. *Acoustics Today*, 1(1):11–17, October 2005.

[26] P. Felisberto, S. M. Jesus, Y. Stephan, and X. Demoulin. Shallow water tomography with a sparse array during the intimate'98 sea trial. In MTS/IEEE, editor, *Proceedings MTS/IEEE Oceans'2003*, pages 571–575, San Diego, USA, 2003.

[27] J.-C. Le Gac, M. Asch, Y. Stéphan, and X. Demoulin. Geoacoustic inversion of broad-band acoustic data in shallow water on a single hydrophone. *IEEE J. Ocean Eng.*, 28:479–493, 2003.

[28] C. Soares, S. M. Jesus, and E. Coelho. Acoustic oceanographic buoy testing during the maritime rapid environmental assessment 2003 sea trial. In D. Simons, editor, *Proc. of European Conference on Underwater Acoustics 2004*, pages 271–279, Delft, Netherlands, 2004.

[29] C. Soares, S. M. Jesus, and E. Coelho. Shallow water tomography in a highly variable scenario. In A. Caiti, R. Chapman, J.-P. Hermand, and S. M. Jesus, editors, *Acoustics Inversion Methods and Experiments for Assessment of the Shallow Water Environment*, pages 41–55, Netherlands, 2004. Kluwer Academic Publishers.

[30] C. Soares and S. M. Jesus. Matched-field tomography using an acoustic oceanographic buoy. In S. M. Jesus, editor, *Proc. of European Conference on Underwater Acoustics 2006*, pages 717–722, Carvoeiro, Portugal, 2006.

[31] S. M. Jesus, C. Soares, A. Silva, J.-P. Hermand, and E. Coelho. Aob - acoustic oceanographic buoy: concept and feasibility. In *Proc. Underwater Defence Technology European Conference (UDT'06)*, Hamburg, Germany, June 2006.

[32] N. R. Chapman, R. M. Dizaji, and R. L. Kirlin. Geoacoustic inversion using broad band ship noise. In *Proc. Fifth European Conf. on Underwater Acoustics, ECUA'00*, pages 787–792, Lyon, France, July 2000.

[33] S. M. Jesus, C. Soares, J. Onofre, E. Coelho, and P. Picco. Experimental testing of the blind ocean acoustic tomography concept. In Pace and Jensen, editors, *Impact

of Littoral Environment Variability on Acoustic Predictions and Sonar Performance, pages 433–440, Kluwer, September 2002.

[34] S. M. Jesus, C. Soares, E. Coelho, and P. Picco. An experimental demonstration of blind ocean acoustic tomography. *J. Acoust. Soc. America*, 3(119):1420–1431, March 2006.

[35] A. M. Thode, G. L. D'Spain, and W. A. Kuperman. Matched-field processing, geoacoustic inversion, and source signature recovery of blue whale vocalizations. *J. Acoust. Soc. Am.*, 107:1286–1300, 2000.

[36] C. F. Mecklenbräuker and A. Gershman. Broadband maximum likelihood estimation of shallow ocean parametersusing shipping noise. In MTS/IEEE, editor, *Proc. on IEEE International Conference on Acoustics, Speech, Signal Processing*, pages 3105–3108, Salt Lake City, USA, 2001.

[37] D. J. Battle, P. Gerstoft, W. A. Kuperman, W. S. Hodgkiss, and M. Siderius. Geoacoustic inversion of tow-ship noise via near-field-matched-field processing. *IEEE J. Ocean Eng.*, 28:454–467, 2003.

[38] C. Park, W. Seong, P. Gerstoft, D. Battle, and P. Nielsen. Time domain geoacoustic inversion using ship noise. In MTS/IEEE, editor, *Proceedings MTS/IEEE Oceans'2003*, pages 586–591, San Diego, USA, 2003.

[39] M. J. Buckingham and S. A. S. Jones. A new shallow-ocean technique for determining the critical angle of the seabed from the vertical directionality of the ambient noise in the water column. *J. Acoust. Soc. America*, 81(4):938–946, April 1987.

[40] M. J. Buckingham and J. R. Potter. Acoustic daylight imaging: vision in the ocean. *GSA Today*, 4:97–102, 1994.

[41] N. M. Carbone, G. B. Deane, and M. J. Buckingham. Estimating the compressional and shear wave speeds of a shallow water seabed from the vertical coherence of ambient noise in the water column. *J. Acoust. Soc. America*, 103(2):801–813, 1998.

[42] C.H. Harrison and A. Baldacci. Bottom reflection properties by inversion of ambient noise. In *Proc. Sixth of European Conf. on Underwater Acoustics, ECUA'02*, pages 471–476, Gdansk, Poland, June 2002.

[43] C.H. Harrison. The influence of noise and coherence fluctuations on a new geo-acoustic inversion technique. In Pace and Jensen, editors, *Impact of Littoral Environment Variability on Acoustic Predictions and Sonar Performance*, pages 139–146, Kluwer, September 2002.

[44] C. H. Harrison and D. G. Simons. Geoacoustic inversion of ambient noise: A simple method. *J. Acoust. Soc. America*, 4(112):1377–1389, October 2002.

[45] M. J. Buckingham, E. M. Giddens, J. B. Pompa, F. Simonet, and T. R. Hahn. A light aircraft as a source of sound for performing ge-acoustic inversion ofthe sea bed. In *Proc. of Sixth European Conf. on Underwater Acoust., ECUA'02*, pages 465–470, Gdansk, Poland, June 2002.

[46] K. V. Mackenzie. Discussion of sea water sound-speed determinations. *J. Acoust. Soc. Am.*, 70:801–806, 1981.

[47] K. V. Mackenzie. Nine term equation for sound speed in the ocean. *J. Acoust. Soc. Am.*, 70:807–812, 1981.

[48] W. Menke. *Geophysical Data Analysis: Discrete Inverse Theory.* Academic Press, Inc, San Diego, California, 1989.

[49] S. M. Jesus, A. Silva, , and C. Soares. INTIFANTE'00 sea trial data report - Events 1, 2 and 3. Data Report 02/01, SiPLAB, Faro, Portugal, 2001.

[50] S. Jesus, A. Silva, and C. Soares. Acoustic Oceanographic Buoy test during the MREA'03 sea trial. Internal Report Rep. 04/03, SiPLAB/CINTAL, Universidade do Algarve, Faro, Portugal, November 2003.

[51] S. Jesus, C. Soares, P. Felisberto, A. Silva, L. Farinha, and C. Martins. Acoustic Maritime Rapid Environmental Assessment during the MREA'04 sea trial. Internal Report Rep. 02/05, SiPLAB/CINTAL, Universidade do Algarve, Faro, Portugal, March 2005.

[52] C. M. Ferla, M. B. Porter, and F. B. Jensen. C-SNAP: Coupled SACLANTCEN normal mode propagation loss model. Memorandum SM-274, SACLANTCEN Undersea Research Center, La Spezia, Italy, 1993.

[53] D. R. DelBalzo, C. Feuillade, and M. M. Rowe. Effects of water depth mismatch on matched-field localization in shallow water. *J. Acoust. Soc. America*, 83:2180–2185, 1988.

[54] M. B. Porter, R. L. Dicus, and R. G. Fizell. Simulations of matched-field processing in a deep-water pacific environment. *IEEE Journal of Oceanic Engineering*, 12(1):173–181, January 1987.

[55] R.M. Hamson and R.M. Heitmeyer. Environmental and system effects on source localization in shallow water by the matched-field processing of a vertical array. *J. Acoust. Soc. America*, 86(5):1950–1959, 1989.

[56] A. Tolstoy. Sensitivity of matched field processing to sound-speed profile mismatch for vertical arrays in a deep water pacific environment. *J. Acoust. Soc. America*, 85(6):2394–2404, June 1989.

[57] D. F. Gingras. Methods for predicting the sensitivity of matched-field processors to mismatch. *J. Acoust. Soc. America*, 86:1940–1949, 1989.

[58] C. Feuillade, D. R. DelBalzo, and M. M. Rowe. Environmental mismatch in shallow water matched-field processing: geoacoustic parameter variability. *J. Acoust. Soc. America*, 85:2354–2364, 1989.

[59] R. M. Hamson and R. M. Heitmeyer. An analytical study of the effects of environmental and system parameters on source localisation in shallow water by matched-field processing of a vertical array. *J. Acoust. Soc. America*, 86:1950–1959, 1989.

[60] S. Jesus. Normal-mode matching localization in shallow water: environmental and system effects. *J. Acoust. Soc. America*, 90:2034–2041, 1991.

[61] A. M. Richardson and L. W. Nolte. *A posteriori* probability source localization in an uncertain sound speed, deep ocean environment. *J. Acoust. Soc. America*, 89(5):2280–2284, 1991.

[62] M. J. Hinich and E.J. Sullivan. Maximum-likelihood passive localization using mode filtering. *J. Acoust. Soc. America*, 85(1):214–219, 1989.

[63] J. M. Ozard. Matched field processing in shallow water for range, depth and bearing determination: Results of experiment and simulation. *J. Acoust. Soc. America*, 86:744–753, 1989.

[64] C. Feuillade, W. A. Kinney, and D. R. DelBalzo. Shallow water matched-field localization off panama city, florida. *J. Acoust. Soc. America*, 88:423–433, 1990.

[65] S. M. Jesus. Broadband matched-field processing of transient signals in shallow water. *J. Acoust. Soc. America*, 4(93):1841–1850, April 1993.

[66] M. V. Greening, P. Zakarauskas, and S. E. Dosso. Matched-field localization for multiple sources in an uncertain environment, with application to arctic ambient noise. *J. Acoust. Soc. America*, 101(6):3525–3538, 1997.

[67] C. Soares, A. Waldhorst, and S. M. Jesus. Matched field processing: Environmental focusing and source tracking with application to the north elba data set. In *Proc. of the Oceans'99 MTS/IEEE conference*, pages 1598–1602, Seattle, Washington, 13-16 September 1999.

[68] C. Soares, M. Siderius, and S. M. Jesus. Source localization in a time-varying ocean waveguide. *J. Acoust. Soc. Am.*, 112(5):1879–1889, November 2002.

[69] L. T. Fialkowski, M. D. Collins, J. S. Perkins, and W. A. Kuperman. Source localization in noisy and uncertain ocean environments. *J. Acoust. Soc. America*, 101(6):3539–3545, 1997.

[70] S. E. Dosso. Matched-field inversion for source localization with uncertain bathymetry. *J. Acoust. Soc. America*, 94:1160–1163, 1993.

[71] C. Soares, M. Siderius, and S. M. Jesus. High frequency source localization in the strait of sicily. In *Proc. of the MTS/IEEE Oceans 2001*, Honolulu, Hawai, USA, November 2001.

[72] C. Soares. Matched-field processing: acoustic focalization with data taken in a shallow water area of the strait of sicily, March 2001.

[73] J. Holland. *Adaptation in Natural and Artificial Systems.* University of Michigan, 1975.

[74] H. L. Van Trees. *Optimum Array Processing, Part IV.* Wiley, New York, 2002.

[75] C. Soares and S. M. Jesus. Broadband matched field processing: Coherent and incoherent approaches. *J. Acoust. Soc. Am.*, 113(5):2587–2598, May 2003.

[76] A. B. Baggeroer, W. A. Kuperman, and H. Schmidt. Matched field processing: Source localization in correlated noise as an optimum parameter estimation problem. *J. Acoust. Soc. Am.*, 80:571–587, 1988.

[77] S. M. Kay. *Fundamentals of Statistical Signal Processing: Estimation Theory.* Prentice Hall, New York, 1993.

[78] A. Tolstoy. Computational aspects of matched field processing in underwater acoustics. In D. Lee, A. Cakmak, and R. Vichnevetsky, editors, *Computational Acoustics*, volume 3, pages 303–310, North-Holland, Amsterdam, 1990.

[79] Z.-H. Michalopoulou. Robust multi-tonal matched-field inversion: A coherent approach. *J. Acoust. Soc. Am.*, 104:163–170, 1998.

[80] G. J. Orris, M. Nicholas, and J. S. Perkins. The matched-phase coherent multi-frequency matched field processor. *J. Acoust. Soc. Am.*, 107:2563–2575, 2000.

[81] P. C. Mignerey and S. Finette. Multichannel deconvolution of an acoustic transient in an oceanic waveguide. *J. Acoust. Soc. Am.*, 92:351–364, 1992.

[82] S. Finette, P. C. Mignerey, J. F. Smith, and C. D. Richmond. Broadband source signature extraction using a vertical array. *J. Acoust. Soc. Am.*, 94:309–318, 1993.

[83] R. G. Fizell and S. C. Wales. Source localization in range and depth in an artic environment. *J. Acoust. Soc. Am., Suppl.*, 78:S57, 1985.

[84] B. A. D. H. Brandwood. A complex gradient operator and its application in adaptive array theory. In *IEE Proc.*, volume 130, pages 11–16, February 1983.

[85] K. Hsu and A. B. Baggeroer. Application of the maximum-likelihood method (mlm) for sonic velocity logging. *Geophysics*, 51:780–787, 1986.

[86] H. Akaike. Information theory and an extension of the maximum likelihood principle. In *Proc. 2nd Int. Symp. Inform. Theory*, pages 267–281, 1973.

[87] G. Schwartz. Estimating the dimension of a model. *Ann. Stat.*, 6:461–464, 1978.

[88] J. Rissanen. Modeling by shortest data description. *Automatica*, 14:465–471, 1978.

[89] M. K. Broadhead, R. L. Field, and J. H. Leclere. Sensitivity of the deconvolution of acoustic transients to green's function mismatch. *J. Acoust. Soc. America*, 94:994–1002, 1993.

[90] M. K. Broadhead. Broadband source signature extraction from underwater acoustics data with sparse environmental information. *J. Acoust. Soc. America*, 97:1322–1325, 1995.

[91] J. F. Boehme. *Advances in Spectrum Analysis and Array Processing*, volume 2, chapter 1, pages 1–63. Prentice Hall, 1991.

[92] M. Wax and T. Kailath. Detection of signals by information theoretic criteria. *Trans. Acoust., Speech, Signal Processing*, ASSP-33(2):387–392, 1985.

[93] A. R. Robinson and J. Sellschopp. *Ocean Forecasting: Conceptual Basis and Applications*, chapter 11, pages 203–232. Springer, 2002.

[94] J. Sellschopp and A. R. Robinson. Describing and forecasting ocean conditions during operation rapid response. In *Proc. of the conf. on rapid environmental assessment*, pages 35–42, Lerici, Italy, March 1997.

[95] A. R. Robinson. Forecasting and simulating coastal ocean processes and variabilities with harvard ocean prediction system. In *Proc. of the conf. on rapid environmental assessment*, pages 187–198, Lerici, Italy, March 1997.

[96] S. M. Jesus, C. Soares, A. J. Silva, J.-P. Hermand, and E. F. Coelho. Aob - an easily deployable, reconfigurable and multifunctional acoustic-oceanographic system. In *Proc. 148th Meeting of the Acoustical Society of America*, San Diego, USA, November 2004.

[97] F. Zabel, C. Martins, and A. Silva. Acoustic Oceanographic Buoy (version 2). Internal Report Rep. 05/05, University of Algarve, Faro, Portugal, 2005.

[98] T. Fassbender. Erweiterte genetische algorithmen zur globalen optimierung multi-modaler funktionen. Diplomarbeit, Ruhr-Universität, Bochum, 1995.

[99] E. L. Hamilton. Geoacoustic modeling of the sea floor. *J. Acoust. Soc. Am.*, 68(5):1313–1340, 1980.

[100] E. L. Hamilton. Sound velocity-density relations in sea-floor sediments and rocks. *J. Acoust. Soc. Am.*, 63(2):366–377, 1978.

[101] S. M. Jesus, E. Coelho, J. Onofre, P. Picco, C. Soares, and C. Lopes. The intifante'00 sea trial: preliminary source localization and ocean tomography data analysis. In *Proc. of the MTS/IEEE Oceans 2001*, Honolulu, Hawai, USA, 5-8 November 2001.

[102] S. M. Jesus. TOMografia PAssiva COstiera, Data Report - Phase 1. Internal Report Rep. 01/01, SiPLAB/CINTAL, Universidade do Algarve, Faro, Portugal, March 2001.

[103] P. Felisberto, C. Lopes, and S. M. Jesus. An autonomous system for ocean acoustic tomography. *Sea-Technology*, 45(4):17–23, April 2004.

[104] P. Felisberto, C. Lopes, and A. Carmo. Ultra Light Vertical Array / Remote Data Acquisition System. Internal Report 03/03, SiPLAB, Faro, Portugal, 2003.

[105] P. Felisberto, L. Farinha, and C. Soares. Ultra Light Vertical Array Remote Data Acquisition System (ULVA/RDAS version 2). Internal Report 03/05, SiPLAB, Faro, Portugal, 2005.

[106] S. M. Jesus, C. Soares, J. Onofre, and P. Picco. Blind ocean acoustic tomography: Experimental results on the intifante'00 data set. In *Proc. Sixth of European Conf. on Underwater Acoustics, ECUA'02*, Gdansk, Poland, June 2002.

[107] S. M. Jesus and C. Soares. Blind ocean acoustic tomography with source spectrum estimation. In *Proc. Int. Conf. on Theoretical and Computational Acoustic*, pages 211–220, Honolulu, Hawai, USA, August 2003.

[108] S. M. Jesus and C. Soares. TOMografia PAssiva COstiera - Inversion results with active data - Phase 2. Internal Report Rep. 06/01, SiPLAB/CINTAL, Universidade do Algarve, Faro, Portugal, December 2001.

[109] S. M. Jesus and C. Soares. TOMografia PAssiva COstiera - Inversion results with passive data - Phase 3. Internal Report Rep. 02/03, SiPLAB/CINTAL, Universidade do Algarve, Faro, Portugal, March 2003.

Appendix A

The Cramer-Rao Lower Bound Theorem

The Cramer-Rao Lower Bound Theorem is stated in Ref. [77] as follows:

Cramer-Rao Lower Bound - Vector Parameter: It is assumed that the probability density function (PDF) $p(\underline{x}; \underline{\theta})$ satisfies the *regularity* conditions

$$\mathrm{E}[\frac{\partial \ln p(\underline{x}; \underline{\theta})}{\partial \underline{\theta}}] = \underline{0} \tag{A.1}$$

for all $\underline{\theta}$, where the expectation is taken with respect to $p(\underline{x}; \underline{\theta})$. Then the covariance matrix of any unbiased estimator $\hat{\underline{\theta}}$ satisfies

$$\mathbf{C}_{\hat{\theta}} - \mathbf{I}^{-1}(\theta) \geq \mathbf{0} \tag{A.2}$$

where $\geq \mathbf{0}$ is interpreted as meaning that the matrix is positive semidefinite. The Fisher information matrix $\mathbf{I}(\theta)$ is given as

$$[\mathbf{I}(\underline{\theta})]_{ij} = -\mathrm{E}[\frac{\partial^2 \ln p(\underline{x}; \underline{\theta})}{\partial \theta_i \partial \theta_j}] \tag{A.3}$$

where the derivatives are taken at the true value of $\underline{\theta}$ and the expectation is taken with respect to $p(\underline{x}; \underline{\theta})$. Furthermore, an unbiased estimator may be found that attains the bound in that $\mathbf{C}_{\hat{\theta}} = \mathbf{I}^{-1}(\underline{\theta})$ if and only if

$$\frac{\partial \ln p(\underline{x}; \underline{\theta})}{\partial \underline{\theta}} = \mathbf{I}(\underline{\theta})(\underline{g}(\underline{x}) - \underline{\theta}) \tag{A.4}$$

for some p-dimensional function $\underline{g}$ and some $p \times p$ matrix $\mathbf{I}$. That estimator, which is the

minimum-variance unbiased (MVU) estimator, $\hat{\underline{\theta}} = \underline{g}(\underline{x})$, and its covariance matrix is $\mathbf{I}^{-1}(\underline{\theta})$.

Appendix B

Synthetic data: the environmental model

For generating the synthetic data used in the present study a range-independent three-layer environmental model was used. Fig. B.1 shows the environmental model used as input to the acoustic propagation model for synthetic data generation.
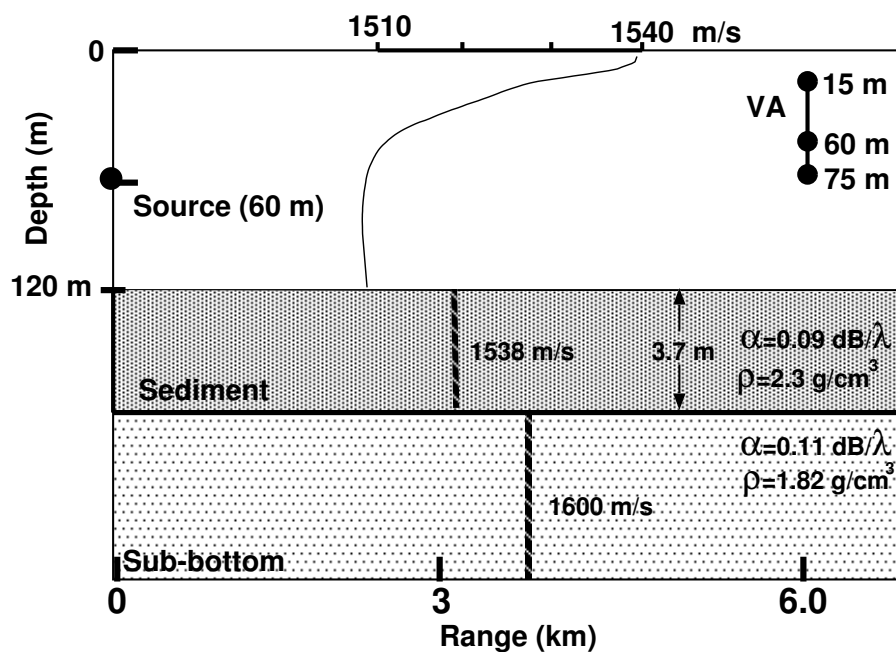
Figure B.1: Environmental model used for synthetic data generation.

The watercolumn sound-speed profile is based on the mean temperature profile of the MREA'03 sea trial (figure 2.1(b)) and the mean salinity profile, and was obtained by ap-

plication of the Mackenzie formula (eq. 2.1). The Empirical Orthogonal Functions (EOF) used along the synthetic study are shown in figure 2.1(e).

The CD-ROM provided with this document contains the mean temperature and salinity, and the EOFs.

Appendix C

Publications

The relevant publications obtained during the progress of the present work are contained in the CD-ROM provided with this document [28, 29, 30, 31, 33, 34, 75, 106, 107].